NASA TECHNICAL MEMORANDUM

NASA TM X-727

NASA TM X-72788

(NASA-TM-X-72788) FLOW VISUALIZATION OF VORTICES LOCKED BY SPANWISE BLOWING OVER WINGS FEATURING A UNIQUE LEADING AND TRAILING-EDGE FLAP SYSTEM (NASA) 103 p HC $5.50 CSCL 01A G3/02

N76-18056

Unclas 14258

FLOW VISUALIZATION OF VORTICES LOCKED BY SPANWISE BLOWING OVER WINGS FEATURING A UNIQUE LEADING- AND TRAILING-EDGE FLAP SYSTEM

By Gary E. Erickson - George Washington University, Joint Institute of Acoustics and Flight Sciences and
James F. Campbell - NASA Langley Research Center

This informal documentation medium is used to provide accelerated or special release of technical information to selected users. The contents may not meet NASA formal editing and publication standards, may be revised, or may be incorporated in another publication.

NATIONAL AERONAUTICS AND SPACE ADMINISTRATION
LANGLEY RESEARCH CENTER, HAMPTON, VIRGINIA 23665

1. Report No.	2. Government Accession No.	3. Recipient's Catalog No.
TM X-72788		

4. Title and Subtitle	5. Report Date
FLOW VISUALIZATION OF VORTICES LOCKED BY SPANWISE BLOWING OVER WINGS FEATURING A UNIQUE LEADING- AND TRAILING-EDGE FLAP SYSTEM	DECEMBER 1975
	6. Performing Organization Code

7. Author(s)	8. Performing Organization Report No.
Gary E. Erickson - George Washington University JIAFS and James F. Campbell - NASA Langley Research Center	
	10. Work Unit No.
9. Performing Organization Name and Address NASA Langley Research Center Hampton, Virginia 23665	11. Contract or Grant No.
	13. Type of Report and Period Covered Technical Memorandum
12. Sponsoring Agency Name and Address National Aeronautics and Space Administration Washington, DC 20546	14. Sponsoring Agency Code

15. Supplementary Notes

16. Abstract

Flow visualization studies were conducted to qualitatively determine the effects of active generation and augmentation of vortex flow over wings by blowing a discrete jet in a spanwise direction in the channel formed by extension of upper surface leading- and trailing-edge flaps. Spanwise blowing from a reflection plane over a rectangular wing was found to generate and "lock" a dual co-rotating vortex system within the channel and, at sufficient blowing rates, cause the separated flow off the upper end of the leading-edge flap to reattach to the trailing-edge flap. Observations suggest the external vortex flow induced by the lateral jet developed a thick, highly-cambered airfoil shape, the effective camber and thickness of which was dependent on flap extension angles. Sweeping the wing leading-edge to 45^{o} appeared to reduce, relative to the rectangular wing, the blowing rate required to develop a dual-vortex system and induce flow reattachment to the trailing-edge flap. Test parameters included wing angle of attack, jet momentum coefficient, leading- and trailing-edge flap deflection angle, and jet location above the wing surface. Effects due to removal of the leading- and trailing-edge flap were also investigated.

17. Key Words (Suggested by Author(s)) (STAR category underlined)	18. Distribution Statement
"Locked" vortex Spanwise blowing high lift	Unclassified - Unlimited

19. Security Classif. (of this report)	20. Security Classif. (of this page)	21. No. of Pages	22. Price*
Unclassified	Unclassified	100	$4.75

*Available from { The National Technical Information Service, Springfield, Virginia 22151
STIF/NASA Scientific and Technical Information Facility, P.O. Box 33, College Park, MD 20740

FLOW VISUALIZATION OF VORTICES LOCKED BY SPANWISE BLOWING OVER WINGS FEATURING A UNIQUE LEADING- AND TRAILING-EDGE FLAP SYSTEM

By Gary E. Erickson - George Washington University, Joint Institute of Acoustics and Flight Sciences and
James F. Campbell - NASA Langley Research Center

ABSTRACT

Flow visualization studies were conducted to qualitatively determine the effects of active generation and augmentation of vortex flow over wings by blowing a discrete jet in a spanwise direction in the channel formed by extension of upper surface leading- and trailing-edge flaps. Spanwise blowing from a reflection plane over a rectangular wing was found to generate and "lock" a dual co-rotating vortex system within the channel and, at sufficient blowing rates, cause the separated flow off the upper end of the leading-edge flap to reattach to the trailing-edge flap. Observations suggest the external vortex flow induced by the lateral jet developed a thick, highly-cambered airfoil shape, the effective camber and thickness of which were dependent on flap extension angles. Sweeping the wing leading-edge to 45° appeared to reduce, relative to the rectangular wing, the blowing rate required to develop a dual-vortex system and induce flow reattachment to the trailing-edge flap. Test parameters included wing angle of attack, jet momentum coefficient, leading- and trailing-edge flap deflection angle, and jet location above the wing surface. Effects due to removal of the leading- and trailing-edge flap were also investigated.

SUMMARY

Flow visualization studies were conducted in a small pilot wind tunnel at the NASA Langley Research Center to qualitatively determine the effects of active generation and augmentation of vortex flow over wings by blowing a discrete jet in a spanwise direction in the channel formed by extension of upper surface leading- and trailing-edge flaps. Test parameters included wing angle of attack, jet momentum coefficient, leading- and trailing-edge flap deflection angle, jet location above the wing surface, and leading-edge sweep angle. Effects due to removal of the leading- and trailing-edge flap were also investigated.

Spanwise blowing from a reflection plane over a rectangular wing featuring extension of leading- and trailing-edge flaps was found to generate and "lock" dual co-rotating vortices within the upper surface channel and at sufficient blowing rates cause the separated flow off the upper end of the leading-edge flap to reattach to the trailing-edge flap. The external vortex flow induced by the lateral jet appears to develop a "fictitious" airfoil shape possessing a large amount of camber and thickness. Extension or retraction of the leading- and trailing-edge flaps increases or decreases, respectively, the volume of the vortex channel, suggesting a possible means of varying the effective wing camber and thickness. Increased blowing rate at a given angle of attack decreases the size and growth rate of the vortices within the channel and appears to influence a larger mass of air passing over the wing. Observations suggest that higher blowing rates are required to maintain a stable vortex system to a given span distance as angle of attack is increased. Test results also indicate that jet location above the wing surface is possibly more effective relative to jet location at the wing surface in generating the vortical flow and inducing flow reattachment to the trailing-edge flap. The flow studies suggest that the presence of the leading- and trailing-edge flaps aids in developing a stable dual-vortex system over the wing. Extension of the leading-edge flap initiates flow separation at all angles of attack whereas the trailing-edge flap appears to act as a "turning vane" which aids in the development of a rotating mass behind the jet. Sweeping the wing leading-edge to 45° induces a favorable spanwise pressure gradient which appears to reduce, relative to the wing with zero leading-edge sweep, the blowing rate required to generate a dual-vortex system and cause flow reattachment to the trailing-edge flap at given flap deflection angles and angle of attack.

INTRODUCTION

The concept of inducing high lift by means of a separation induced vortex flow over a wing has received considerable attention in recent years. Vortex-induced lift increments for take-off and landing are a design feature of supersonic cruise aircraft such as the Anglo-French Concorde which features a thin highly-swept, low aspect ratio wing and the type of flow involved is shown in Figure 1. Development of a vortex flow over a wing is also important to the maneuver performance of the F-16 fighter. In order to achieve these beneficial lifting effects associated with the vortex, the flow over the wing

must separate near the leading edge, which results in high wing drag. It is, therefore, desirable to incorporate into the wing design the capability of transitioning from a high-lift configuration featuring external vortex flow to a low-drag cruise configuration without compromising the aerodynamic efficienc during either flight mode.

Reference 1 has investigated one promising concept which consists of "locking" an external vortex flow over a semi-span rectangular wing by spanwise blowing in the channel formed by extension of upper surface leading- and trailing-edge flaps. The configuration and flow situation are illustrated in Figure 2 which shows how the flow separates from the upper end of the leading-edge flap and rolls up into two discrete vortices within the channel. At sufficient blowing rates the separated flow reattaches to the trailing-edge flap after passing over the vortex channel, which results in large increases in lift. This flow situation is somewhat analogous to the stable, leading-edge vortices which are passively generated over thin, highly-swept low aspect ratio wings, previously shown in Figure 1, and also to the leading-edge separation vortices augmented by spanwise blowing over moderately-swept, higher aspect ratio wings which have been investigated in refs. 2-7 and are illustrated in Figure 3. Figure 4 shows data taken from reference 1 which indicate the significant vortex-induced lift increments obtained at all angles of attac by blowing spanwise in the wing cavity. The data also suggest that increased blowing rate increases the positive lift increments induced by the vortex flow

The present qualitative flow visualization studies were conducted to obtain additional information on the rectangular wing "locked" vortex concept considered in ref. 1 and to extend the concept to swept wing configurations. Test parameters included wing angle of attack, jet momentum coefficient, flap deflection angle and jet location above the wing surface. The effects on the flow situation due to removal of the leading- and trailing-edge flap were also investigated for a range of angle of attack, blowing rate, and flap deflection angle. Tests were conducted in a small pilot wind tunnel at the NASA Langley Research Center. Visualization of the flow process was made possible by a unique helium-filled bubble generator which produced neutrally-buoyant bubbles

NOMENCLATURE

a_e	Sonic velocity at nozzle exit
A_e	Nozzle exit area
AR	Aspect ratio, ($= b^2/S$)
b	Wing span
c_l	2-D lift coefficient
c_r	Wing root chord

c_t	Wing tip chord
C_L	3-D lift coefficient
C_μ	Jet momentum coefficient, $\left(\equiv \frac{2(\rho_e A_e V_e)V_e}{\rho_\infty V_\infty^2 S} \right)$
d	Nozzle diameter
h	Normal distance from wing upper surface to nozzle center line
LE	Leading-edge
M_e	Mach number at nozzle exit
p_e	Static pressure at nozzle exit
p_∞	Free-stream static pressure
$p_{t,e}$	Total pressure at nozzle exit
S	Wing planform area
T	Nozzle thrust
TE	Trailing edge
V_e	Jet exit velocity (See eq. 1)
V_∞	Free-stream velocity
x_n	Nozzle chordwise location measured from wing apex
α	Wing angle of attack
γ	Ratio of specific heats (air: $\gamma = 1.4$)
δ_{LE}, δ_{TE}	Leading- and trailing-edge flap deflection angles, respectively
ρ_e	Air density at jet exit (assumed equal to ρ_∞)
ρ_∞	Air density of free stream
2y/b	Wing span location

WIND TUNNEL TESTS

Flow visualization tests were conducted in a small pilot wind tunnel at the NASA Langley Research Center. The semi-span wing models were mounted on a vertical reflection plane located in the tunnel test section. A circular insert provided angle of attack capability. A free-stream dynamic pressure of 1.5 psf and free-stream velocity of 35.5 fps were maintained throughout the tests.

MODELS

Two models constructed of 0.25" - thick plexiglass were used in the experiments, and the wing and jet assemblies which were mounted on a circular insert made of 0.25" - thick plexiglass are illustrated in Figures 5(a) and 5(b). The AR= 2.0 rectangular wing shown in Figure 5(a) had a chord length (flaps retracted) of 6.0 inches, semi-span length of 6.0 inches, and leading- and trailing-edge flaps having constant-chord dimensions of 1.8 in. and 3.0 in., respectively. The leading-edge flap, which was an arbitrary airfoil shape with round leading edge and sharp trailing edge, was hinged at its quarter-chord whereas the trailing-edge flap having sharp leading and trailing edges was hinged at its half-chord line. The AR= 1.8 45° swept trapezoidal wing illustrated in Figure 5(b) had root and tip chord lengths of 10.0 in. and 3.5 in., respectively, when the flaps were fully retracted. The leading-edge flap had a round leading edge, sharp trailing edge, and chord dimension which tapered linearly from 2.5 in. at the root to 0.7 in. at the tip. The trailing-edge flap, with sharp leading and trailing edges, had a constant-chord dimension of 3.0 in. The leading- and trailing-edge flaps were hinged at the quarter-chord and half-chord lines, respectively. Test configurations considered in the flow visualization studies are illustrated in Figure 6.

Compressed air was brought over the wing through flexible tubing coupled to a length of stainless steel tubing having an inner diameter of 0.17 in. which extended outward slightly from the reflection plane and in a direction parallel to the wing leading edge.

INSTRUMENTATION

A flow meter indicated the volume flow rate (CFM) through the air supply system and the flow was regulated by a valve between the flow meter and nozzle. The volume flow rate and the compressed air pressure were adjusted to provide the desired nozzle flow conditions.

The total pressure at the nozzle exit ($p_{t,e}$) was measured with a pitot tube, and jet exit velocities were calculated using the compressible flow equation:

$$V_e = a_e M_e = \frac{2}{\gamma-1}\left\{\left[1-\left(\frac{p_e}{p_{t,e}}\right)^{\frac{\gamma-1}{\gamma}}\right]\left(\frac{p_e}{p_{t,e}}\right)^{\frac{\gamma-1}{\gamma}}\right\}^{1/2} \quad (1)$$

V_e is the jet velocity that results when the flow expands isentropically from $p_{t,e}$ to p_e, where it is assumed that $p_e = p_\infty$.

Nozzle thrust was estimated by suspending the nozzle vertically at one end of a platform balance and measuring the thrust for a range of blowing rates. This measured thrust is plotted as a function of C_μ in Figure 7 along with the thrust calculated from the equation:

$$T = (\rho_e A_e V_e) V_e \quad (2)$$

A helium - filled bubble generator was used to produce neutrally-buoyant bubbles which, when emitted into the flow, would reveal the general flow about the model. A mixture of air, helium, and soap solution ejected at the end of a converging nozzle produced bubbles, the diameter of which could be varied by adjusting the air, helium, and soap supplies. A bubble diameter of about 0.1" was found to provide good flow definition. A sketch of the nozzle arrangement is presented in Figure 8. The flow at any wing station could be examined by moving the bubble nozzle to the desired location.

A high-intensity light source was placed behind the model and facing upstream such that the bubbles would appear white in constrast to the black surfaces of the model and reflection plane. Proper location of the light source was most critical in obtaining good flow photographs. Placement of a high-intensity lamp downstream from the model and oriented approximately parallel to the wing chord plane ensured that the bubbles passing over the wing would be exposed to the light for a sufficient length of time. A second light source directed into the cavity defined the vortical flow within the channel and also the flow slightly forward of the wing which was not exposed to the light source located downstream. In general, the location(s) of the lamp(s) was dependent on model configuration and angle of attack.

A Hasselblad 500 EL-M camera mounted on a tripod was used in the tests. F-stop and shutter speed settings were 5.6 and 1/8 second, respectively, which enabled each bubble to appear as a streakline in the photographs. The camera was positioned so as to minimize glare from the model and reflection plane surfaces, and the distance between the camera and model was generally 1.5 - 2.0 ft. The development process of the Kodak Tri-X Pan 70mm film (ASA 400) increased the ASA rating to 1000 to heighten the contrast between the helium-filled bubbles and the wing and reflection plane surfaces.

RESULTS AND DISCUSSION

The results of this study are in the form of photographs taken of the flow visualization process for the test configurations previously shown in Figure 6. In all of these photographs, the free-stream flow is from left to right. The photographs are side views taken approximately in the wing chordal plane. Exceptions are noted in the discussion and the figures.

The following sections discuss the principle parameters investigated in the flow studies and are summarized in Table 1. A comparison of theoretical and experimental values of lift for the rectangular wing is presented at the end of section 2.

TABLE 1

Section	Wing Model	Principle Parameters
1	Rectangular	Jet momentum coefficient; angle of attack
2	Rectangular	Flap deflection angle
3	Rectangular	TE flap removal
4	Rectangular	LE flap removal
5	Rectangular	Nozzle displacement above wing surface
6	45° swept trapezoidal	LE sweep; jet momentum coefficient; angle of attack

The results presented in sections 1-4, and 6 were obtained with the jet located at $x_n/c_r = 0.4$ and $h/d = 1.0$.

Spanwise Blowing on the Rectangular Wing

1. Fixed Flap Deflection Angles, $\delta_{LE} = \delta_{TE} = 60^{\circ}$

The results obtained for blowing in the channel of the rectangular wing for $\delta_{LE} = \delta_{TE} = 60^{\circ}$ are presented in Figures 9 - 35 for angles of attack from 10° to 40° and jet momentum coefficients from 0.0 to 0.75.

In general, with blowing off flow separation occurs at the upper end of the leading-edge flap at all angles of attack and a large rotating mass exists

downstream of the wing. A typical result obtained with blowing off ($C_\mu = 0.0$) is shown in Figure 9 at $\alpha = 30^\circ$.

Blowing spanwise from $x_n/c_r = 0.40$ and h/d = 1.0 generates and augments vortex flow within the cavity as illustrated in Figures 10 - 12 for $\alpha = 10^\circ$. The separated flow off the upper end of the leading-edge flap rolls up into a dual co-rotating vortex system within the cavity for the range of blowing rates from 0.21 to 0.57. Figures 10 and 11 are for $C_\mu = 0.21$ and 0.30, respectively, and show the clockwise-rotating vortex of relatively large diameter behind the jet within the cavity and also indicate the flow reattachment on the trailing-edge flap. The vortex appears bounded by the lateral jet, wing surface, trailing-edge flap, and the flow passing over the "locked" vortex channel. The vortex located forward of the jet is shown in Figure 12 for $C_\mu = 0.57$. At this blowing rate, a large number of helium-filled bubbles constitute the forward vortex flow, which suggests that at higher blowing rates the induced pressure created by the spanwise jet influences a greater fluid mass passing over the wing. The investigation of ref. 1 did not observe this vortex forward of the jet. This may be a result of an inherent disadvantage in generating smoke forward of the model, which was the flow visualization technique used in ref. 1. The helium-filled bubble generator used in the present studies is unique in that the details of the flow are better revealed by the individual bubbles, and the flow at a particular location along the wing may be isolated and closely examined by moving the nozzle to the desired location.

Figures 13 - 21, 22 - 29, and 30 - 35 present results obtained for $\alpha = 20^\circ$, 30°, and 40°, respectively. The effect of increased angle of attack is to increase the blowing rate required to "lock" the vortex system within the channel and to cause flow reattachment on the trailing-edge flap. The discussion of the vortical flow at $\alpha = 10^\circ$ applies equally well to the flow situation observed for $\alpha = 20^\circ$, 30°, and 40°.

Figures 19 - 21 and 26 - 29 are oblique views which indicate the effect of blowing rate on the vortex flow ahead of the jet for $\alpha = 20^\circ$ and 30°, respectively. (Note: The large obstruction in the photographs is the bubble nozzle, tubing, and support assembly. Proper visualization of the forward vortex required emission of the bubbles in close proximity to the wing.) At a given angle of attack, increased blowing rate increased the spanwise effectiveness of the lateral jet, as suggested by a decrease in vortex size and growth rate and a delay of vortex bursting to greater span distances. Figure 29 is a result for $\alpha = 30^\circ$ and $C_\mu = 0.75$ which shows that vortex stability is maintained to approximately one-half of the semi-span. The vortex maintains a nearly constant circular cross-section to the bursting point. The vortex axis also remains approximately parallel to the leading edge as a result of the shielding provided by the leading-edge flap from local cross-flow effects. The photographs suggest that vortex size and growth rate increase rapidly due to jet decay and consequent insufficient flow along the vortex axes. The vortices and jet appear to coalesce and emerge prematurely from the channel, at which point the cross-flow deflects the jet-vortex system downstream. Inboard of the bursting point, the dual-vortex and jet system appears to develop a flow situation somewhat analogous to the flow about a

rotating cylinder in a uniform stream.

2. Variation of Flap Deflection Angles

Figures 36 - 50 illustrate typical results obtained by blowing for $x_n/c_r = 0.40$, $h/d = 1.0$ for various leading- and trailing-edge flap deflection angles. The majority of photographs shown are for $\alpha = 30^o$, except as noted, and are indicative of the results obtained for all angles of attack.

The presence of the vortices in the channel appears to develop a "fictitious" airfoil surface possessing a large amount of camber and thickness. Observations suggest it may be possible to generate a series of airfoil shapes by variation of leading- and trailing-edge flap deflection angles. Figures 36 - 38 and 39 - 42 show for $\delta_{LE} = 60^o$, $\delta_{TE} = 30^o$, and $\delta_{LE} = 90^o$, $\delta_{TE} = 45^o$, respectively, how the flow passes over the closed turbulent region, which consists of the vortices and jet, and at sufficient blowing rates reattaches to the trailing-edge flap. A "tear-drop" airfoil shape is developed which appears dependent on flap deflection angles and blowing rate. Figures 43 - 50 depict further airfoil shapes that might be developed by changing the flap extension angles.

The data suggest that as δ_{LE} is increased, larger blowing rates are required to "lock" the vortex system in the wing channel and to reattach the flow to the trailing-edge flap. This appears to be a result of the larger distance between the jet and the separated region that occurs when δ_{LE} is increased. The C_μ value must be appropriately larger in order for the jet pressure field to influence a given mass of air at larger distances. A compromise appears to exist, therefore, between the generator of a thick or highly-cambered airfoil shape and the blowing rate available.

Calculations were performed utilizing a numerical procedure from ref. 8 to obtain theoretical lift coefficients for two-dimensional inviscid flow about a 25 percent-thick, highly-cambered airfoil for angles of attack from 0^o to 40^o. Airfoil coordinates were estimated by assuming smooth flow off the upper end of the leading-edge flap and reattached flow on the trailing-edge flap of the semi-span rectangular wing of ref. 1. Leading- and trailing-edge flap deflection angles for that investigation were 30^o and 20^o, respectively. A computer plot of pressure coefficient versus chordal distance and also a plot of airfoil surface coordinates are shown in Figure 51 along with the integrated aerodynamic characteristics at each angle of attack. The two-dimensional lift coefficients were adjusted to three-dimensional lift values for incompressible flow by the technique described in ref. 9. The two- and three-dimensional results are compared in Figure 52 to the experimental data previously shown in Figure 4. Applying the theory from ref. 8 to the assumed airfoil shape and correcting the results to 3-D by the method of ref. 9 appears to yield a reasonable estimate of the experimental lift values of ref. 1 for $C_\mu = 0.3$ and 0.4 for a wide range of angle of attack. Care should be exercised however, in interpreting the results since the experimental data of ref. 1 were highly dependent on Reynolds number. The theory presented in Figures 51 and

52 may be a possible method of estimating the induced-lift increments due to the "locked" vortex flow, but investigation of the dependence of this flow phenomenon upon Reynolds number is necessary before a direct comparison of experiment and theory can be attempted.

3. Leading-Edge Flap On, Trailing-Edge Flap Off

Results for the case with upper surface trailing-edge flap off are presented in Figures 53 - 56 for $\alpha = 30^{\circ}$, $\delta_{LE} = 60^{\circ}$, and C_{μ} values from 0.0 to 0.57 and are typical of the observations for $\alpha = 10^{\circ}$, 20°, and 40°.

With blowing on, a distinct vortex was developed ahead of the jet, but a stable vortex was not observed behind the jet for the range of blowing rates considered from $C_{\mu} = 0.21$ to 0.57. The results suggest an analogy to the flow situation previously sketched in Figure 3 for spanwise blowing over a thin, moderately-swept wing at moderate to high angles of attack. In both cases, the separated flow in the vicinity of the leading edge rolls up into a discrete vortex ahead of the jet and flow reattachment is forced to occur aft of the jet. Figures 53 - 56 indicate, however, a tendency for the flow to roll up into a vortex behind the jet which implies that a stable vortex might possibly be developed for particular values of C_{μ}, δ_{LE}, and α. The photographs suggest that the trailing-edge flap acts as a "turning vane" which aids in deflecting the flow which is entrained into the cavity forward towards the jet. The trapped fluid is drawn towards the jet-induced low pressure region and is subsequently deflected by the jet, which appears to act essentially as a solid body in the flow. The boundaries created by the trailing-edge flap, wing surface, jet, and fluid passing over the wing appear to "lock" the vortex within the cavity.

4. Leading-Edge Flap Off, Trailing-Edge Flap On
(Sharp Leading Edge)

Results were obtained for the rectangular wing with the trailing-edge flap on and the leading-edge flap removed. The remaining leading edge was sharpened to obtain the photographs presented in Figures 57 - 59 and 60 - 61 for $\delta_{TE} = 30^{\circ}$ and 60°, respectively, and $\alpha = 30^{\circ}$.

A leading-edge vortex was observed to roll up ahead of the jet for the range of blowing rates considered from $C_{\mu} = 0.21$ to 0.57, but the generator of a stable, rotating flow aft of the jet appeared to be very dependent on blowing rate and flap deflection angle. Since a well-defined dual-vortex system was not observed for the range of angle of attack, blowing rate and flap deflection angle considered, this phase of the test program was terminated.

5. Vertical Jet Location

Shown in Figures 62 - 67 are comparative results obtained for blowing from h/d = 1.0 and 4.0 for $\alpha = 30^{\circ}$, $x_n/c_r = 0.40$ and $\delta_{LE} = \delta_{TE} = 45^{\circ}$. Figures 68 - 71 further illustrate the effect of vertical displacement of the nozzle for similar conditions with the exception that $\delta_{LE} = \delta_{TE} = 60^{\circ}$.

Observations suggest that vertical displacement of the nozzle reduces the blowing rate required at given flap deflection angles and angle of attack to develop an external vortex flow and cause flow reattachment to the trailing-edge flap. The relative distance between the lateral jet and separated region is reduced by raising the nozzle above the wing surface and, at a given blowing rate, a larger mass of air appears to be influenced by the jet relative to the low nozzle location. This is indicated in the photographs by a compression of the streaklines and a greater deflection of the flow passing over the wing.

Spanwise Blowing on the 45° Swept Trapezoidal Wing

6. Fixed Flap Deflection Angles, $\delta_{LE} = \delta_{TE} = 60^{\circ}$

The results obtained for the case of blowing at $x_n/c_r = 0.40$, $h/d = 1.0$ in the channel of a 45° swept trapezoidal wing are summarized in Figures 72 - 86 for the range of angle of attack from $\alpha = 10^{\circ}$ to 40°, blowing rate from $C_\mu = 0.0$ to 0.095, and $\delta_{LE} = \delta_{TE} = 60^{\circ}$.

With blowing off ($C_\mu = 0.0$), a weak vortex was observed over the channel emanating from the trailing edge of the leading-edge flap, and the flow passing over the wing appeared to experience a downward deflection as shown in Figures 72, 75, 79, and 83 for $\alpha = 10^{\circ}$, 20°, 30°, and 40°, respectively.

With blowing on, the vortex previously observed without blowing was enhanced and drawn into the channel and a second rotating flow was generated behind the jet. The discussion pertaining to the vortex flow within the channel for the rectangular wing applies equally well to the flow situation for the 45° swept trapezoidal wing. The favorable spanwise pressure gradient provided by leading-edge sweep appears to reduce the blowing rate required, relative to the rectangular wing, to induce vortex flow within the channel and to cause flow reattachment to the trailing-edge flap, as indicated in Figures 73 - 74, 76 - 78, 80 - 82, and 84 - 86 at $\alpha = 10^{\circ}$, 20°, 30°, and 40°, respectively. Observations suggest that at blowing rates sufficient to maintain vortex stability to the wing tip, the tip vortex might possibly be displaced outboard

RECOMMENDATIONS

The encouraging qualitative results obtained from the present flow visualization studies and also force data for a semi-span rectangular wing from ref. 1 indicate the desirability for further investigation of the concept of vortex-induced lift by spanwise blowing over wings featuring upper surface leading- and trailing-edge flaps. The latter type of configuration may have possible application to short take-off and landing (STOL) aircraft and is appealing in that the flow phenomenon described in this report might possibly be generated at low angles of attack, thus improving pilot visibility at take-off and approach. Wing design featuring the "locked" vortex flow at low speed must provide the capability of transitioning to an efficient, low-drag cruise configuration by retraction of the leading- and trailing-edge flaps. Further design considerations might include a low-speed flap arrangement coupled with spanwise blowing over moderately-swept wings of existing jet aircraft.

Recommended areas of research include parametric wind tunnel studies of full-span wings to determine quantitative effects of blowing rate, angle of attack, flap deflection angles, nozzle location, and leading-edge sweep angle, and investigation of Reynolds number effects on vortex characteristics and blowing effectiveness.

CONCLUDING REMARKS

Flow visualization studies were conducted in a small pilot wind tunnel at the NASA Langley Research Center to determine qualitative effects of generating and "locking" vortex flow over wings by spanwise blowing in a channel formed by extension of upper surface leading- and trailing-edge flaps. Blowing from a reflection plane in the upper surface channel of a rectangular wing induces a dual, co-rotational vortex system within the channel and, at sufficient blowing rates, causes the separated flow off the upper end of the leading-edge flap to reattach to the trailing-edge flap. Increased blowing rate increases the spanwise effectiveness of blowing at a given angle of attack, as indicated by a decrease in size and growth rate of the vortices bounding the jet and a delay of vortex bursting to greater span distances. The effect of increased angle of attack is to increase the blowing rate required to maintain vortex stability to a given span distance and to cause flow reattachment on the trailing-edge flap. The vortex flow appears to energize the flow such that attached flow is provided over an "effective" airfoil shape possessing a large amount of camber and thickness. Two-dimensional inviscid flow calculations were performed applying the theory of ref. 8 to an airfoil shape comparable to that which might be developed by the model of ref. 1 and these results were corrected to three dimensions by the technique of ref. 9. The theory appears to estimate reasonably well the experimental data from ref. 1 for a wide range of angle of attack, but the apparent dependence of the "locked" vortex flow phenomenon upon Reynolds number necessitates discretion when making a direct comparison of theory and experiment. Variation of flap deflection angle and blowing rate appear to be two means of altering the effective wing camber or thickness. Observations suggest that the presence of both the leading- and trailing-edge flaps aids in the development of the two distinct vortex flows over the wing, the former component initiating flow separation at all angles of attack and the latter acting as a "turning vane" which is a factor in the formation of a second rotating mass in the channel. Test results indicate that a jet located above the wing surface is more effective relative to blowing at the surface in developing the vortical flow. Test results also suggest that leading-edge sweep, which provides a favorable spanwise pressure gradient, reduces the blowing rate required, relative to the rectangular wing, to generate and "lock" vortex flow in the channel and to induce reattached flow to the trailing-edge flap.

REFERENCES

1. Westesson, R. A.; and Clareus, V.: Turbulent Lift. Comments on Some Preliminary Wind Tunnel Tests. Saab-Scania Report, TP-74-51, March 1974.

2. Bradley, R. G., et. al.: An Experimental Investigation of Leading-Edge Vortex Augmentation by Blowing. NASA CR-132415, April 1974.

3. Campbell, J. F.: Effect of Spanwise Blowing on the Pressure Field and Vortex-Lift Characteristics of a 44° Swept Trapezoidal Wing. NASA TN D-7907, April 1975.

4. Dixon, C. J.: Lift Augmentation by Lateral Blowing Over a Lifting Surface. AIAA Paper No. 69-193, February 1969.

5. Cornish, J. J.: High-Lift Applications of Spanwise Blowing. ICAS Paper No. 70-09, September 1970.

6. Bradley, R. G., et. al.: Leading-Edge-Vortex Augmentation In Compressible Flow. AIAA Paper No. 75-124, January 1975.

7. Dixon, C. J., et. al.: Theoretical and Experimental Investigations of Vortex-Lift Control by Spanwise Blowing. LG 73 ER-0169, September 1973.

8. Stevens, W. A., et. al.: Mathematical Model for Two-Dimensional Multi-Component Airfoils in Viscous Flow. NASA CR-1843, July 1971.

9. Lowry, J. G., and Polhamus, E. C.: A Method for Predicting Lift Increments Due to Flap Deflection at Low Angles of Attack in Incompressible Flow. NACA TN 3911, January 1957.

PRECEDING PAGE BLANK NOT FILMED

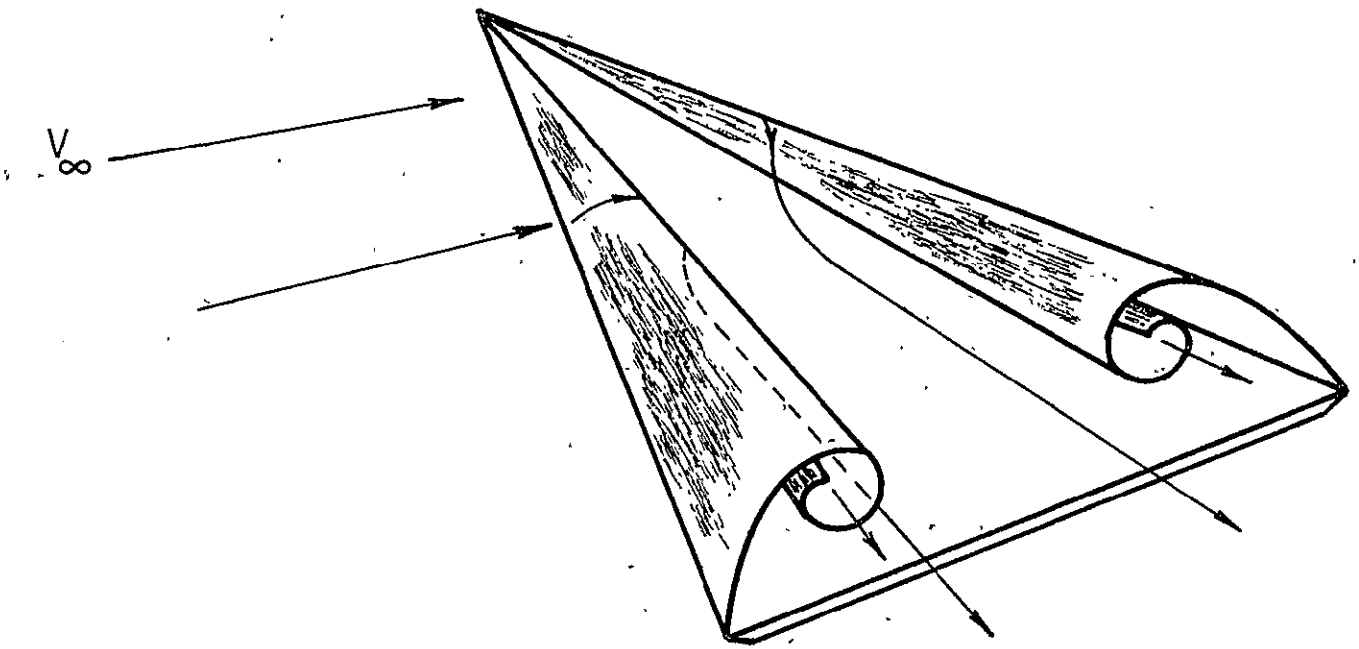

Figure 1.- Stable leading-edge vortices over a slender wing.

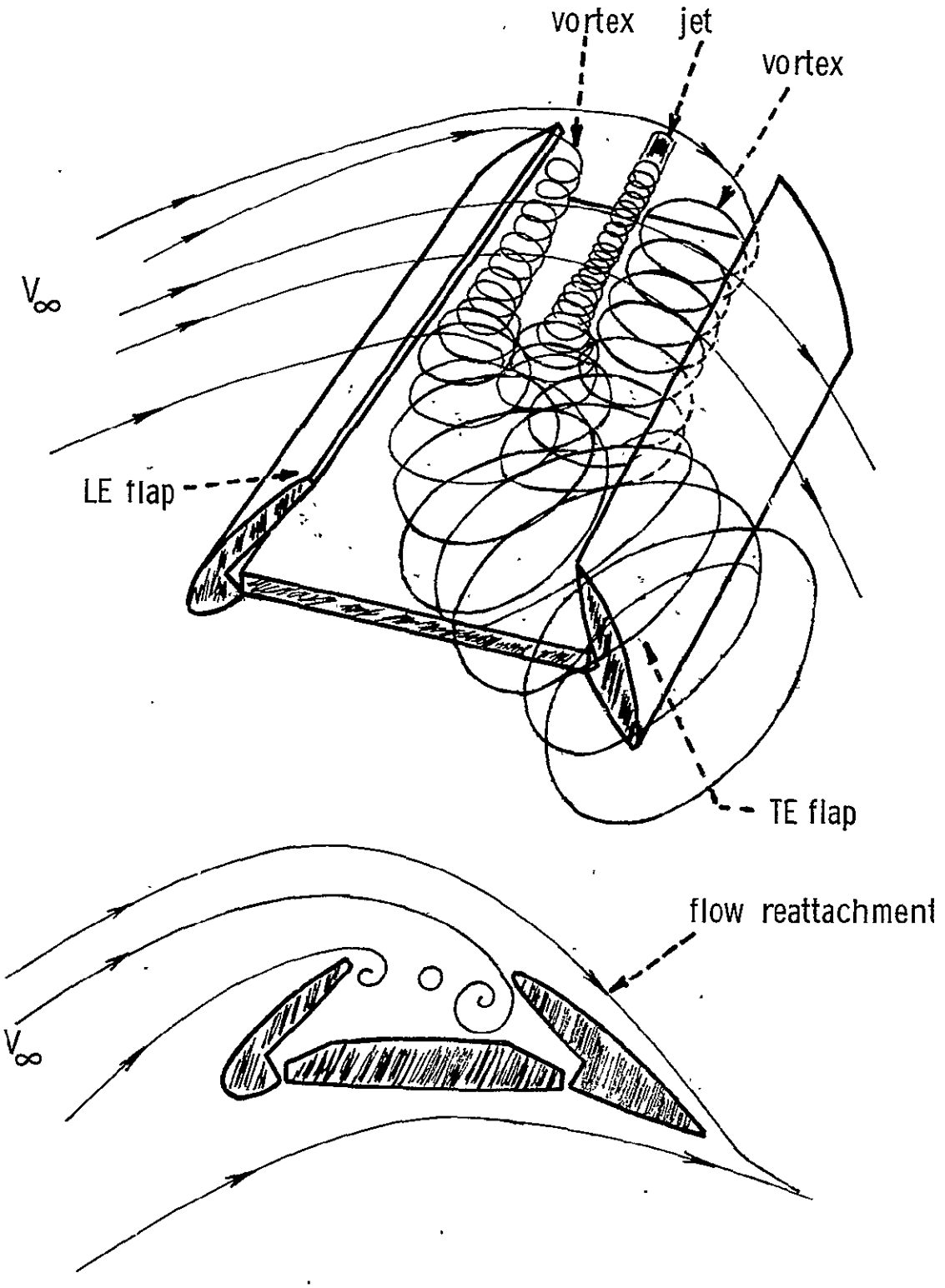

Figure 2.- Generation of a dual vortex system by spanwise blowing over a rectangular wing.

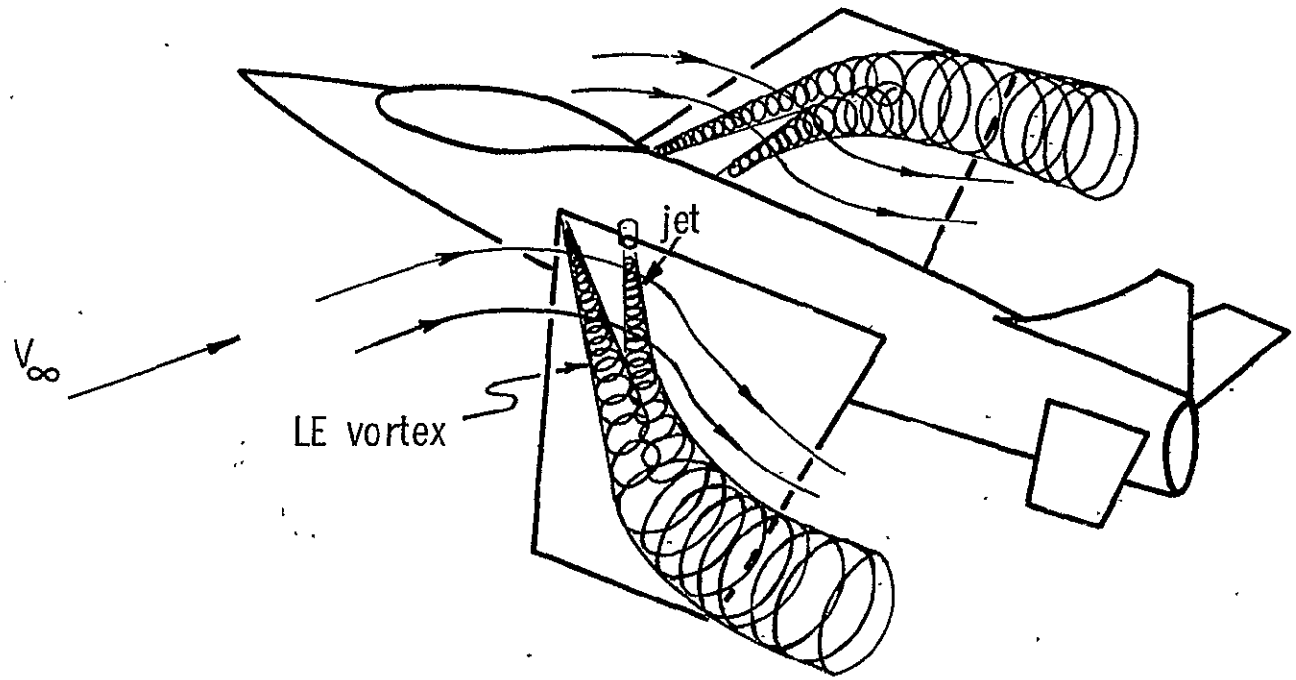

Figure 3.- Leading-edge vortex enhancement by spanwise blowing.

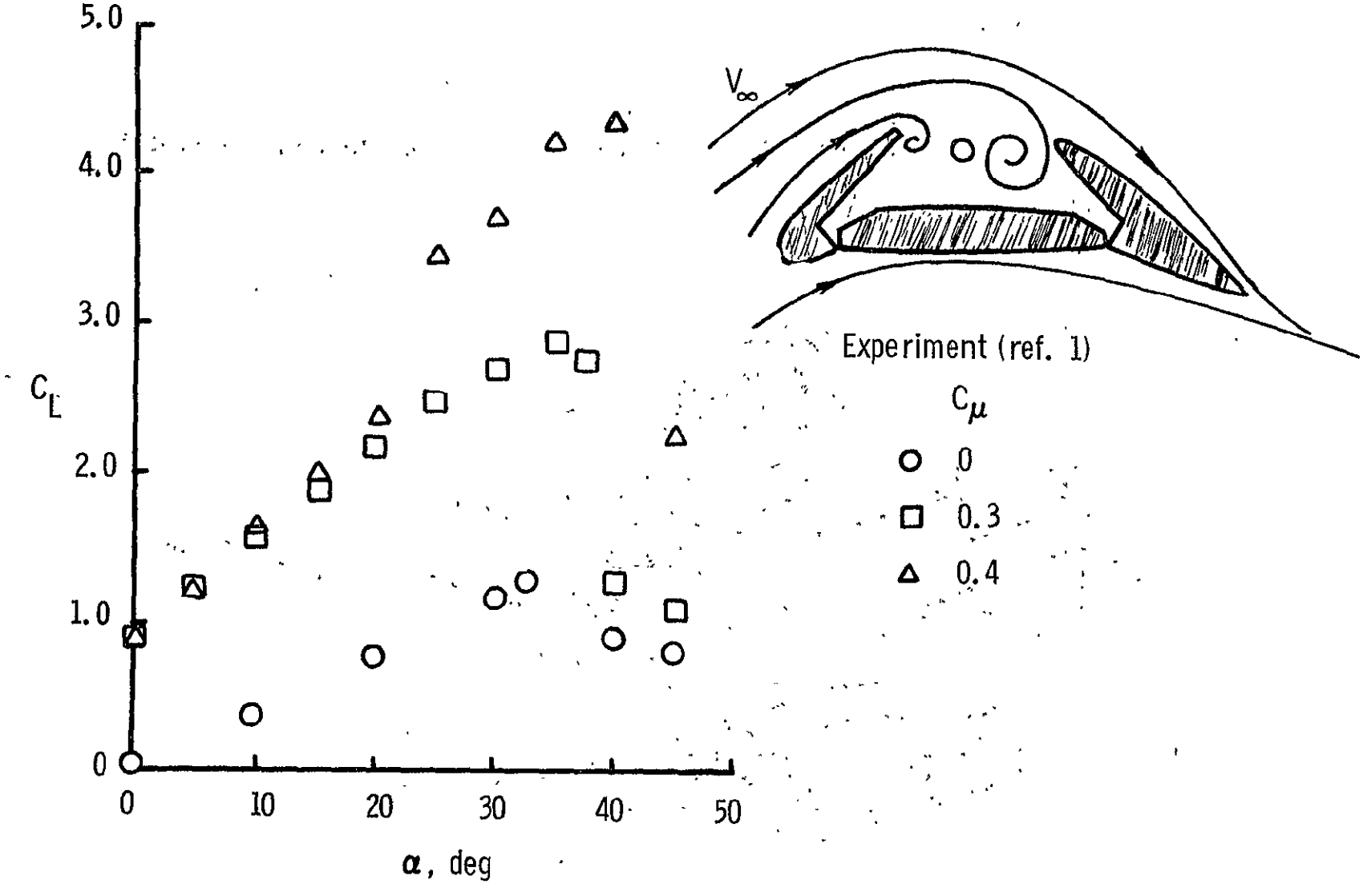

Figure 4.- Lift augmentation by spanwise blowing over an AR = 4.0 rectangular wing; V_∞ = 68.9 fps; Re = 150,000; $\delta_{LE} = 30^0$; $\delta_{TE} = 20^0$

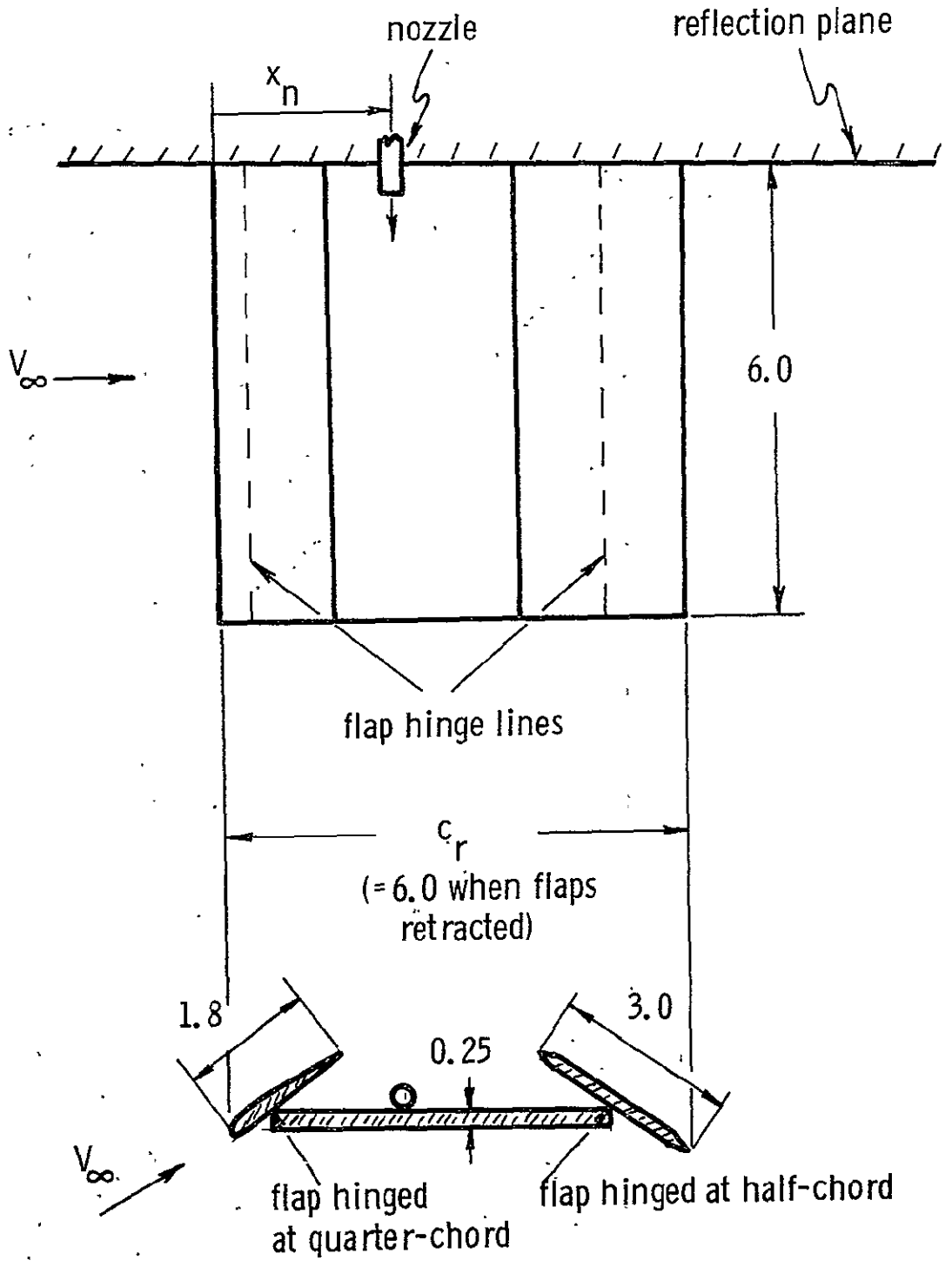

(a) AR = 2.0 rectangular wing.

Figure 5. - Flow visualization models. (all dimensions in inches)

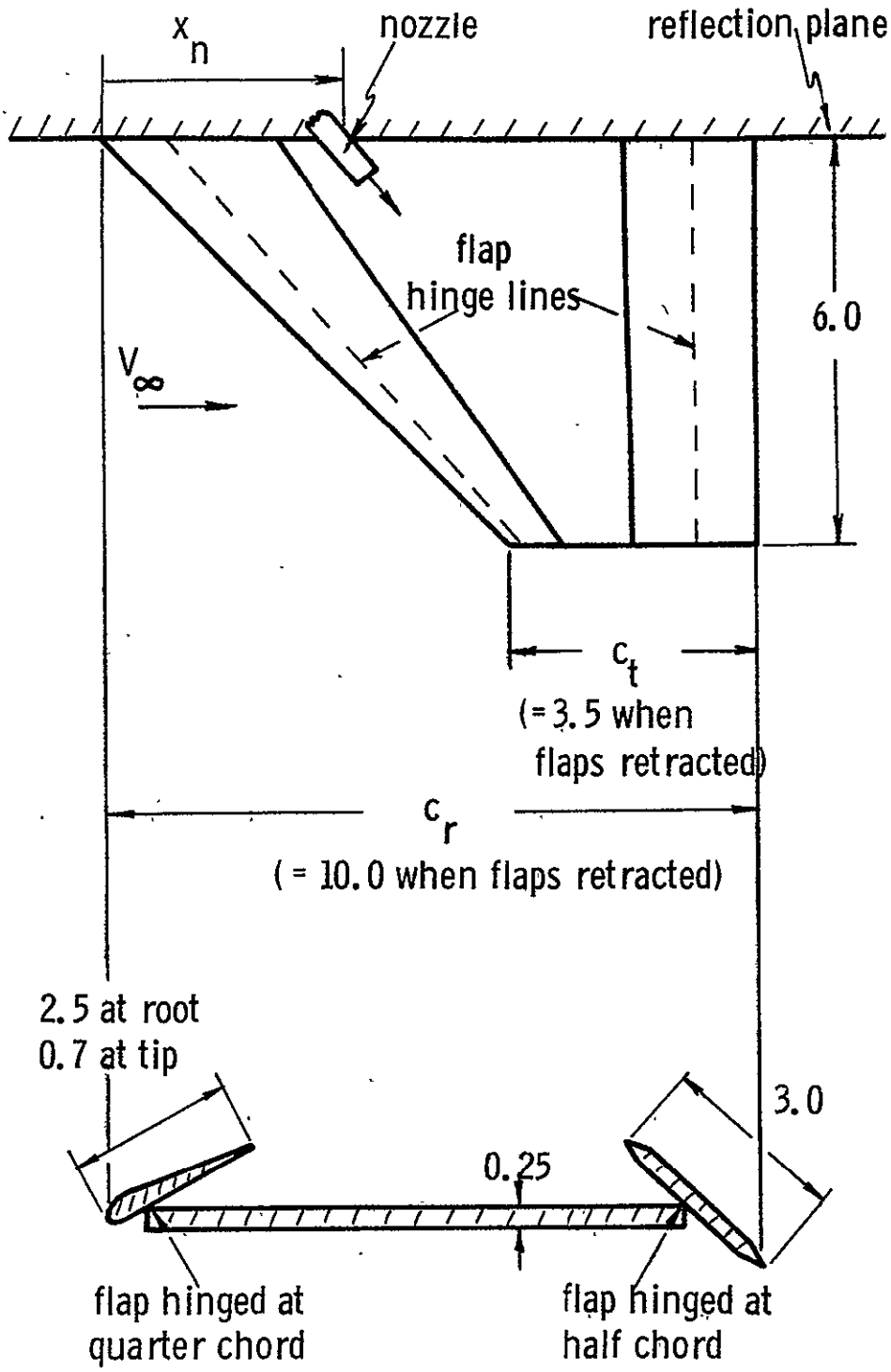

(b) AR = 1.8 45^0 swept trapezoidal wing

Figure 5. - Concluded. (all dimensions in inches)

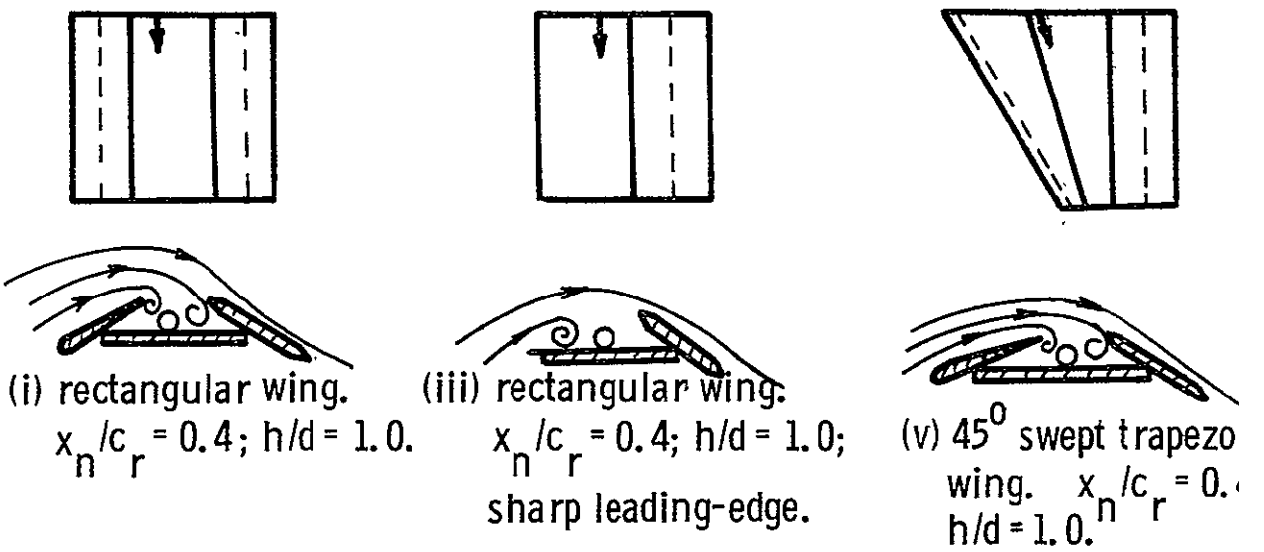

(i) rectangular wing. $x_n/c_r = 0.4$; $h/d = 1.0$.

(iii) rectangular wing. $x_n/c_r = 0.4$; $h/d = 1.0$; sharp leading-edge.

(v) 45^o swept trapezo wing. $x_n/c_r = 0.$ $h/d = 1.0$.

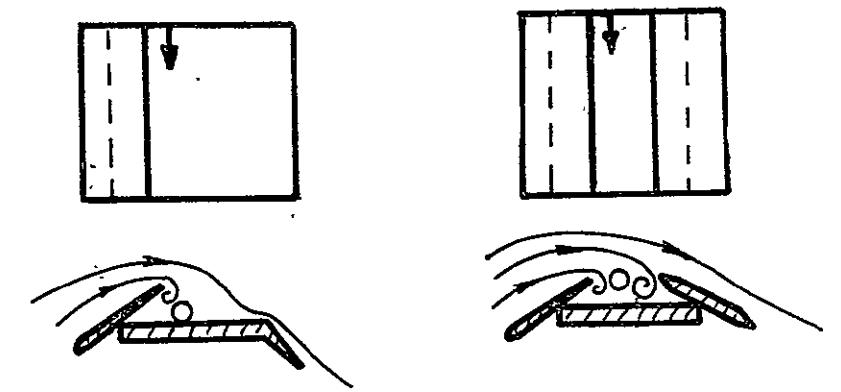

(ii) rectangular wing; upper surface TE flap removed. $x_n/c_r = 0.4$; $h/d = 1.0$.

(iv) rectangular wing. $x_n/c_r = 0.4$; $h/d = 3.0$.

Figure 6. - Experimental configurations.

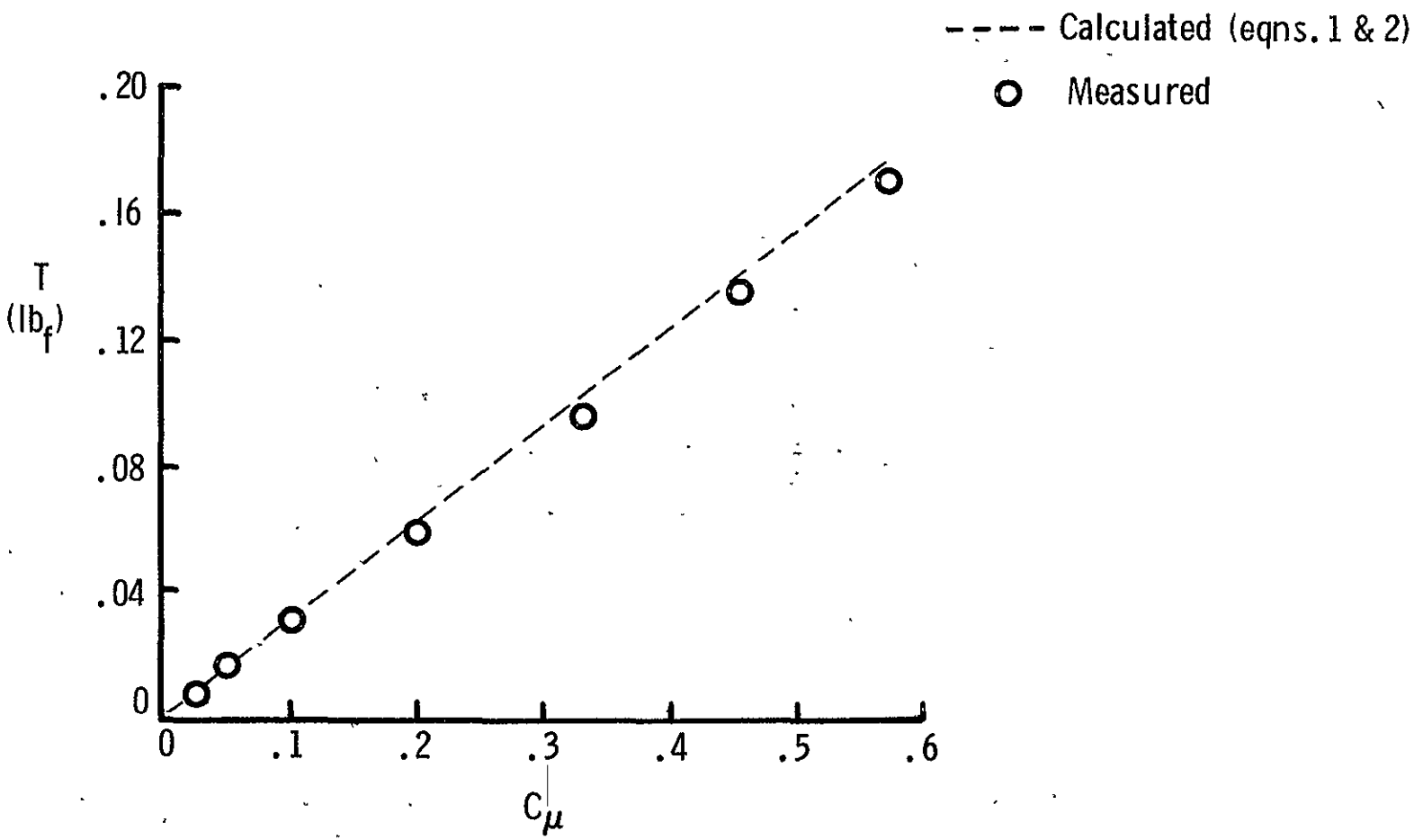

Figure 7.- Nozzle thrust versus jet momentum coefficient.

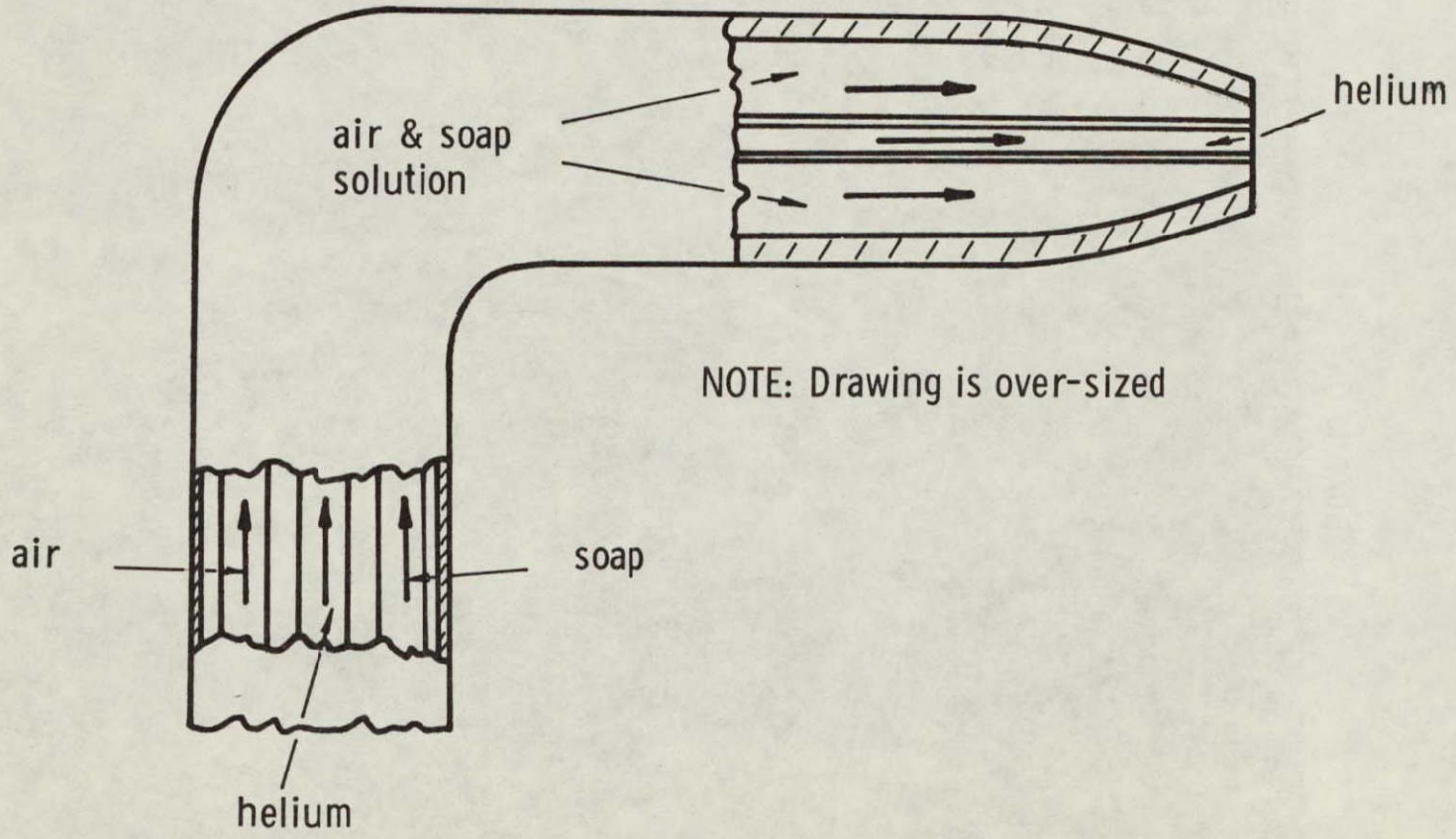

Figure 8.- Helium-filled bubble nozzle and supply lines.

Blowing Off

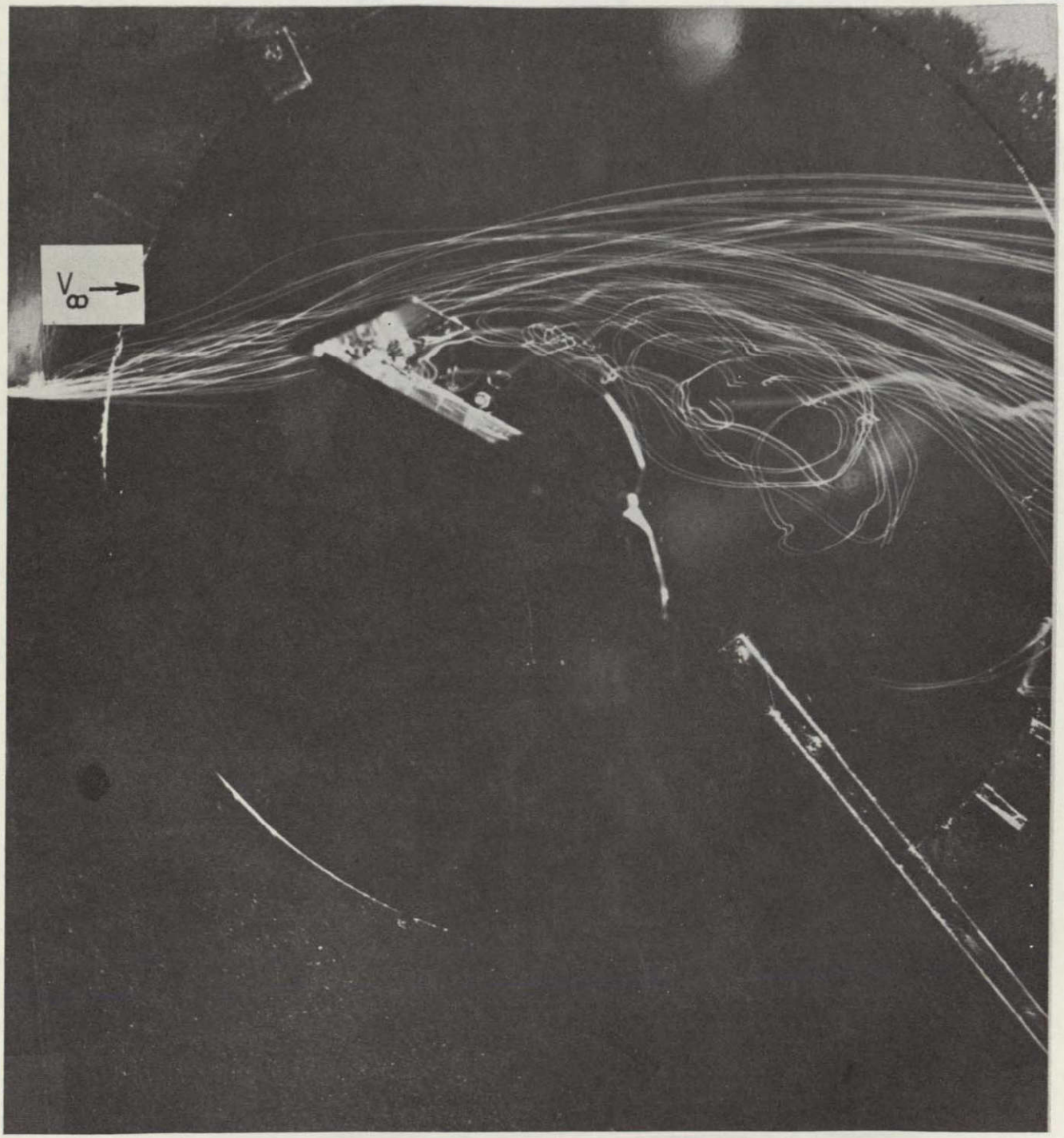

Figure 9.- Flow about the rectangular wing without blowing for $\alpha = 30^0$; $\delta_{LE} = \delta_{TE} = 60^0$.

ORIGINAL PAGE IS
OF POOR QUALITY

Blowing On

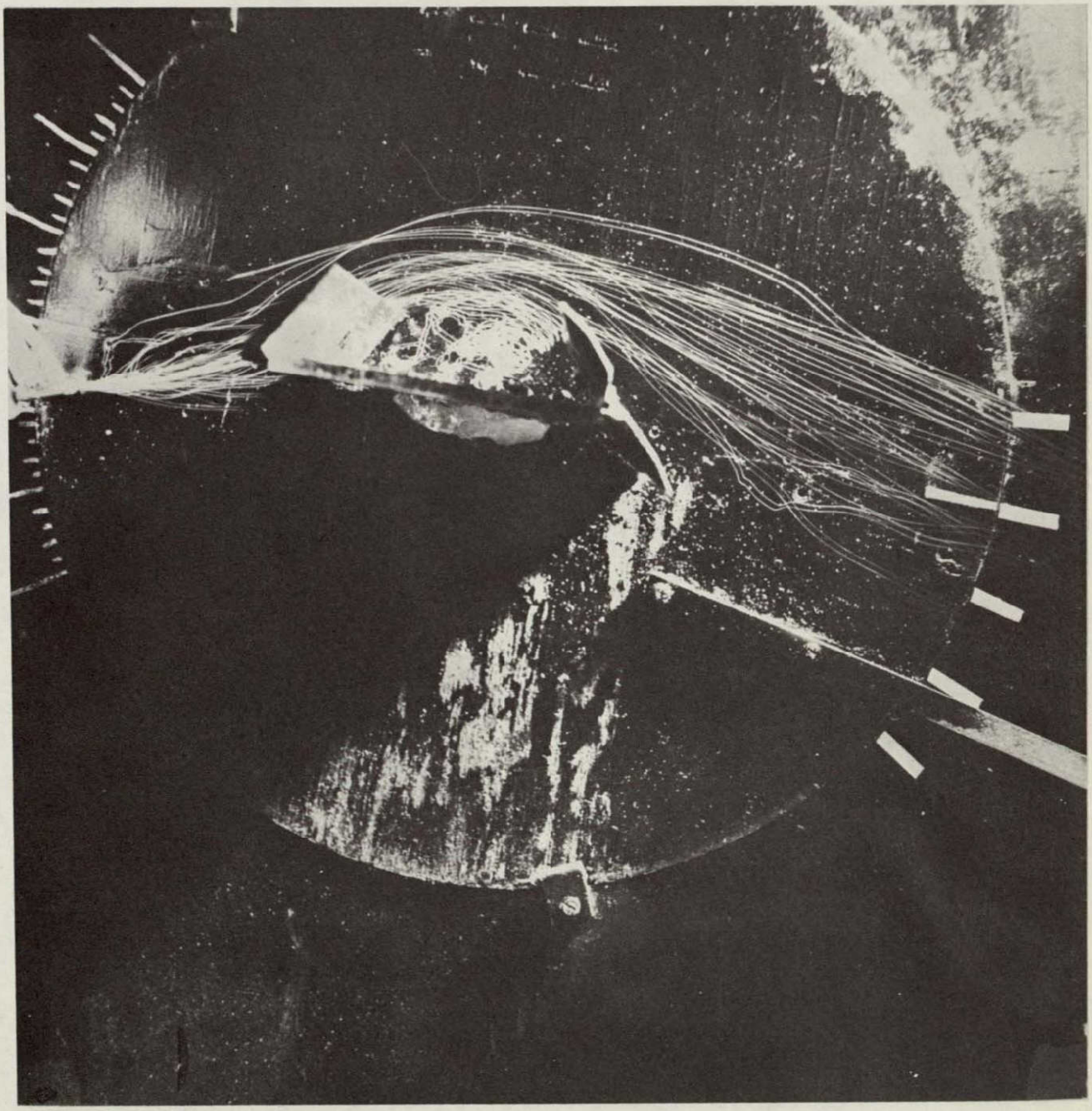

Figure 10.- Spanwise blowing on the rectangular wing for $\alpha = 10^0$ and $C_\mu = 0.21$; $\delta_{LE} = \delta_{TE} = 60^0$; $x_n/c_r = 0.40$; $h/d = 1.0$.

ORIGINAL PAGE IS
OF POOR QUALITY

Blowing On

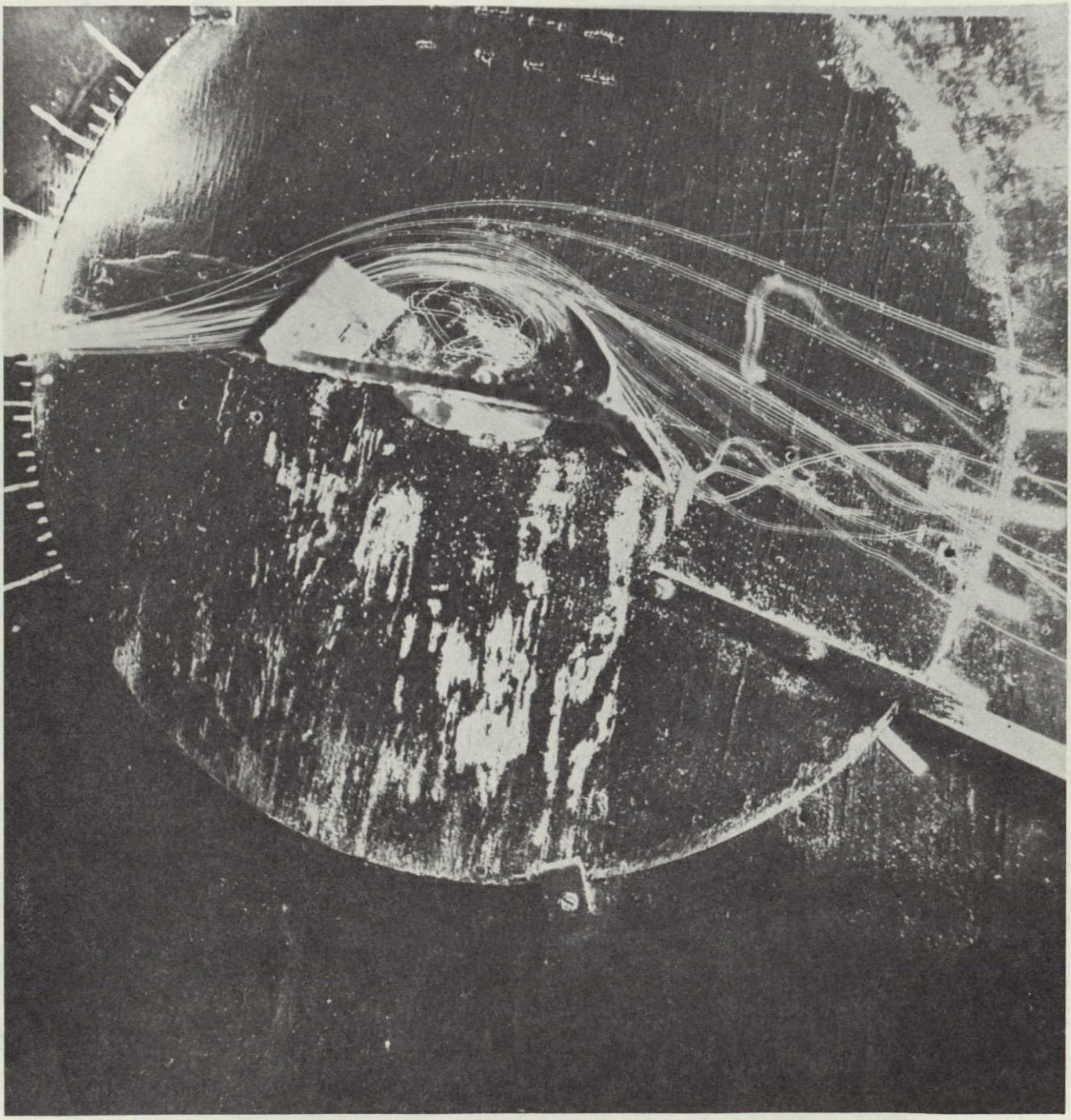

Figure 11.- Spanwise blowing on the rectangular wing for $\alpha = 10^0$ and $C_\mu = 0.30$; $\delta_{LE} = \delta_{TE} = 60^0$; $x_n/c_r = 0.40$; $h/d = 1.0$.

Blowing On

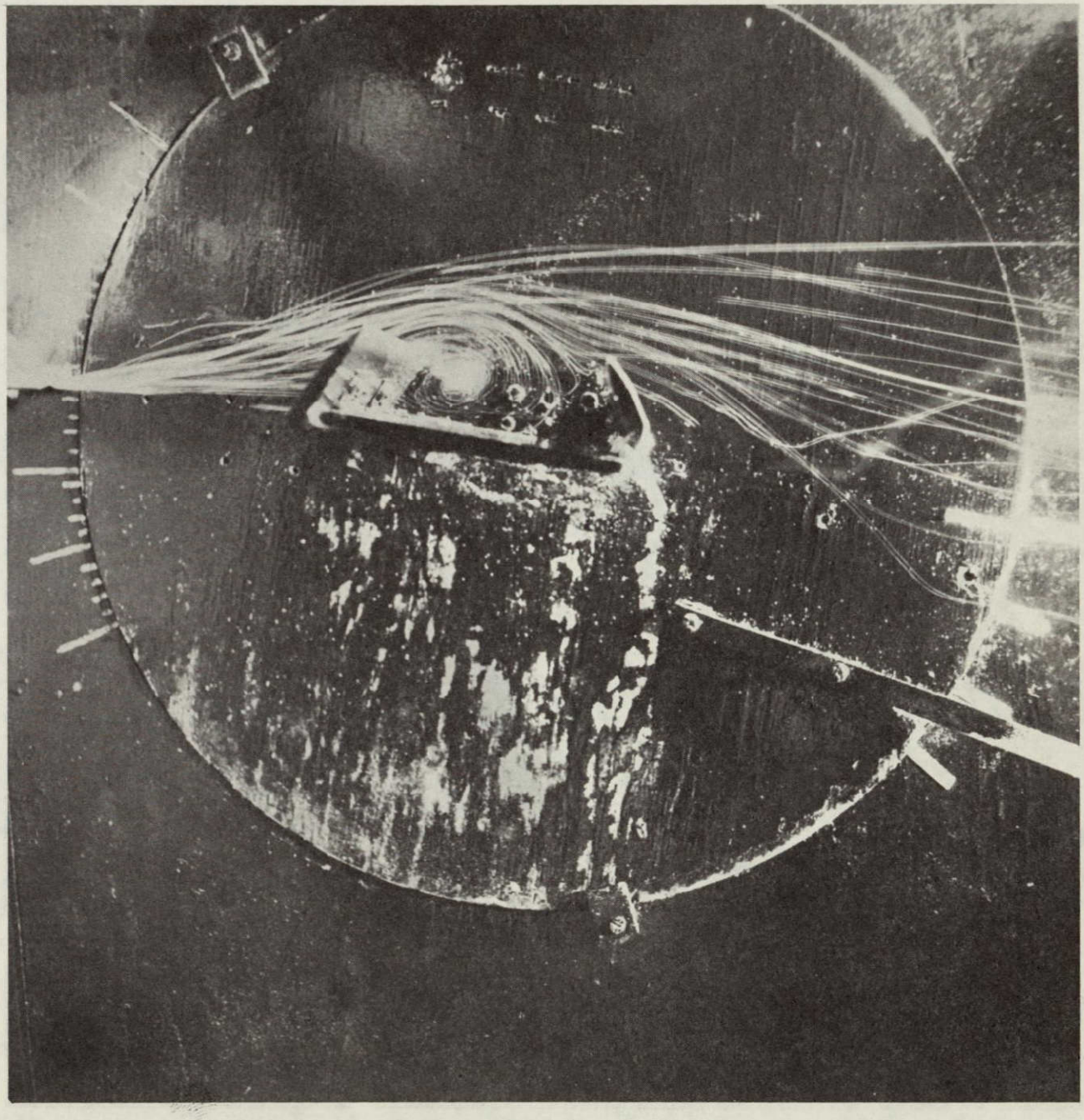

Figure 12. - Spanwise blowing on the rectangular wing for $\alpha = 10^0$ and $C_\mu = 0.57$; $\delta_{LE} = \delta_{TE} = 60^0$; $x_n/c_r = 0.40$; $h/d = 1.0$.

ORIGINAL PAGE IS
OF POOR QUALITY

Blowing On

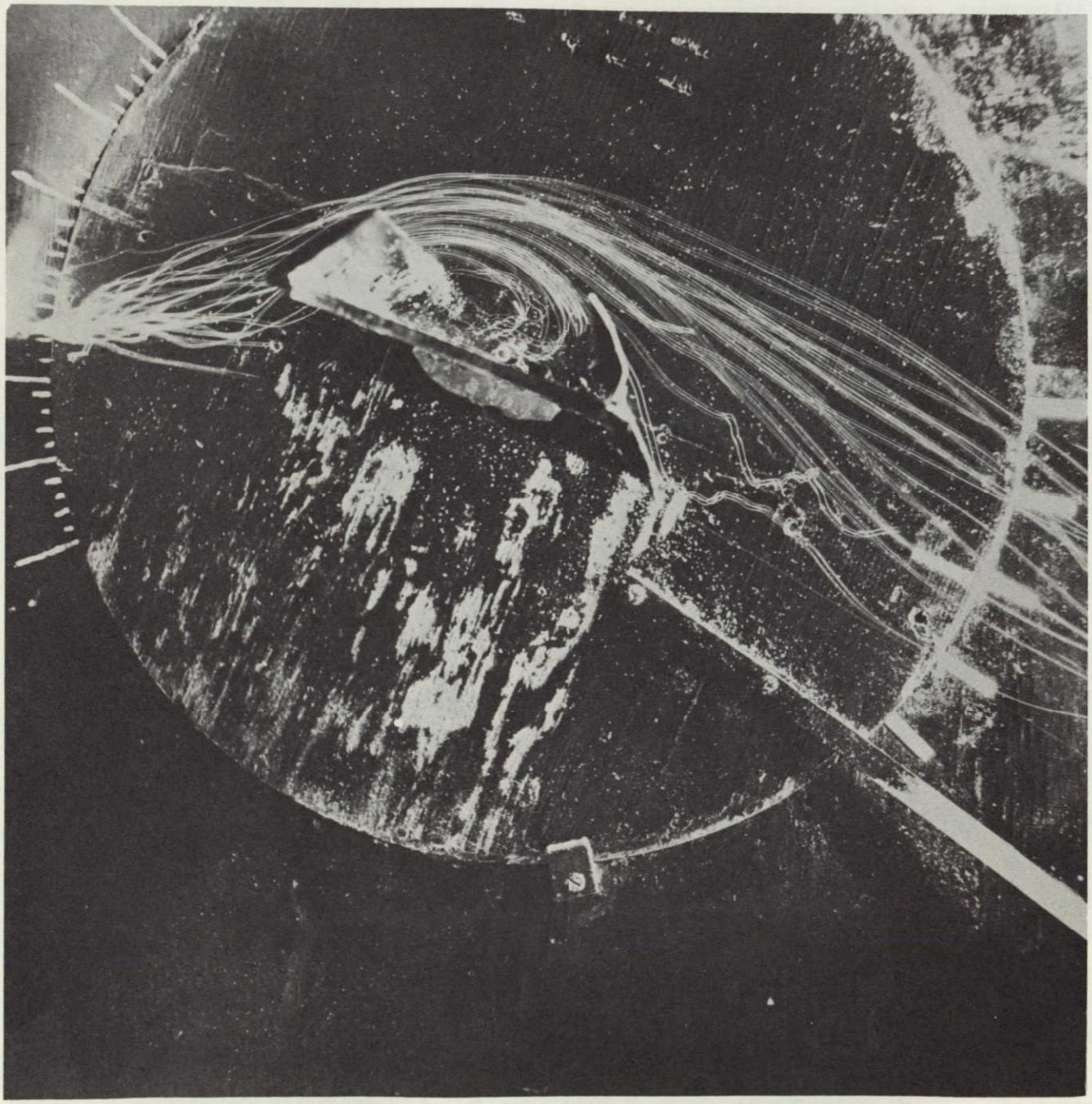

Figure 13. - Spanwise blowing on the rectangular wing for $\alpha = 20^{0}$ and $C_{\mu} = 0.30$; $\delta_{LE} = \delta_{TE} = 60^{0}$; $x_n/c_r = 0.40$; $h/d = 1.0$.

Blowing On

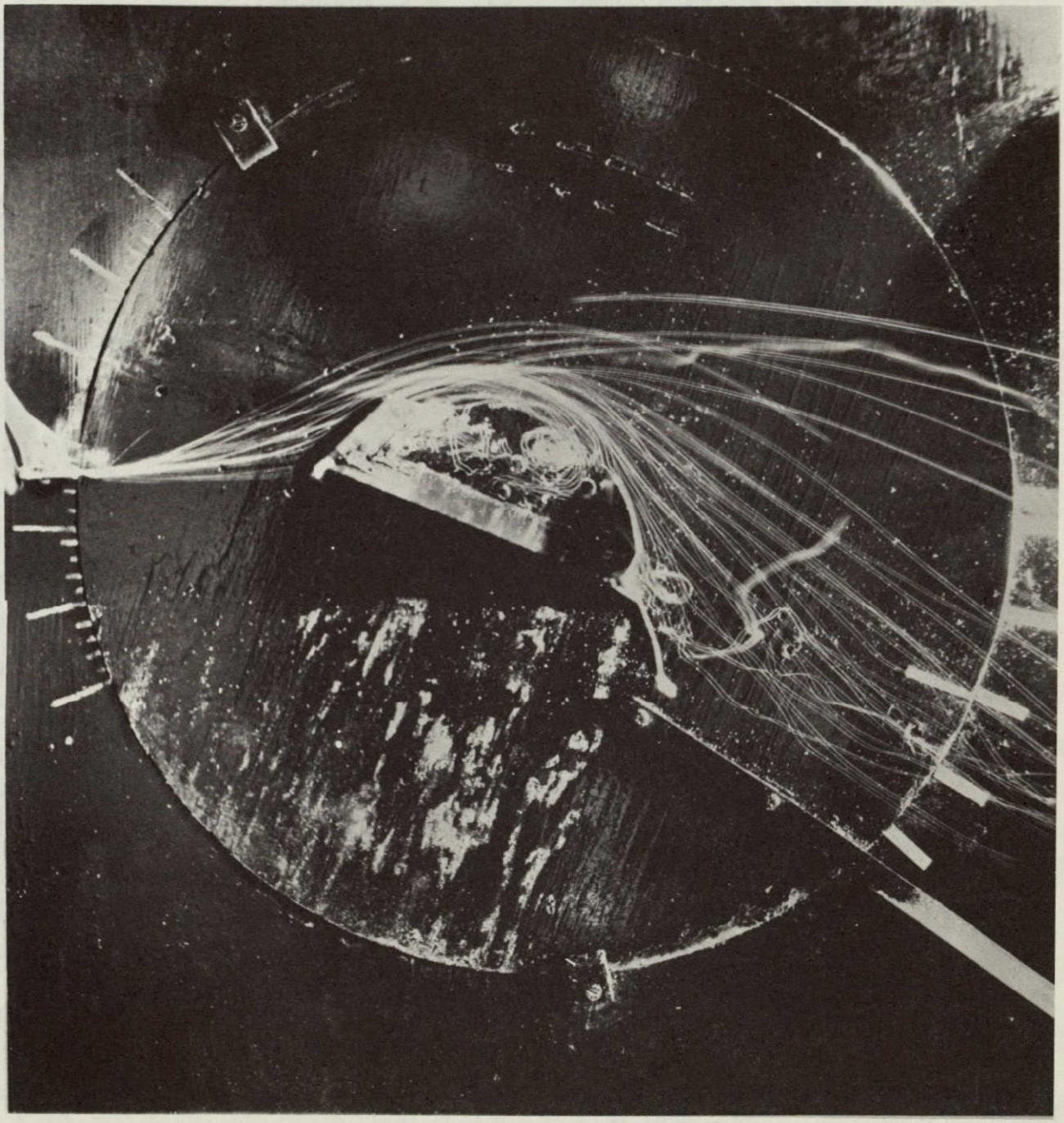

Figure 14. - Spanwise blowing on the rectangular wing for $\alpha = 20^{0}$ and $C_{\mu} = 0.35$; $\delta_{LE} = \delta_{TE} = 60^{0}$; $x_n/c_r = 0.40$; $h/d = 1.0$.

ORIGINAL PAGE IS
OF POOR QUALITY

Blowing On

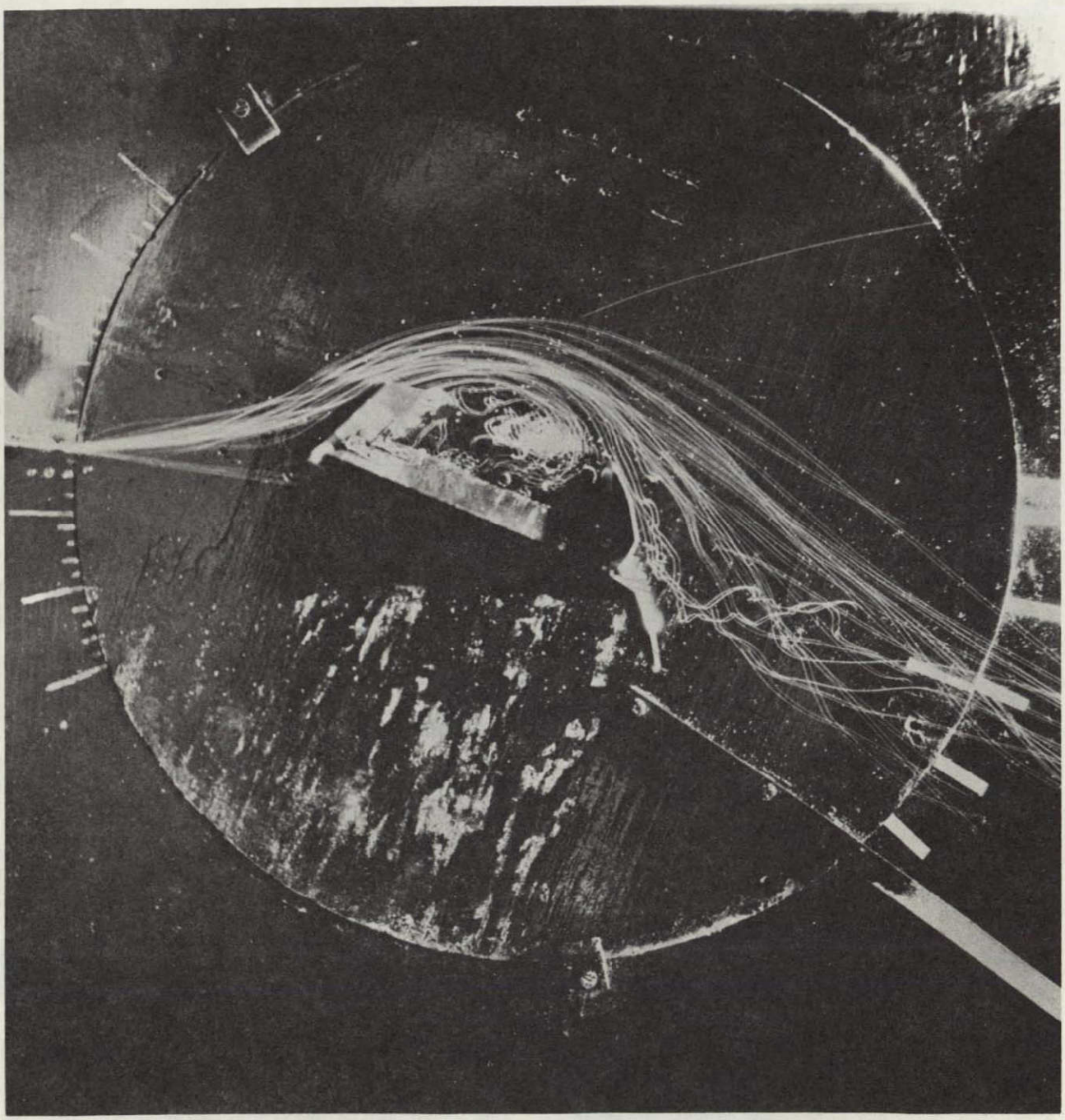

Figure 15. - Spanwise blowing on the rectangular wing for $\alpha = 20^{0}$ and $C_{\mu} = 0.40$; $\delta_{LE} = \delta_{TE} = 60^{0}$; $x_n/c_r = 0.40$; $h/d = 1.0$.

Blowing On

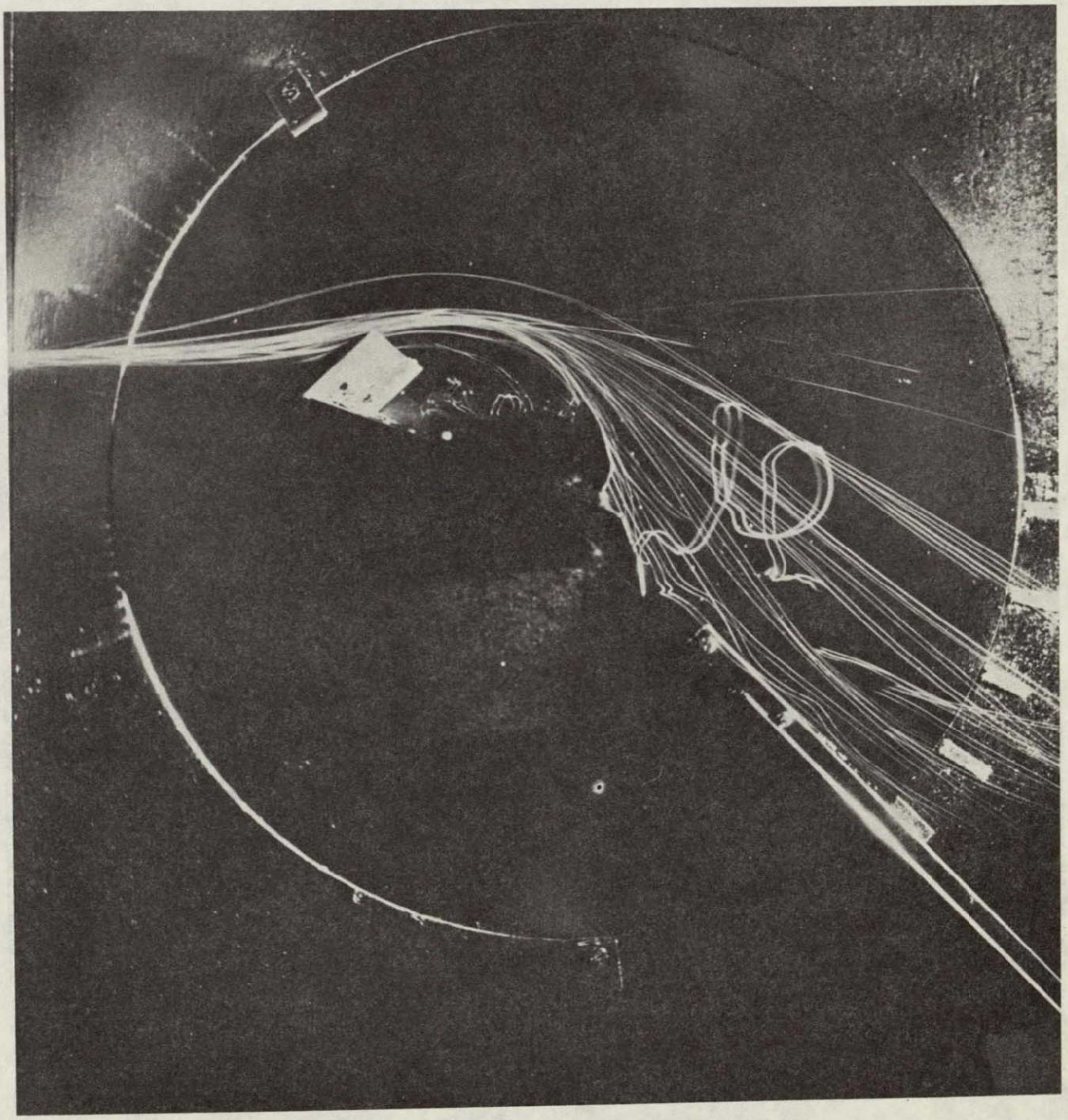

Figure 16. - Spanwise blowing on the rectangular wing for $\alpha = 20^0$ and $C_\mu = 0.45$; $\delta_{LE} = \delta_{TE} = 60^0$; $x_n/c_r = 0.40$; $h/d = 1.0$.

ORIGINAL PAGE IS
OF POOR QUALITY

Blowing On

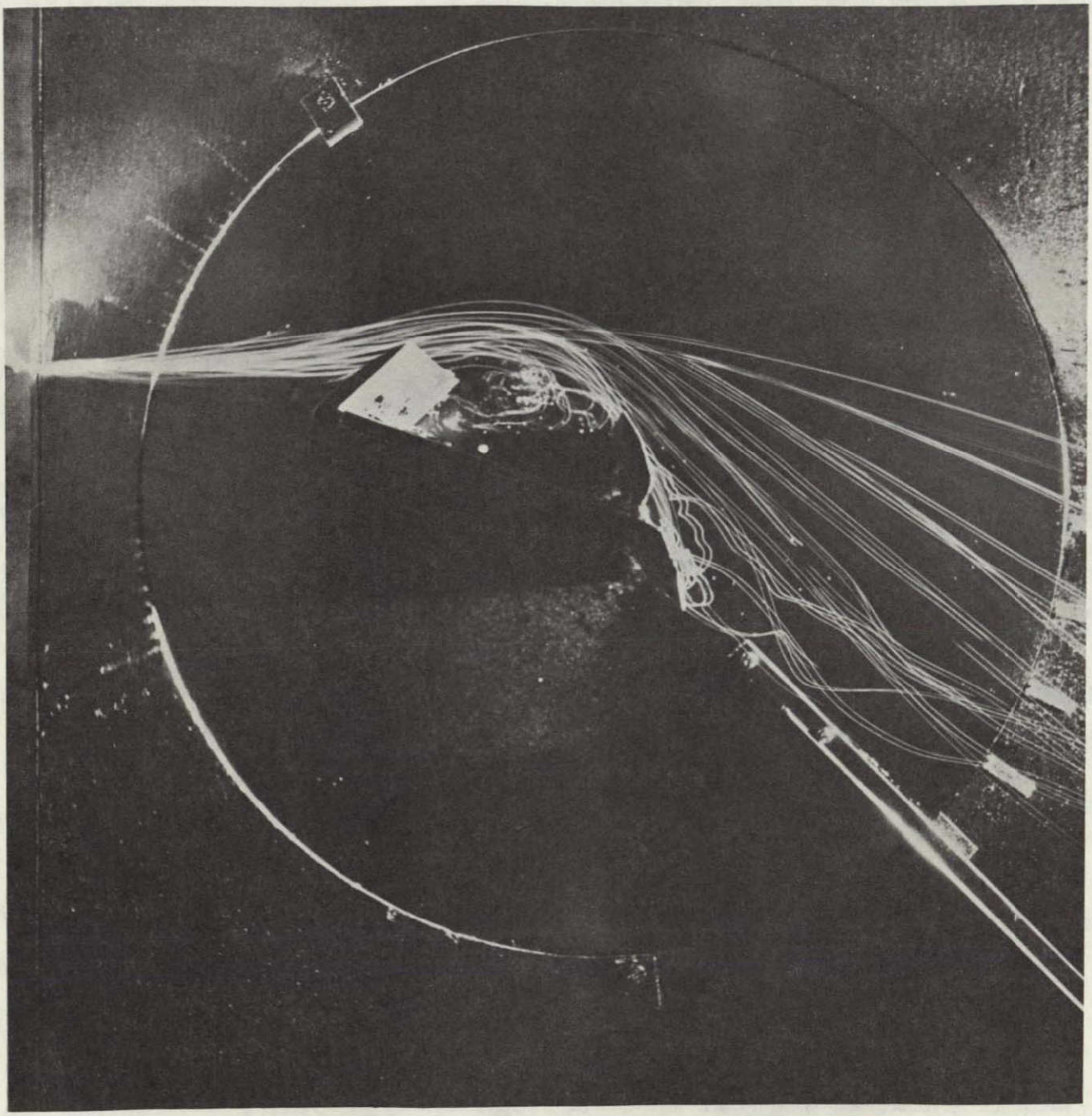

Figure 17. - Spanwise blowing on the rectangular wing for $\alpha = 20^{0}$ and $C_{\mu} = 0.50$; $\delta_{LE} = \delta_{TE} = 60^{0}$; $x_n/c_r = 0.40$; $h/d = 1.0$.

Blowing On

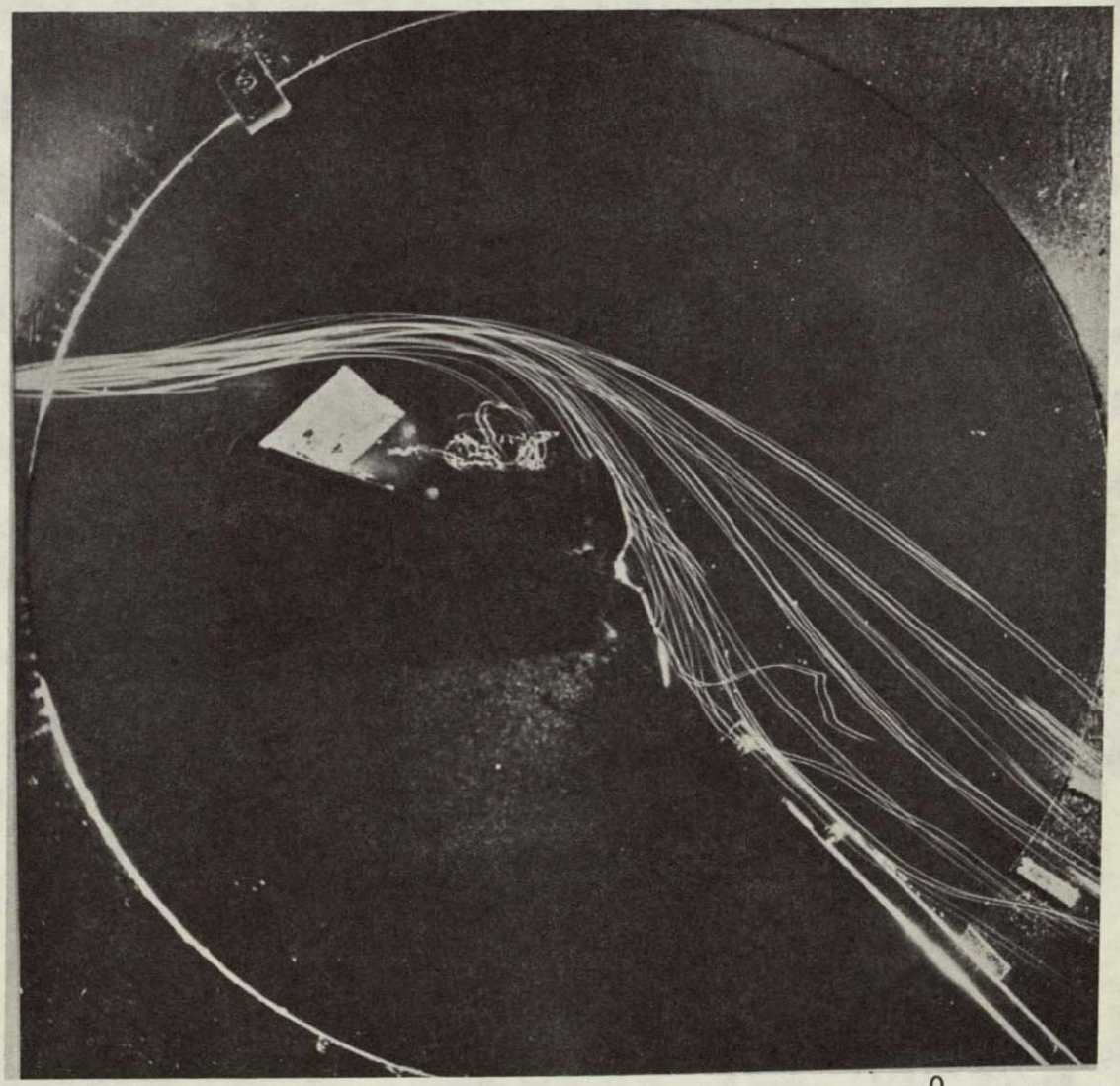

Figure 18. - Spanwise blowing on the rectangular wing for $\alpha = 20^0$ and $C_\mu = 0.55$; $\delta_{LE} = \delta_{TE} = 60^0$; $x_n/c_r = 0.40$; $h/d = 1.0$.

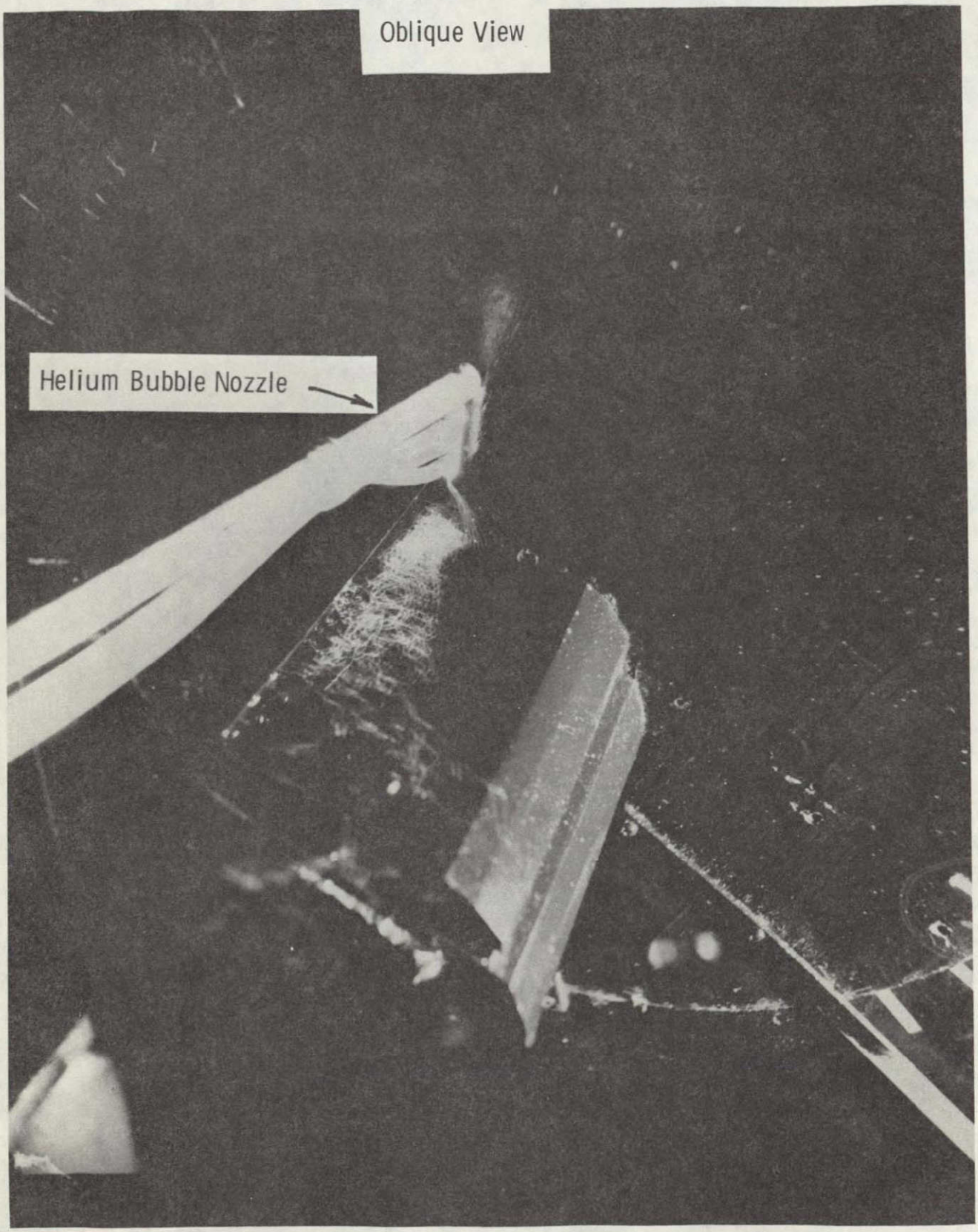

Figure 19.- Spanwise blowing on the rectangular wing for $\alpha = 20^{0}$ and $C_{\mu} = 0.35$; $\delta_{LE} = \delta_{TE} = 60^{0}$; $x_n/c_r = 0.40$; $h/d = 1.0$.

ORIGINAL PAGE IS
OF POOR QUALITY

Blowing On

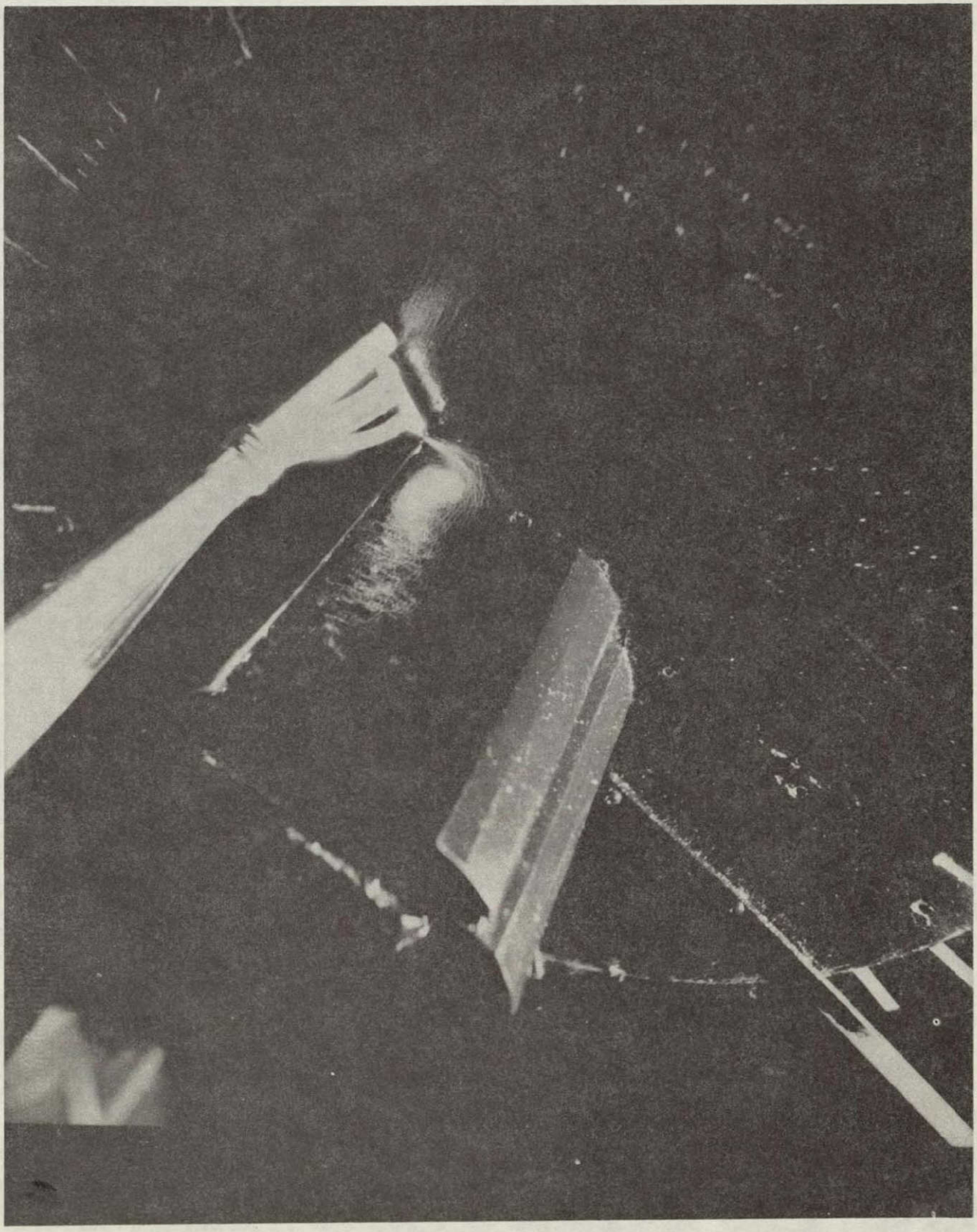

Figure 20. - Spanwise blowing on the rectangular wing for $\alpha = 20^{0}$ and $C_{\mu} = 0.45$; $\delta_{LE} = \delta_{TE} = 60^{0}$; $x_n/c_r = 0.40$; $h/d = 1.0$.

Blowing On

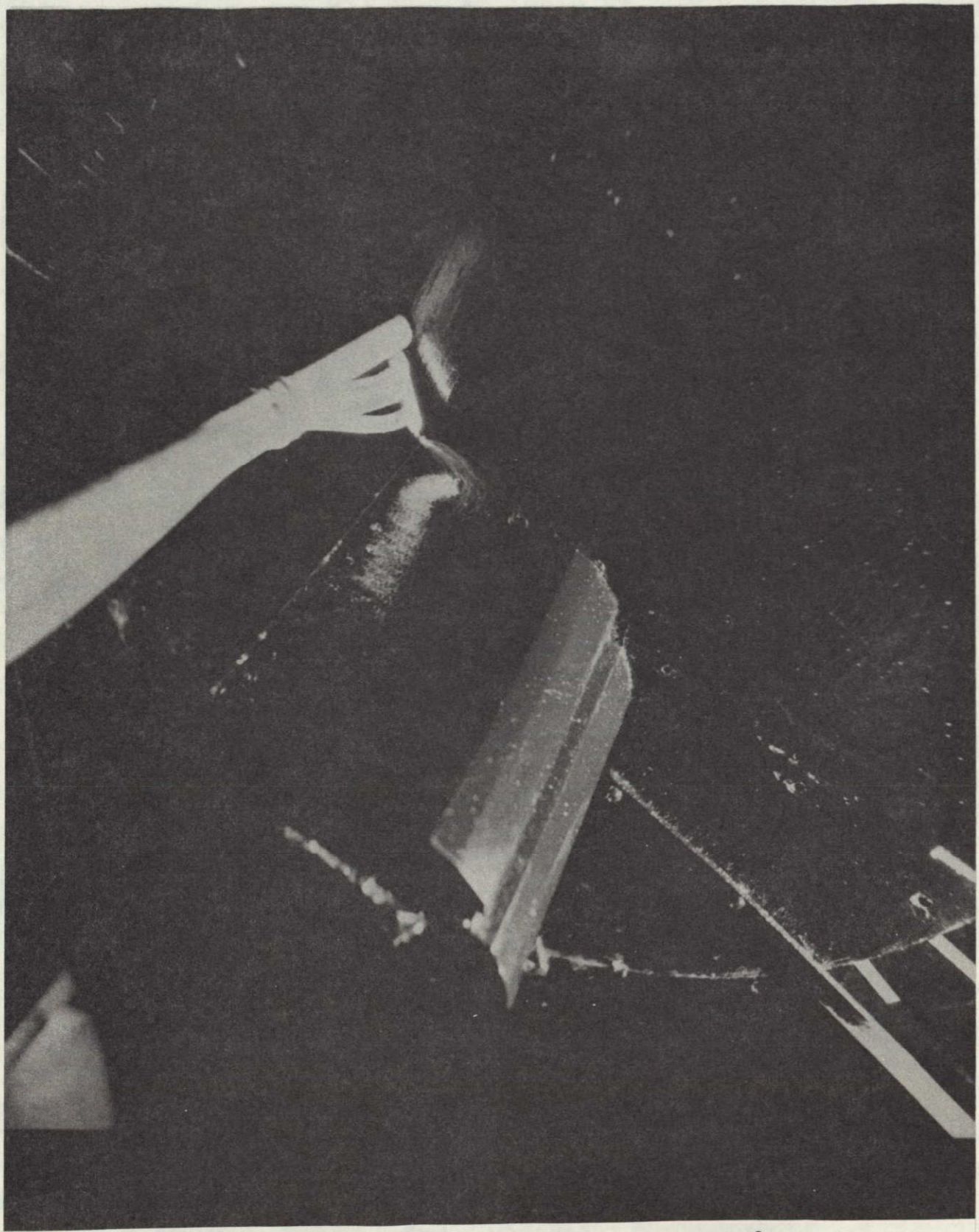

Figure 21. - Spanwise blowing on the rectangular wing for $\alpha = 20^{\circ}$ and $C_{\mu} = 0.65$; $\delta_{LE} = \delta_{TE} = 60^{\circ}$; $x_n/c_r = 0.40$; $h/d = 1.0$.

Blowing On

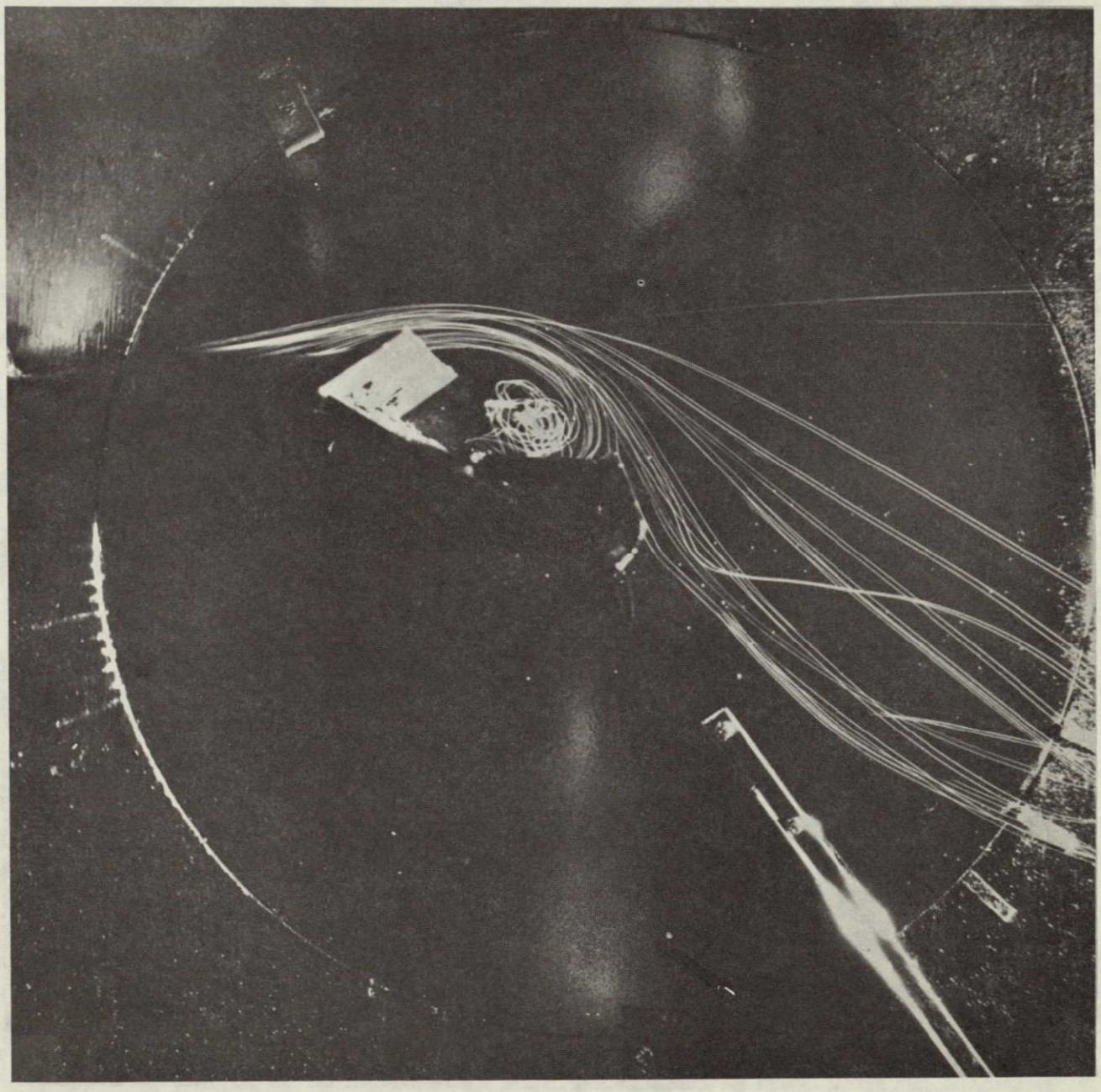

Figure 22. - Spanwise blowing on the rectangular wing for $\alpha = 30^{0}$ and $C_{\mu} = 0.50$; $\delta_{LE} = \delta_{TE} = 60^{0}$; $x_n/c_r = 0.40$; $h/d = 1.0$.

ORIGINAL PAGE IS
OF POOR QUALITY

Blowing On

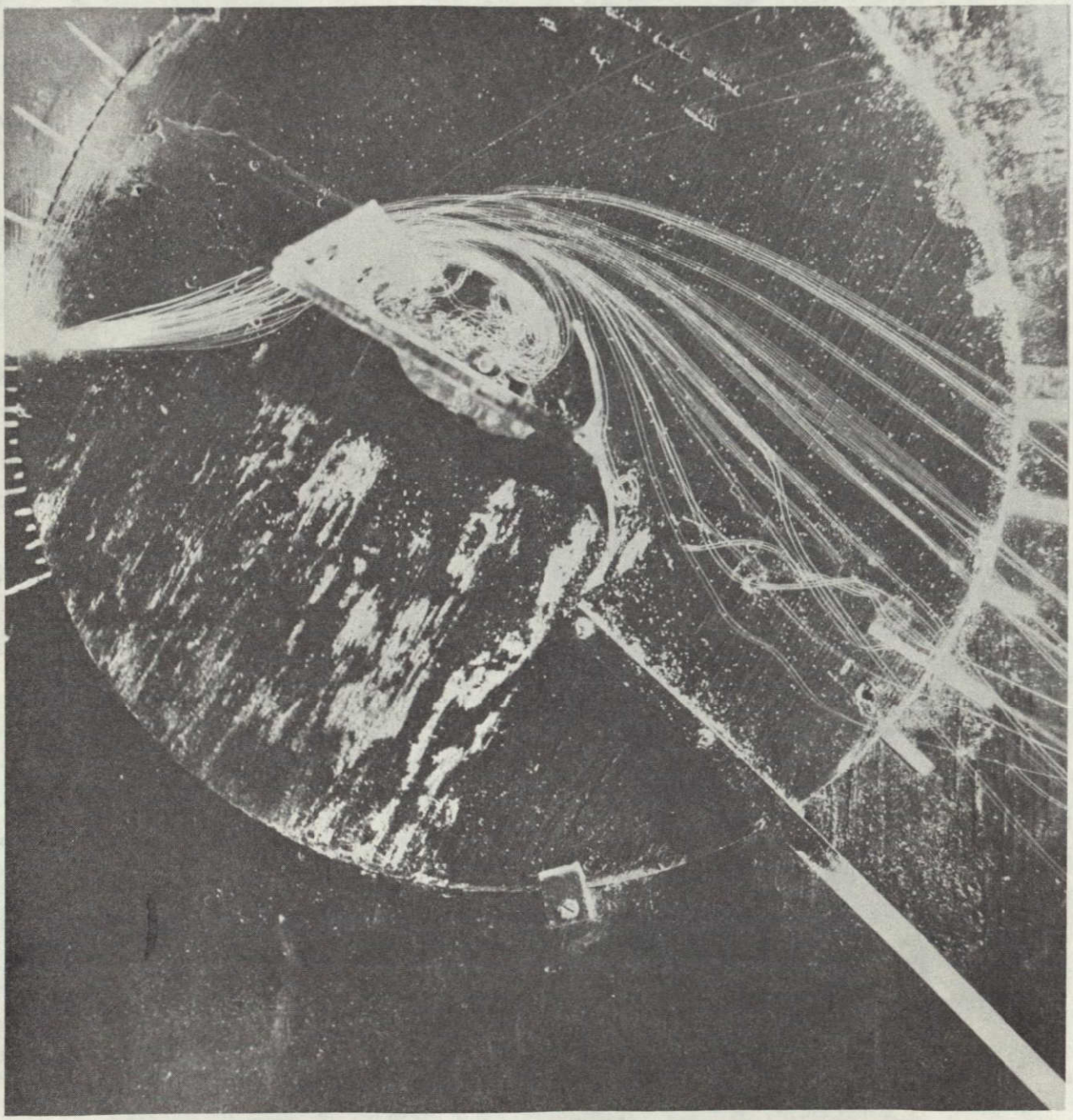

Figure 23. - Spanwise blowing on the rectangular wing for $\alpha = 30^{0}$ and $C_{\mu} = 0.57$; $\delta_{LE} = \delta_{TE} = 60^{0}$; $x_n/c_r = 0.40$; $h/d = 1.0$.

Blowing On

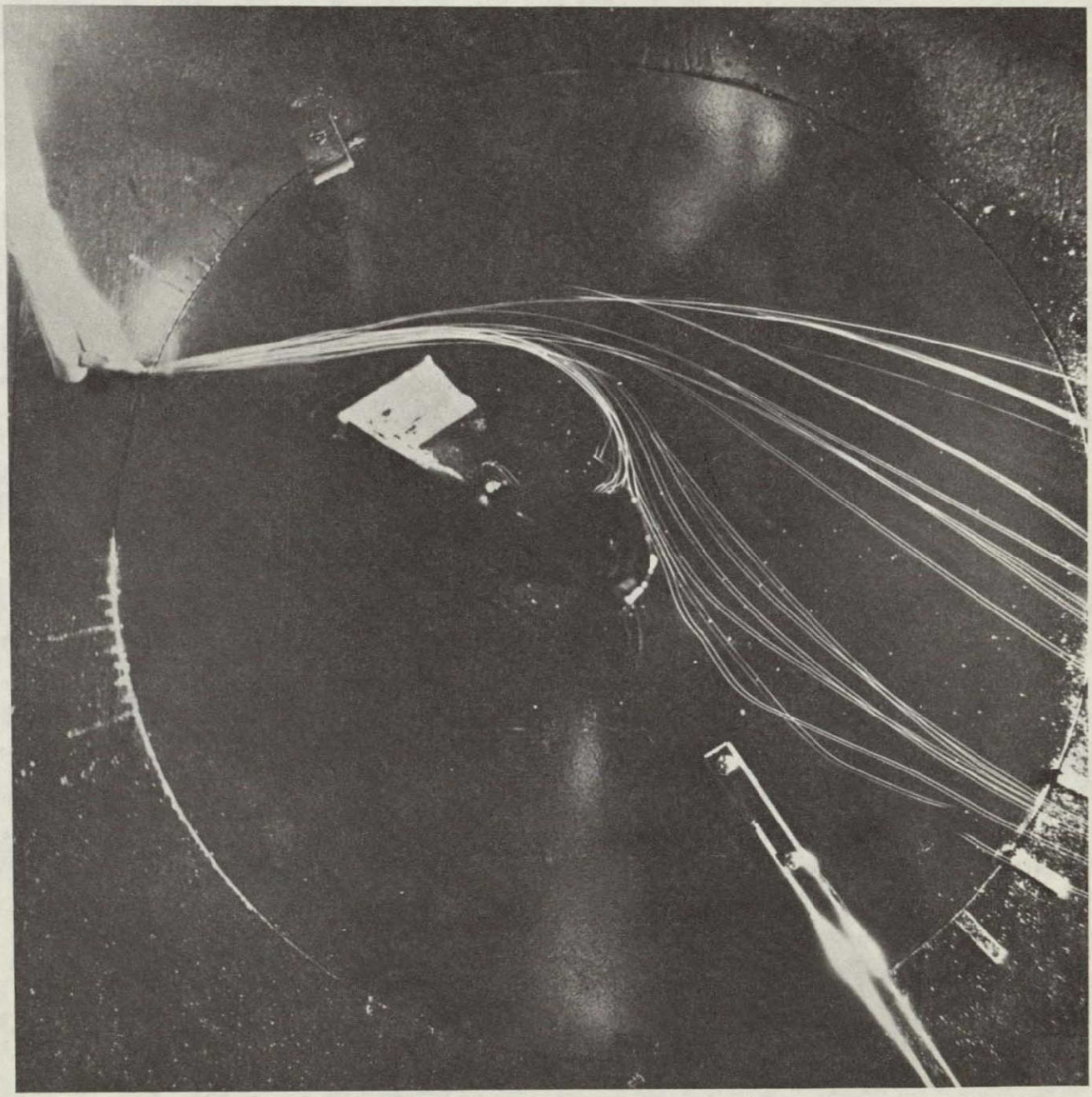

Figure 24. - Spanwise blowing on the rectangular wing for $\alpha = 30^0$ and $C_\mu = 0.60$; $\delta_{LE} = \delta_{TE} = 60^0$; $x_n/c_r = 0.40$; $h/d = 1.0$.

Blowing On

Figure 25. - Spanwise blowing on the rectangular wing for $\alpha = 30^{0}$ and $C_{\mu} = 0.65$;

$\delta_{LE} = \delta_{TE} = 60^{0}$; $x_n/c_r = 0.40$; $h/d = 1.0$.

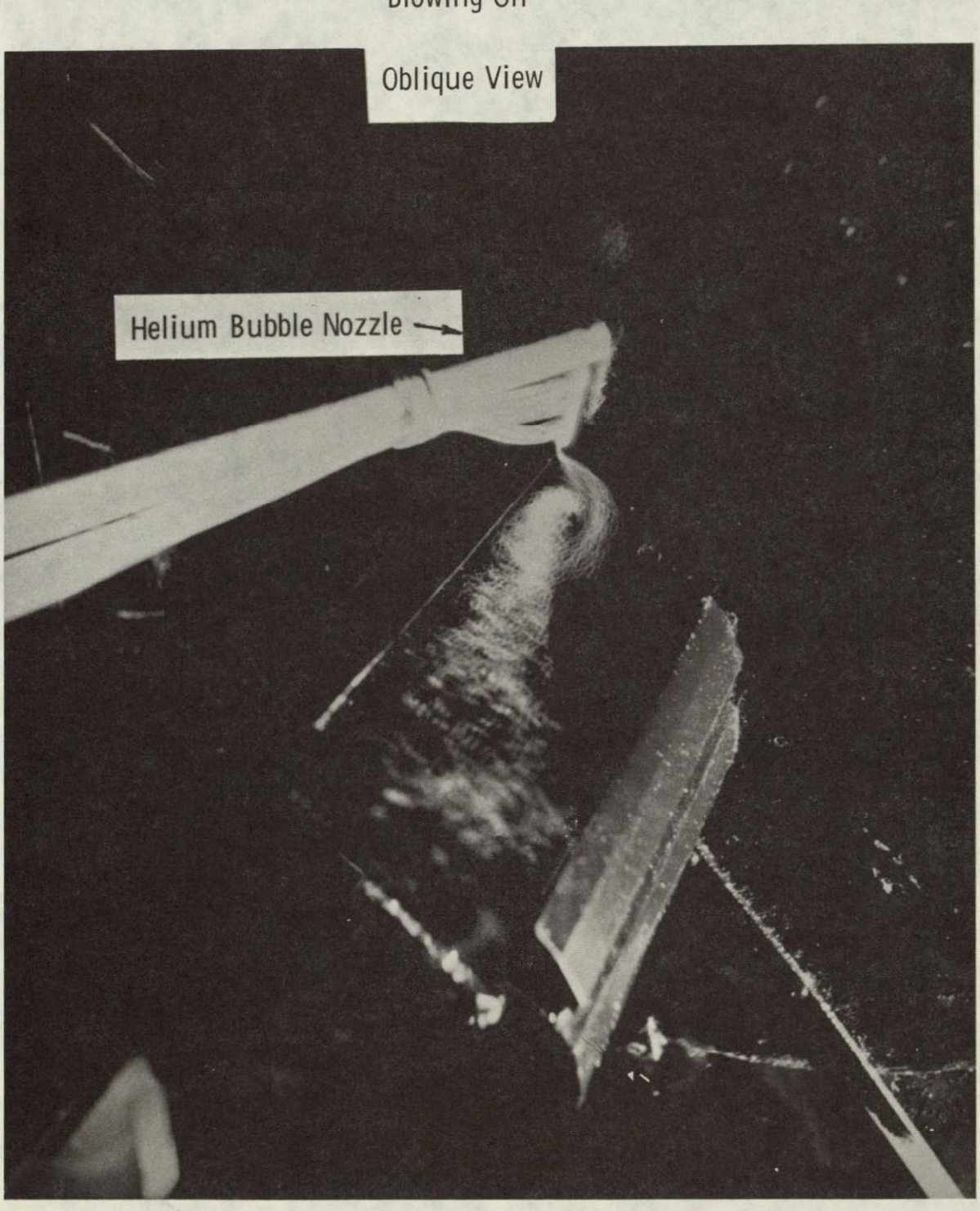

Figure 26. - Spanwise blowing on the rectangular wing for $\alpha = 30^{0}$ and $C_{\mu} = 0.45$; $\delta_{LE} = \delta_{TE} = 60^{0}$; $x_n/c_r = 0.40$; $h/d = 1.0$.

ORIGINAL PAGE IS
OF POOR QUALITY

Blowing On

Figure 27.- Spanwise blowing on the rectangular wing for $\alpha = 30^0$ and $C_\mu = 0.50$; $\delta_{LE} = \delta_{TE} = 60^0$; $x_n/c_r = 0.40$; $h/d = 1.0$.

Blowing On

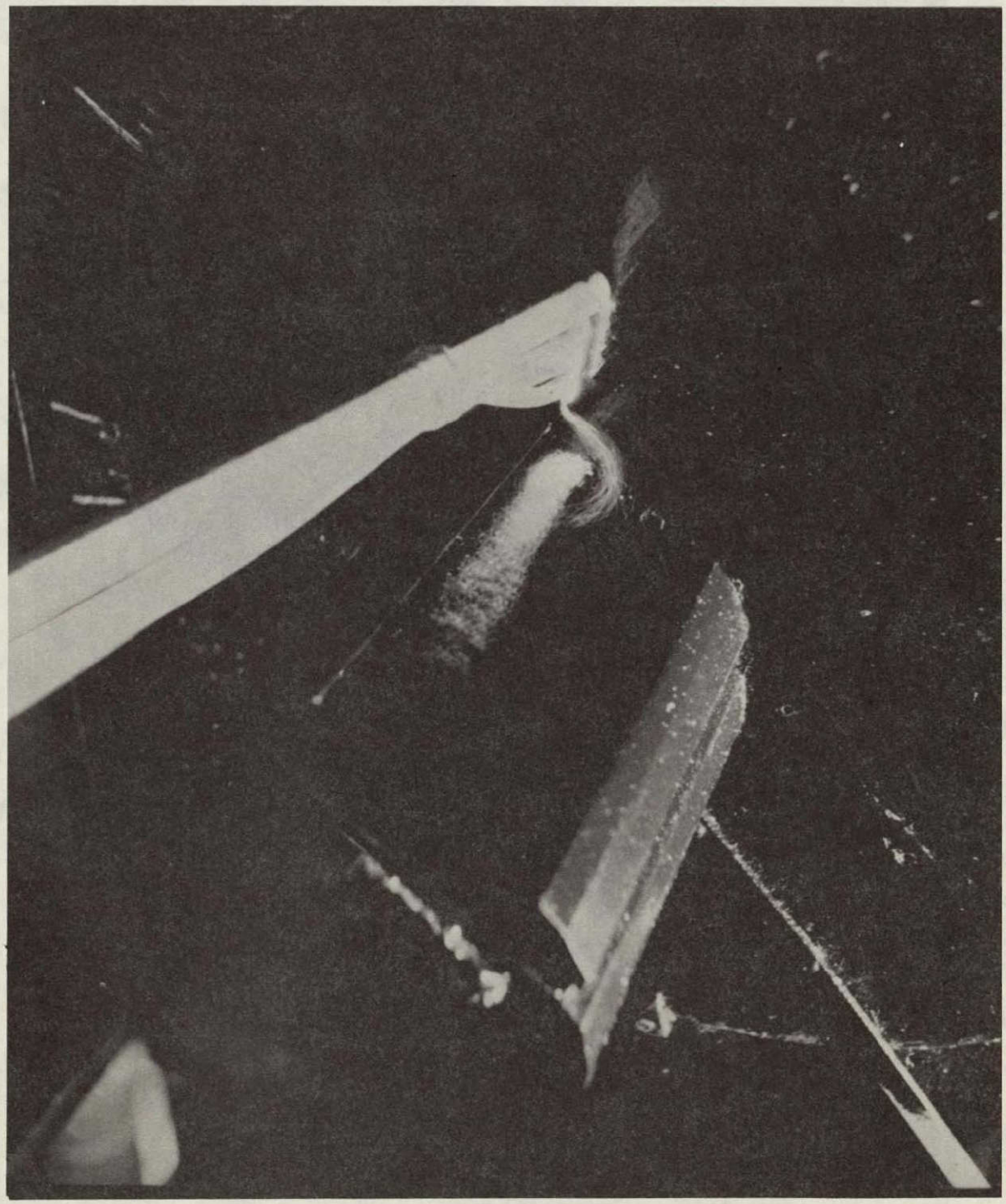

Figure 28. - Spanwise blowing on the rectangular wing for $\alpha = 30^{0}$ and $C_{\mu} = 0.65$; $\delta_{LE} = \delta_{TE} = 60^{0}$; $x_n/c_r = 0.40$; $h/d = 1.0$.

Blowing On

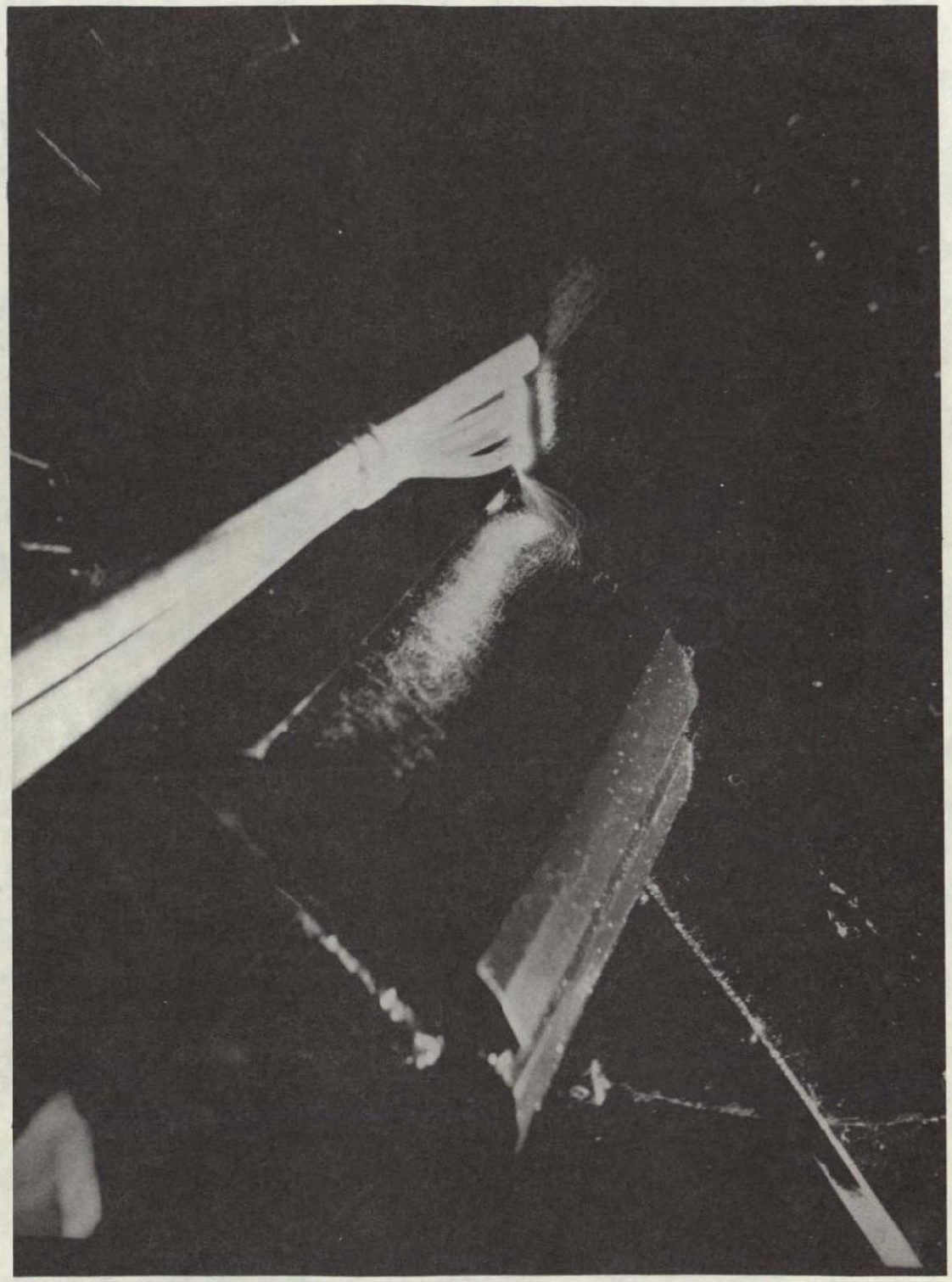

Figure 29.- Spanwise blowing on the rectangular wing for $\alpha = 30^{0}$ and $C_{\mu} = 0.75$; $\delta_{LE} = \delta_{TE} = 60^{0}$; $x_n/c_r = 0.40$; $h/d = 1.0$.

Blowing On

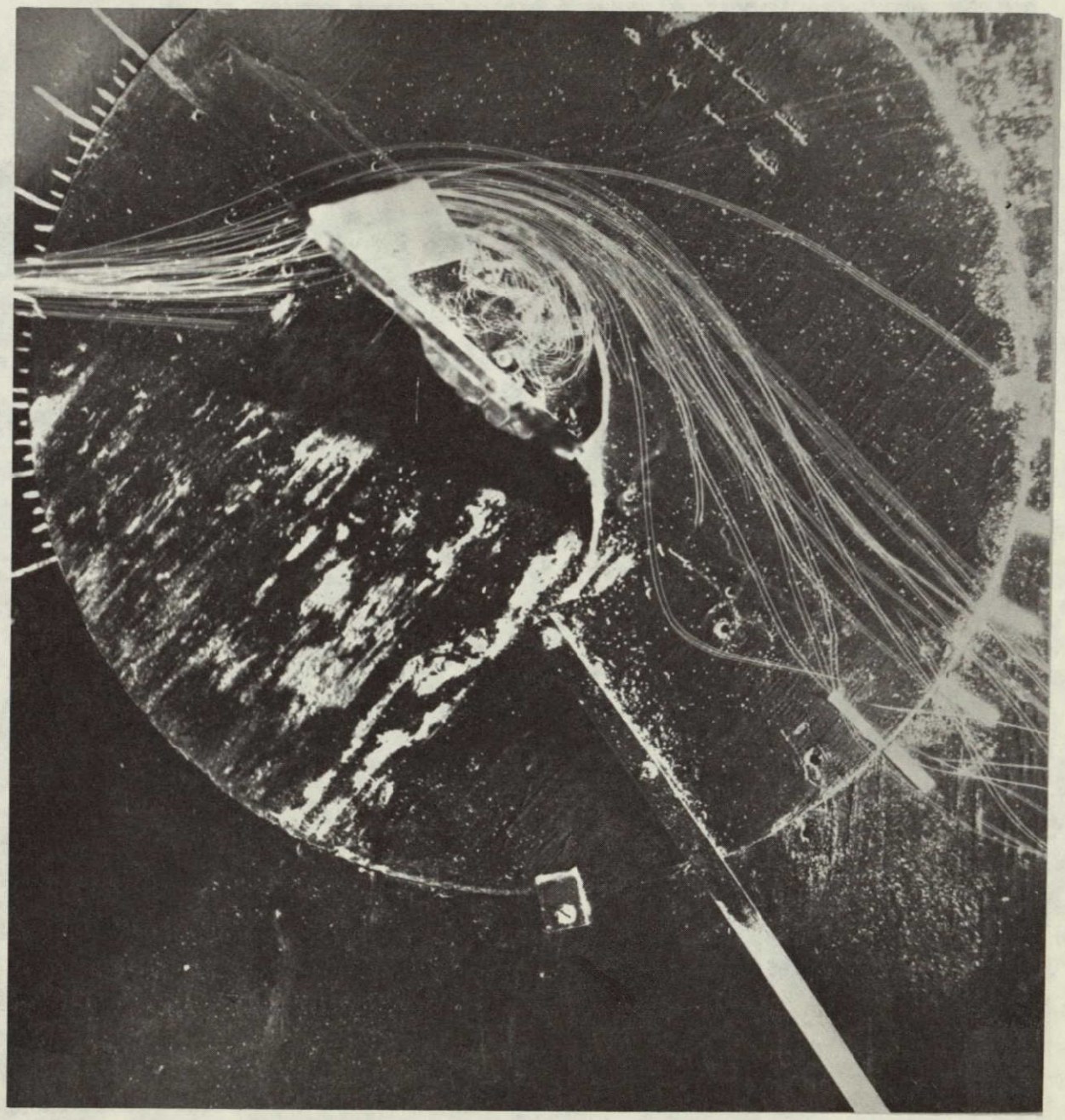

Figure 30. - Spanwise blowing on the rectangular wing for $\alpha = 40^{0}$ and $C_{\mu} = 0.50$; $\delta_{LE} = \delta_{TE} = 60^{0}$; $x_n/c_r = 0.40$; h/d = 1.0.

ORIGINAL PAGE IS
OF POOR QUALITY

Blowing On

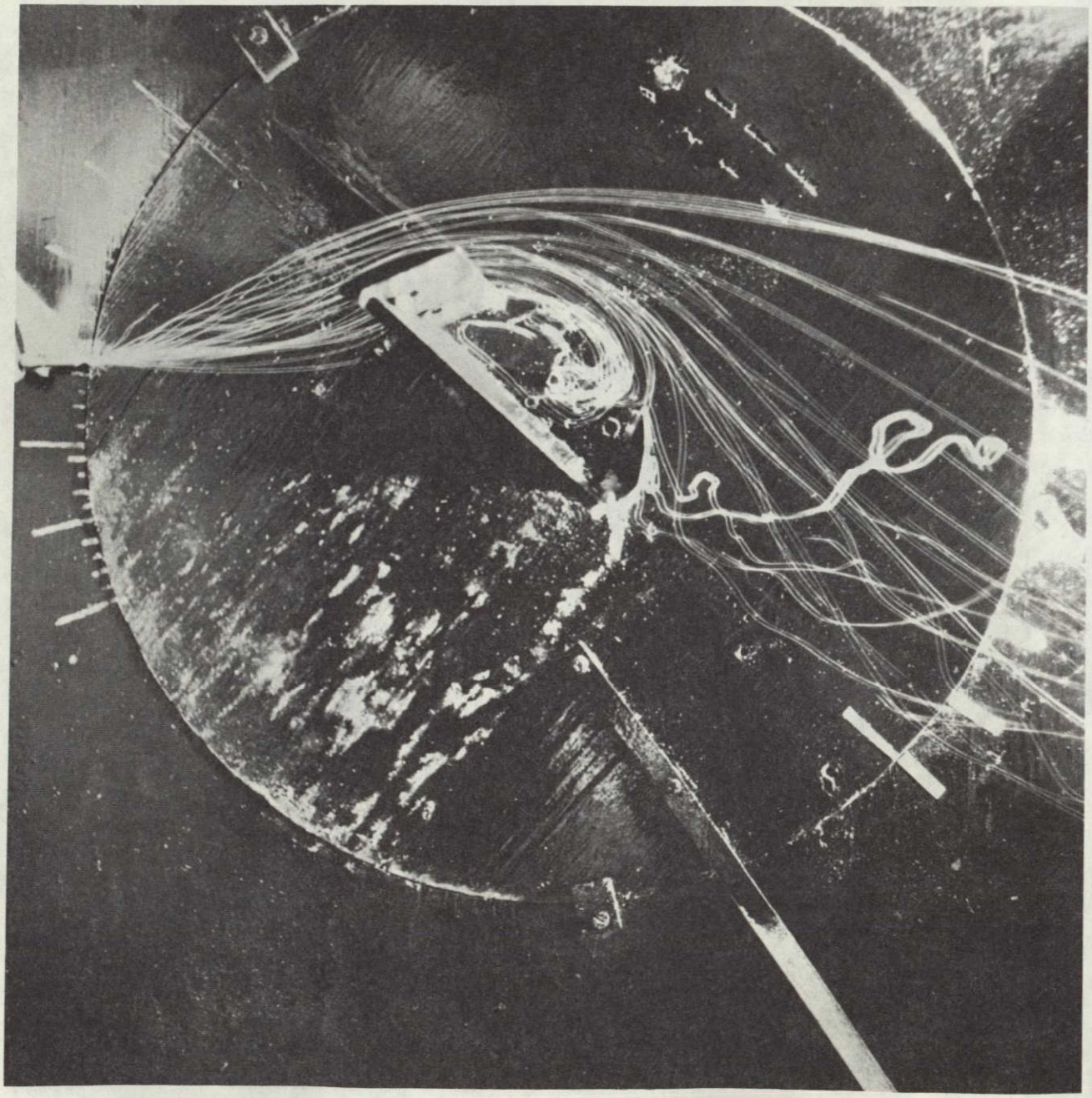

Figure 31. - Spanwise blowing on the rectangular wing for $\alpha = 40^0$ and $C_\mu = 0.55$; $\delta_{LE} = \delta_{TE} = 60^0$; $x_n/c_r = 0.40$; $h/d = 1.0$.

Blowing On

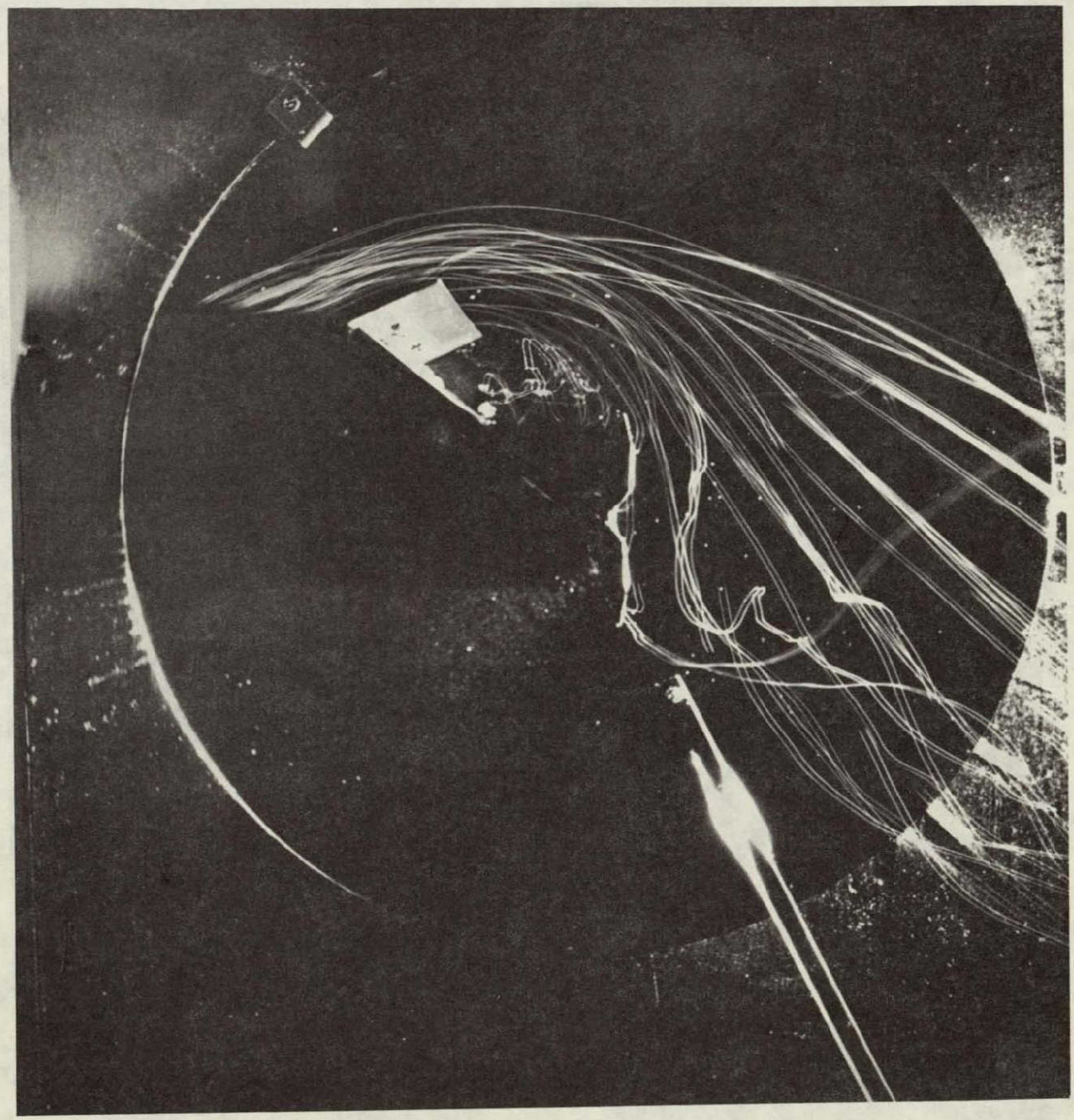

Figure 32.- Spanwise blowing on the rectangular wing for $\alpha = 40^0$ and $C_\mu = 0.60$; $\delta_{LE} = \delta_{TE} = 60^0$; $x_n/c_r = 0.40$; $h/d = 1.0$.

Blowing On

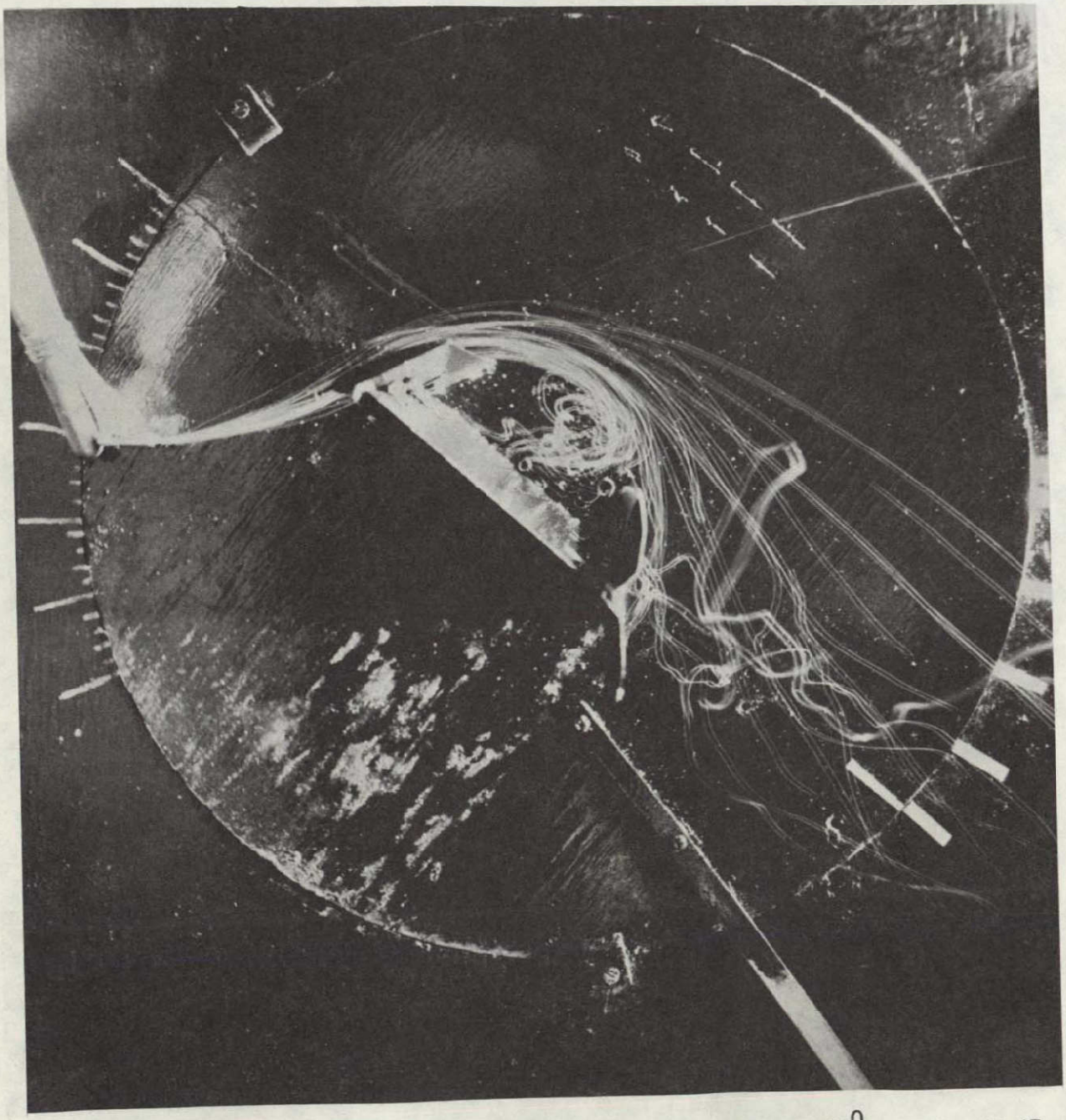

Figure 33.- Spanwise blowing on the rectangular wing for $\alpha = 40^0$ and $C_\mu = 0.65$; $\delta_{LE} = \delta_{TE} = 60^0$; $x_n/c_r = 0.40$; $h/d = 1.0$.

Blowing On

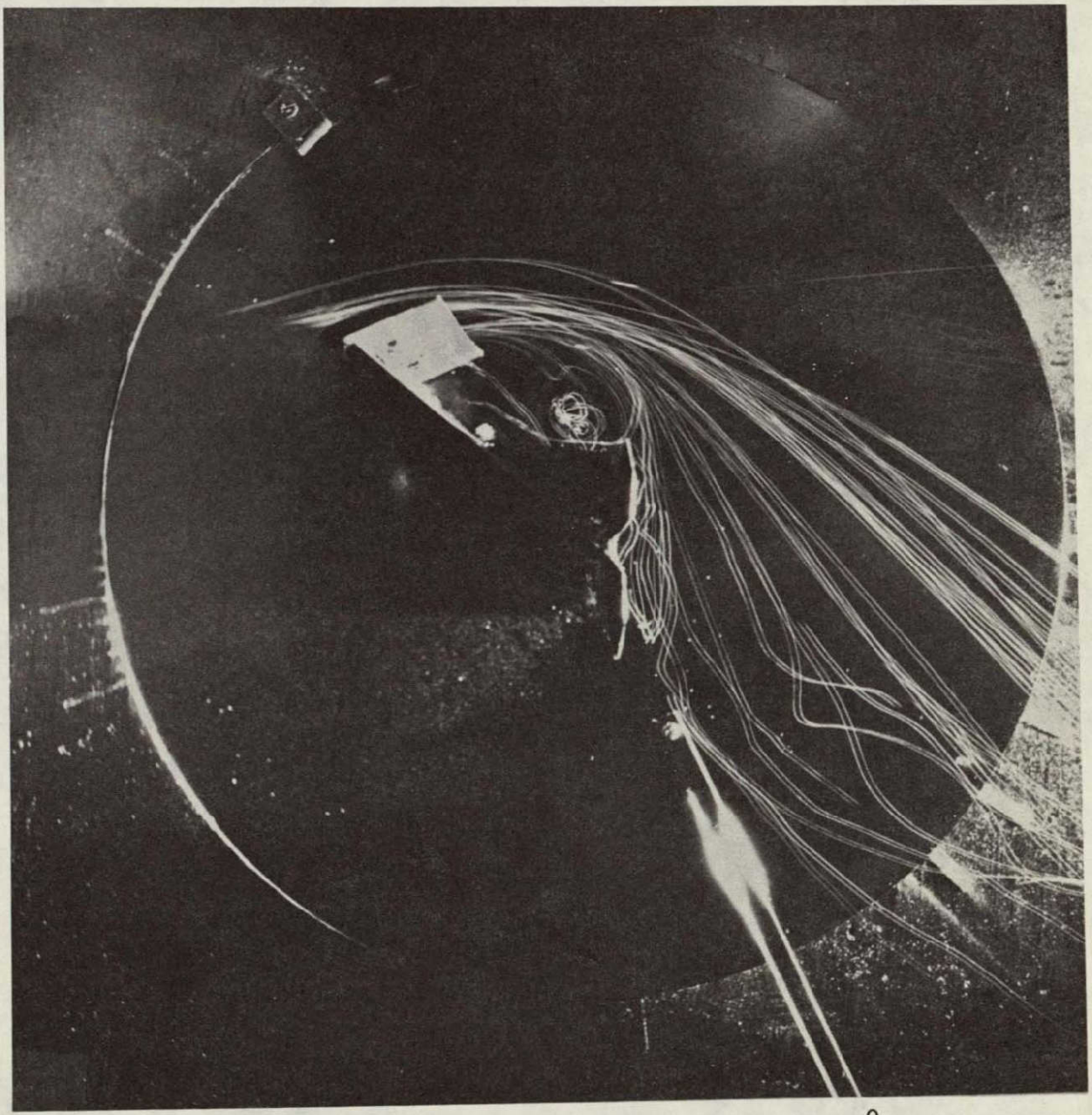

Figure 34. - Spanwise blowing on the rectangular wing for $\alpha = 40^0$ and $C_\mu = 0.70$; $\delta_{LE} = \delta_{TE} = 60^0$; $x_j/c_r = 0.40$; $h/d = 1.0$.

ORIGINAL PAGE IS
OF POOR QUALITY

Blowing On

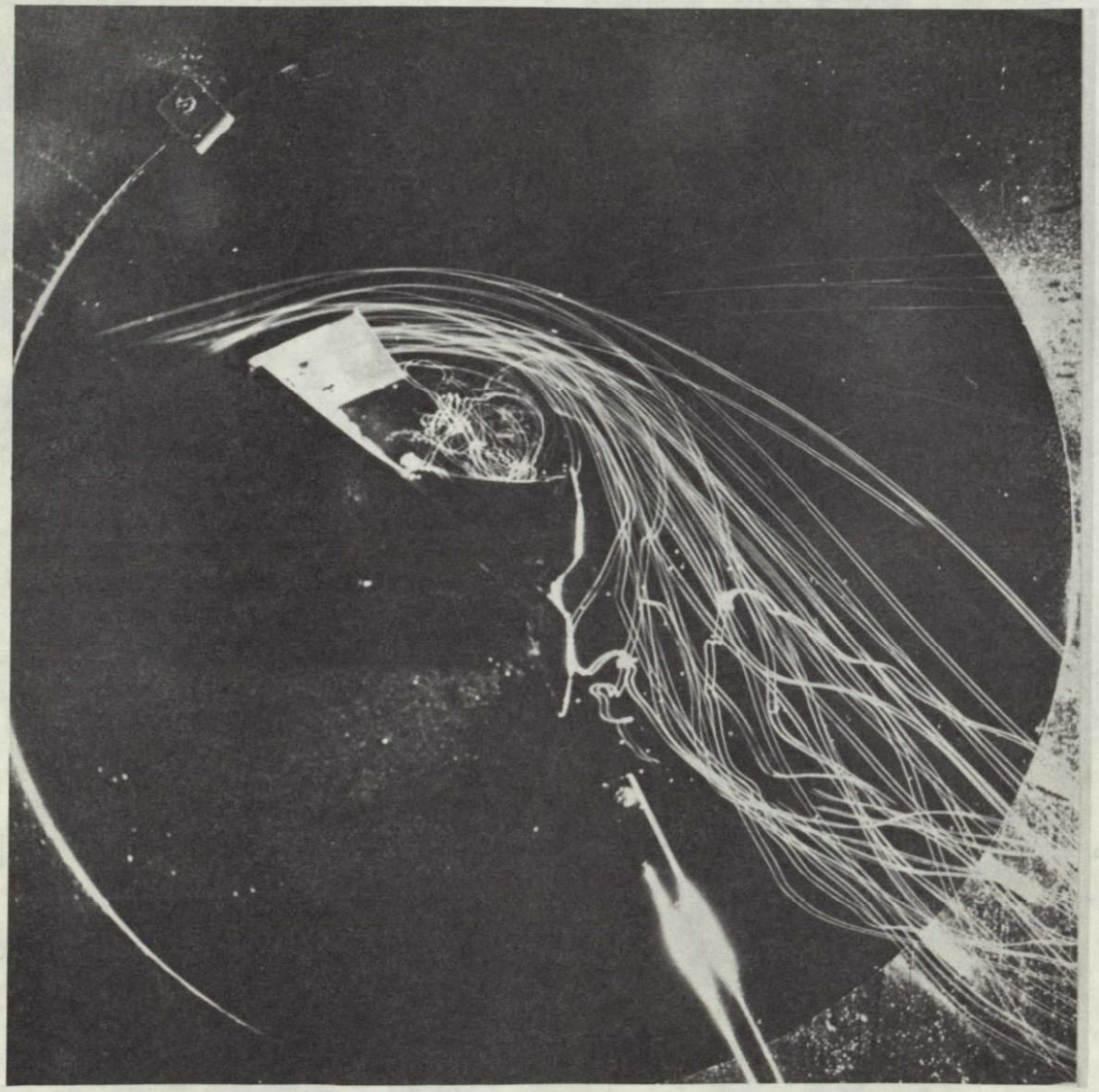

Figure 35. - Spanwise blowing on the rectangular wing for $\alpha = 40^0$ and $C_\mu = 0.75$; $\delta_{LE} = \delta_{TE} = 60^0$; $x_n/c_r = 0.40$; $h/d = 1.0$.

Blowing On

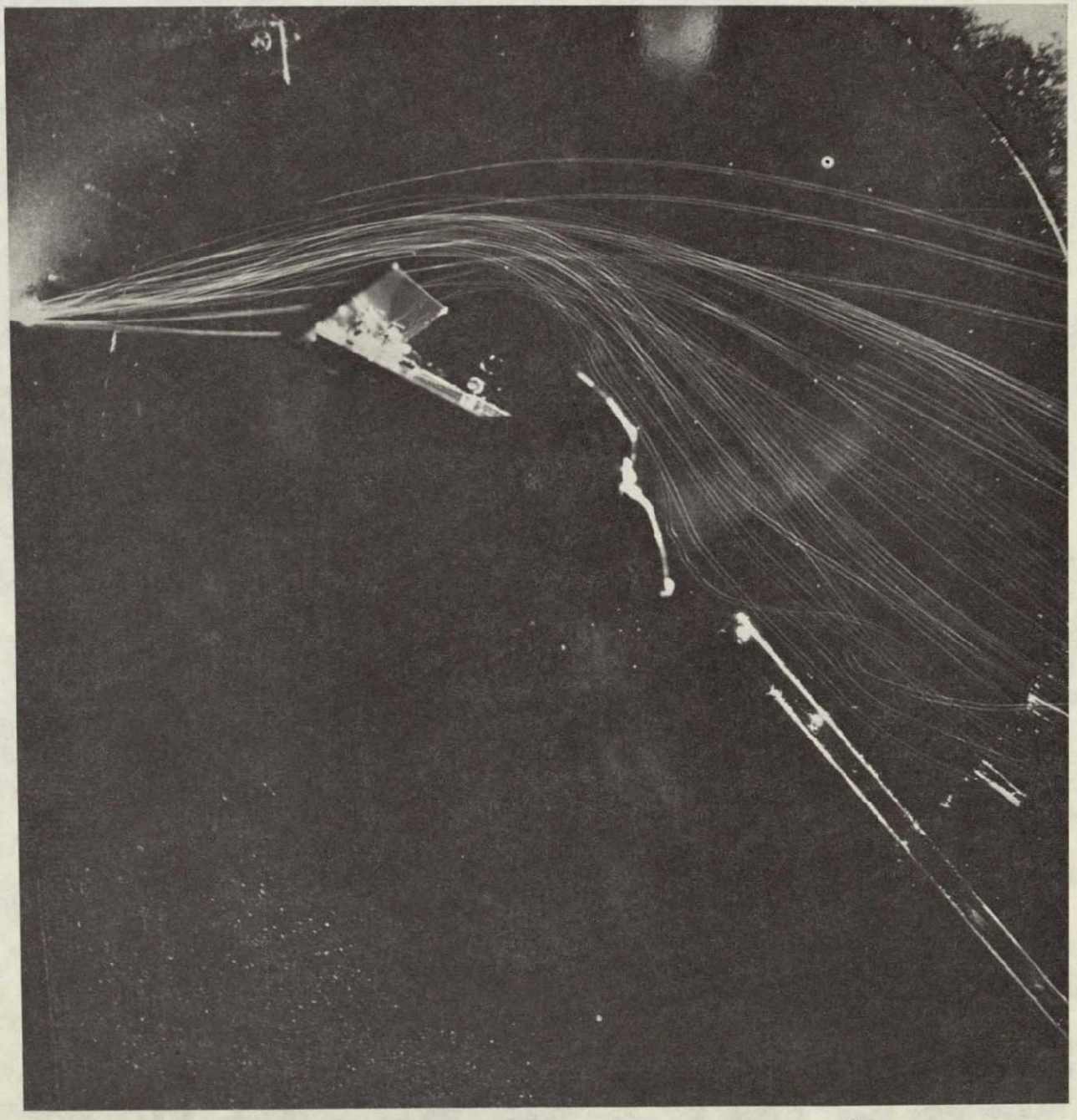

Figure 36. - Spanwise blowing on the rectangular wing for $\alpha = 30^{0}$ and $C_{\mu} = 0.45$; $\delta_{LE} = 60^{0}$; $\delta_{TE} = 30^{0}$; $x_n/c_r = 0.40$; $h/d = 1.0$.

Blowing On

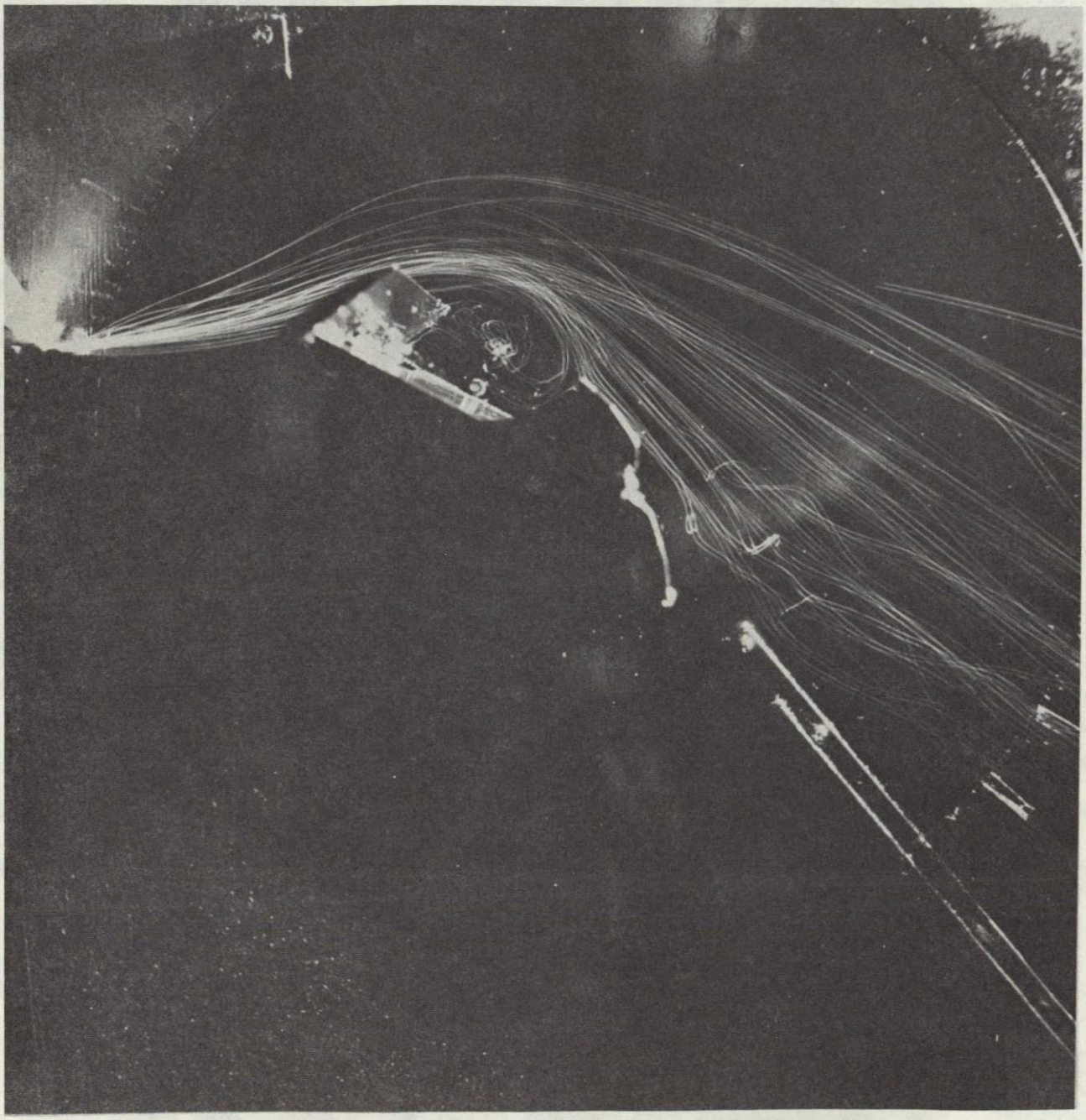

Figure 37. - Spanwise blowing on the rectangular wing for $\alpha = 30^{0}$ and $C_{\mu} = 0.55$; $\delta_{LE} = 60^{0}$; $\delta_{TE} = 30^{0}$; $x_n/c_r = 0.40$; $h/d = 1.0$.

Blowing On

Figure 38. - Spanwise blowing on the rectangular wing for $\alpha = 30^{0}$ and $C_{\mu} = 0.60$; $\delta_{LE} = 60^{0}$; $\delta_{TE} = 30^{0}$; $x_n/c_r = 0.40$; $h/d = 1.0$.

ORIGINAL PAGE IS
OF POOR QUALITY

Blowing On

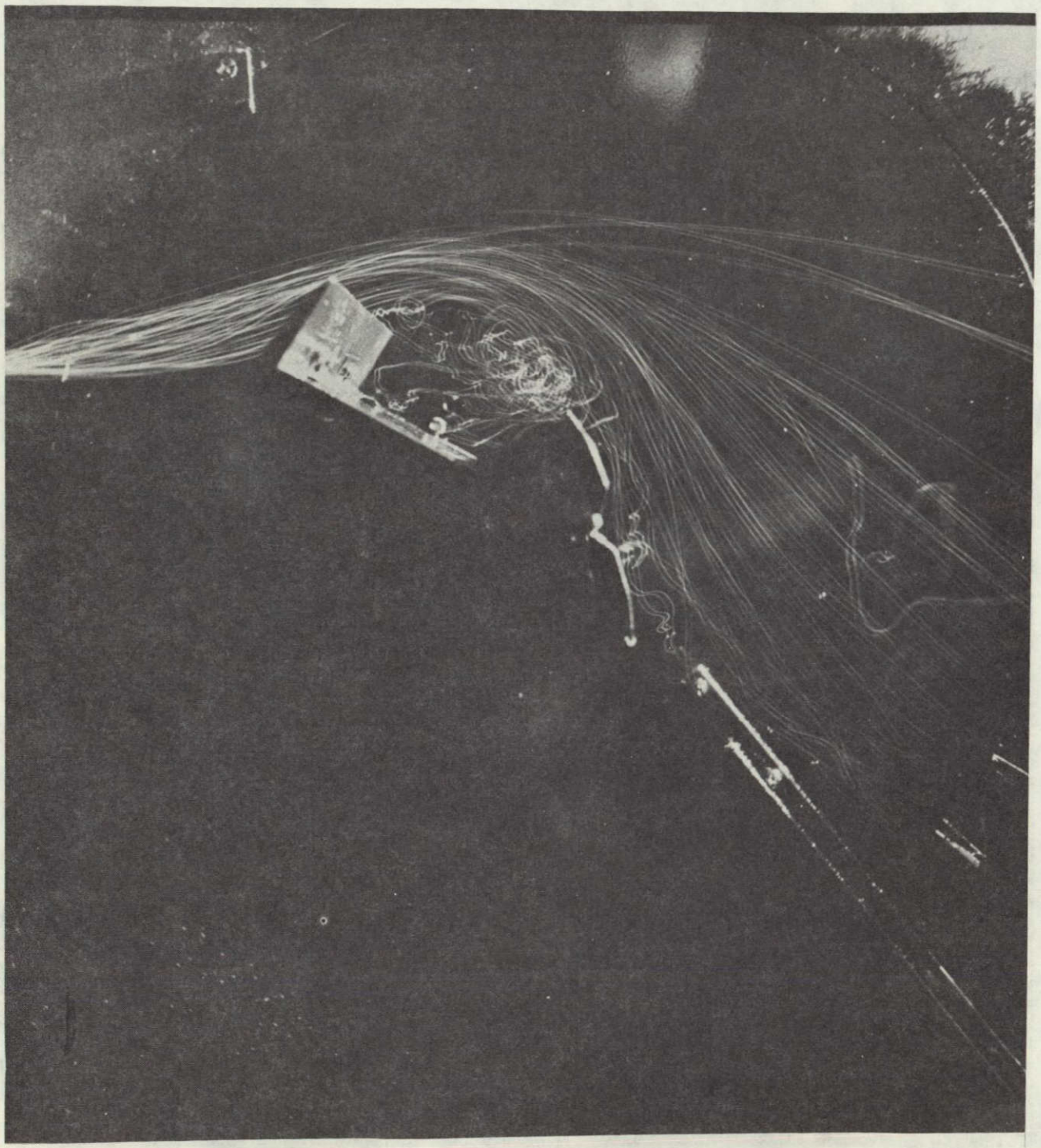

Figure 39.- Spanwise blowing on the rectangular wing for $\alpha = 30^0$ and $C_\mu = 0.55$; $\delta_{LE} = 90^0$; $\delta_{TE} = 45^0$; $x_n/c_r = 0.40$; $h/d = 1.0$.

Blowing On

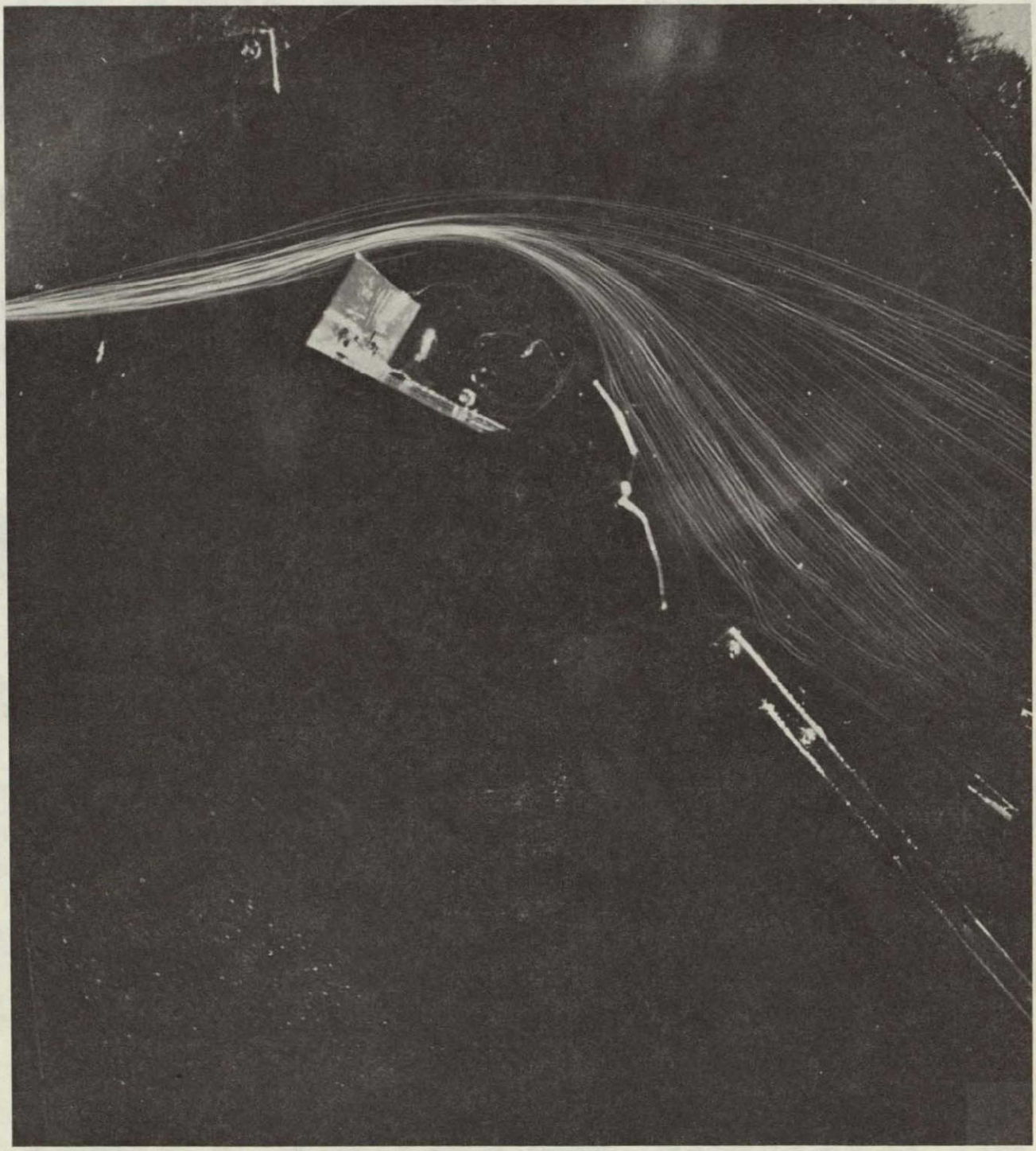

Figure 40. - Spanwise blowing on the rectangular wing for $\alpha = 30^0$ and $C_\mu = 0.60$; $\delta_{LE} = 90^0$; $\delta_{TE} = 45^0$; $x_n/c_r = 0.40$; $h/d = 1.0$.

Blowing On

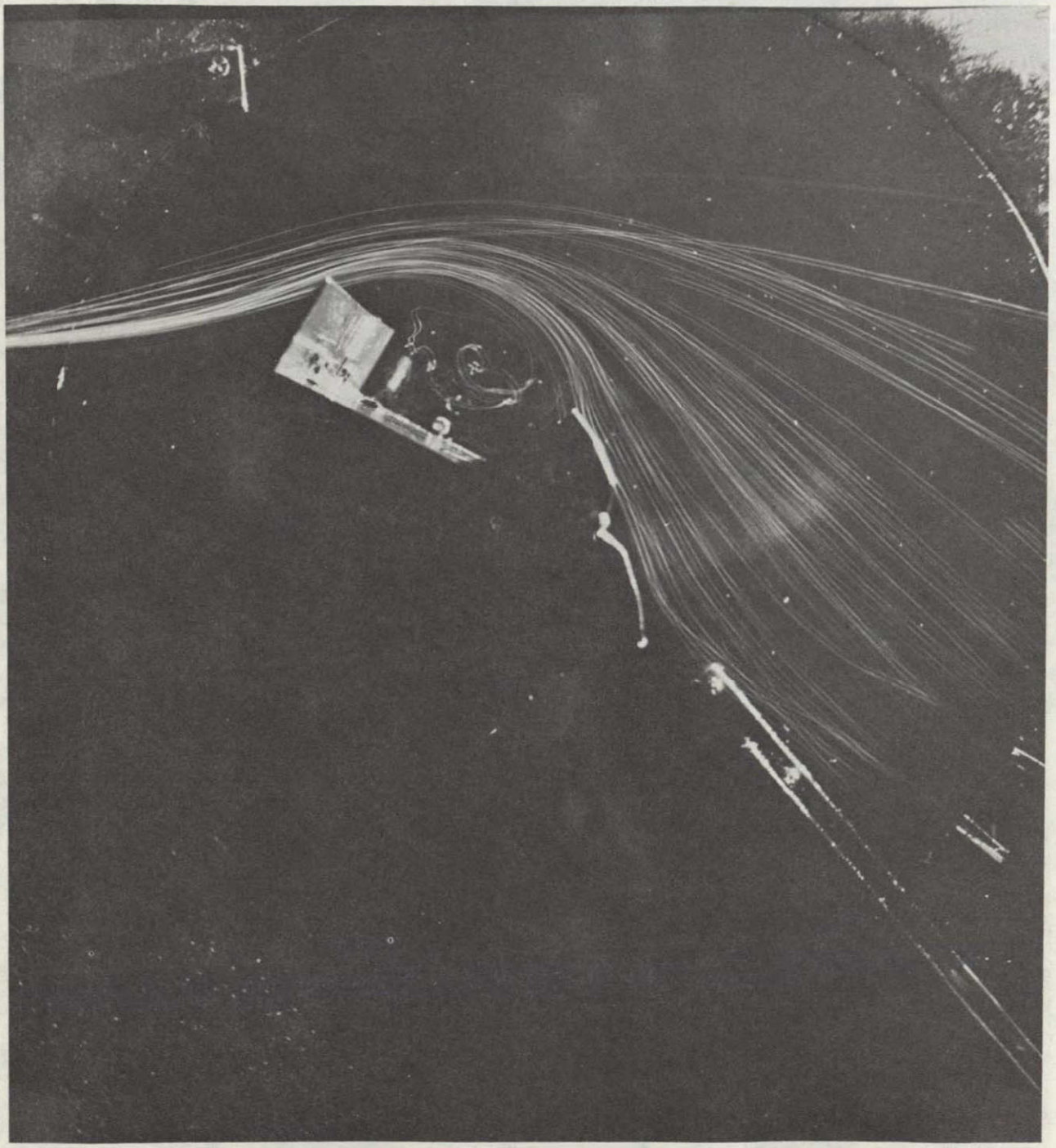

Figure 41. - Spanwise blowing on the rectangular wing for $\alpha = 30^{0}$ and $C_{\mu} = 0.70$; $\varepsilon_{LE} = 90^{0}$; $\delta_{TE} = 45^{0}$; $x_n/c_r = 0.40$; $h/d = 1.0$.

Blowing On

Figure 42.- Spanwise blowing on the rectangular wing for $\alpha = 30^0$ and $C_\mu = 0.75$; $\delta_{LE} = 90^0$; $\delta_{TE} = 45^0$; $x_n/c_r = 0.40$; $h/d = 1.0$.

ORIGINAL PAGE IS
OF POOR QUALITY

Blowing On

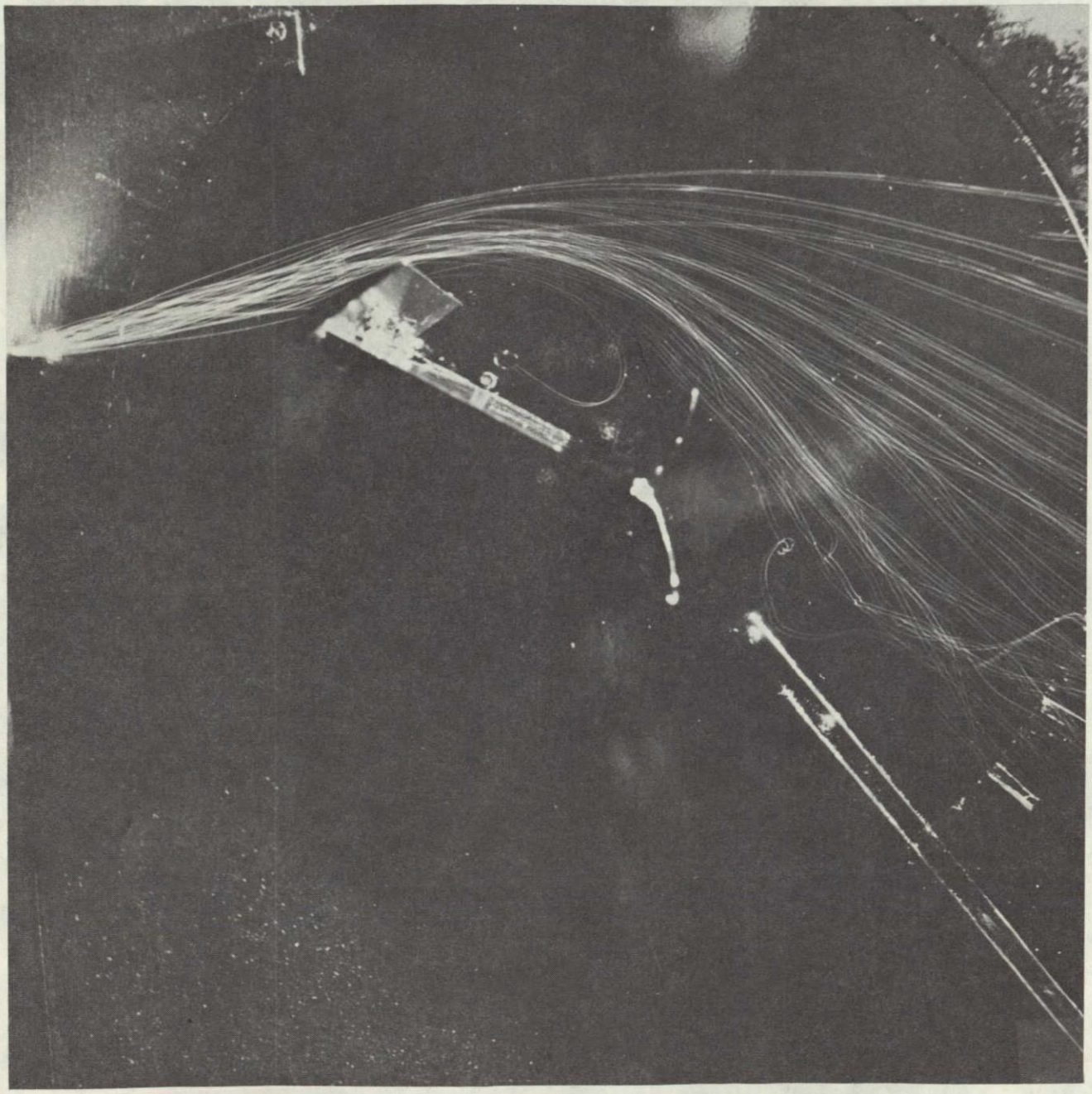

Figure 43. - Spanwise blowing on the rectangular wing for $\alpha = 30^{0}$ and $C_{\mu} = 0.40$; $\delta_{LE} = 60^{0}$; $\delta_{TE} = 90^{0}$; $x_n/c_r = 0.40$; $h/d = 1.0$.

Blowing On

Figure 44. - Spanwise blowing on the rectangular wing for $\alpha = 30^0$ and $C_\mu = 0.45$; $\delta_{LE} = 60^0$; $\delta_{TE} = 90^0$; $x_n/c_r = 0.40$; $h/d = 1.0$.

Blowing On

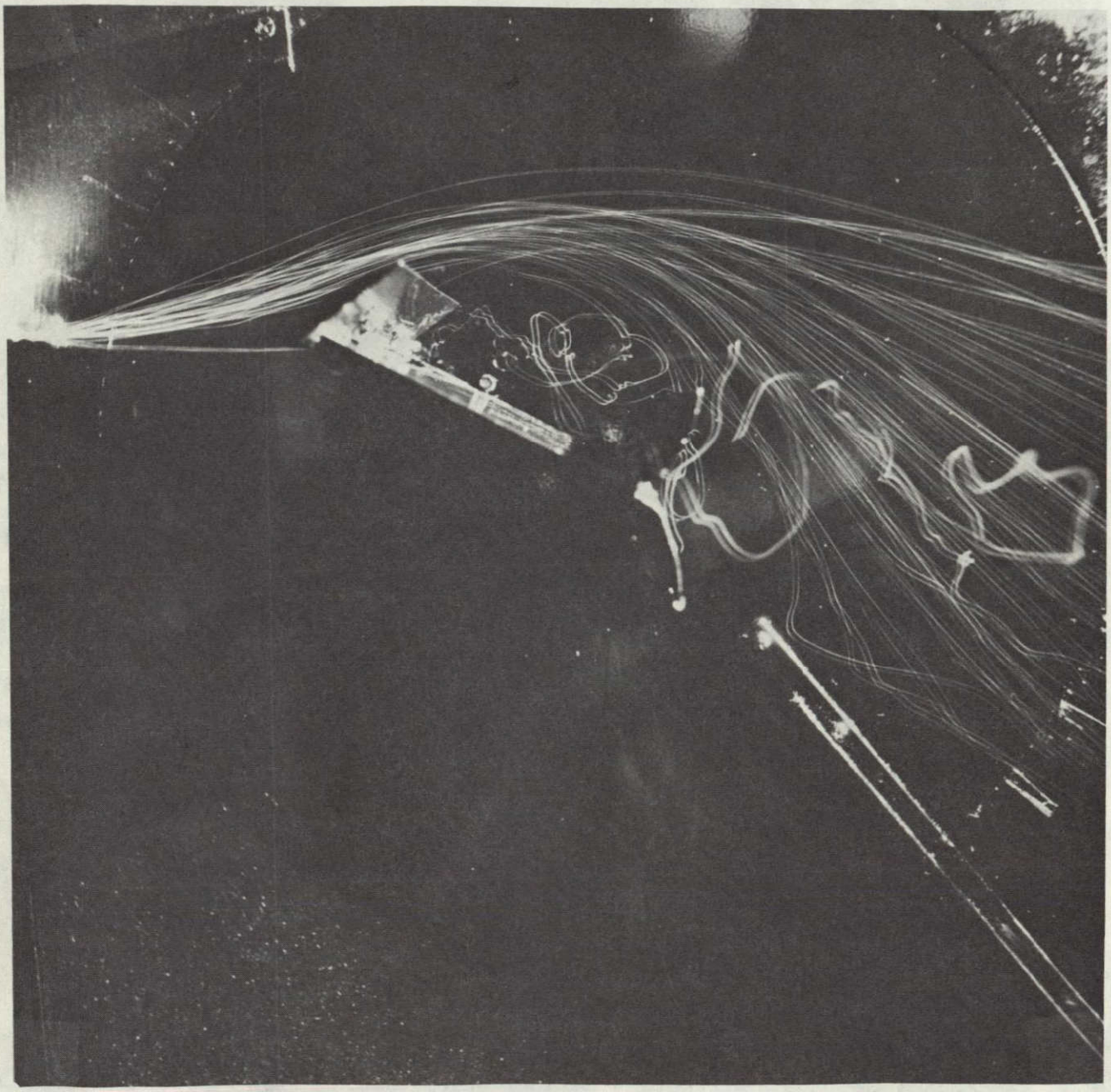

Figure 45. - Spanwise blowing on the rectangular wing for $\alpha = 30^{0}$ and $C_{\mu} = 0.50$; $\delta_{LE} = 60^{0}$; $\delta_{TE} = 90^{0}$; $x_n/c_r = 0.40$; $h/d = 1.0$.

Blowing On

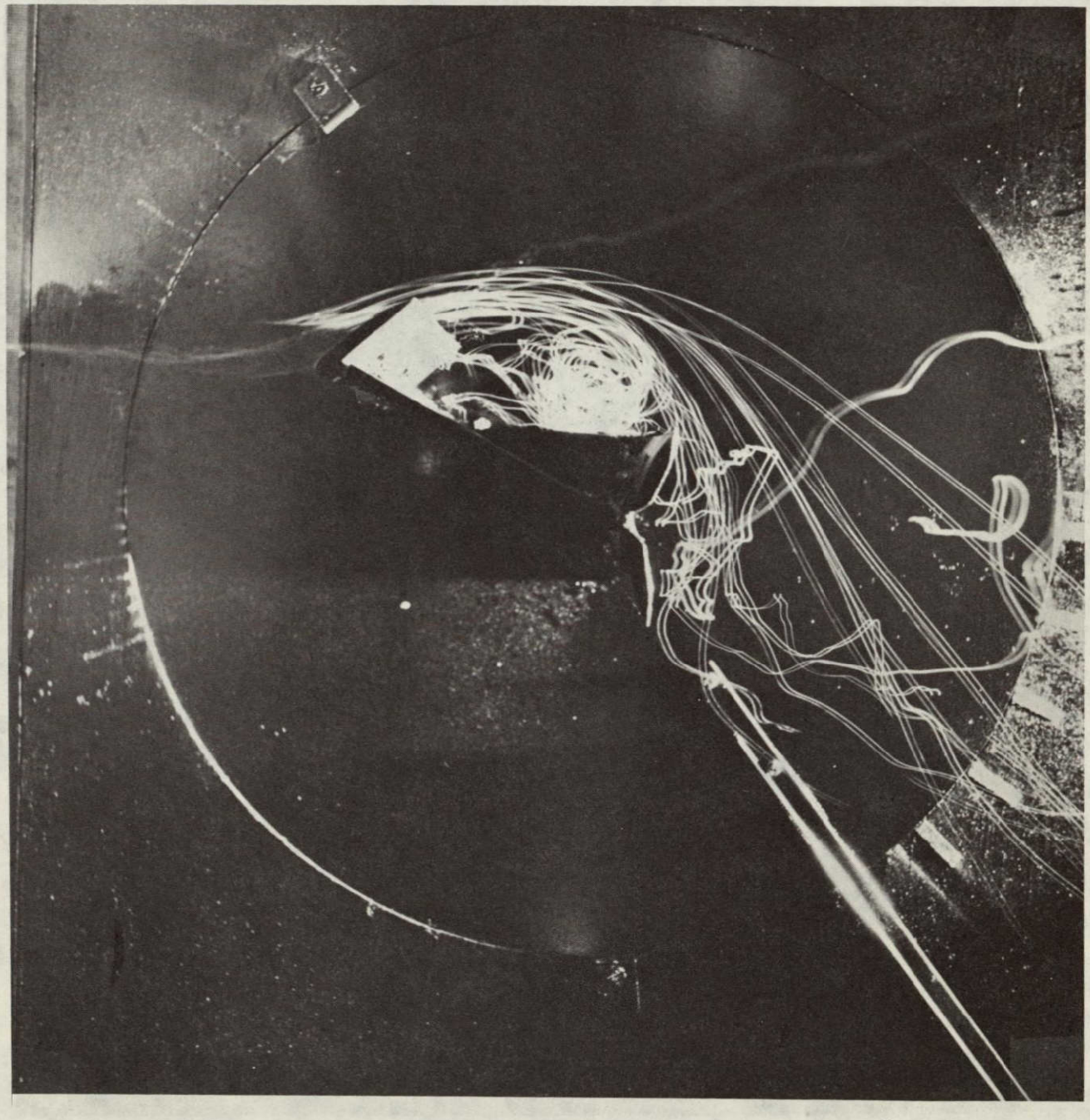

Figure 46. - Spanwise blowing on the rectangular wing for $\alpha = 30^0$ and $C_\mu = 0.57$; $\delta_{LE} = 60^0$; $\delta_{TE} = 90^0$; $x_n/c_r = 0.40$; $h/d = 1.0$.

ORIGINAL PAGE IS OF POOR QUALITY

Blowing On

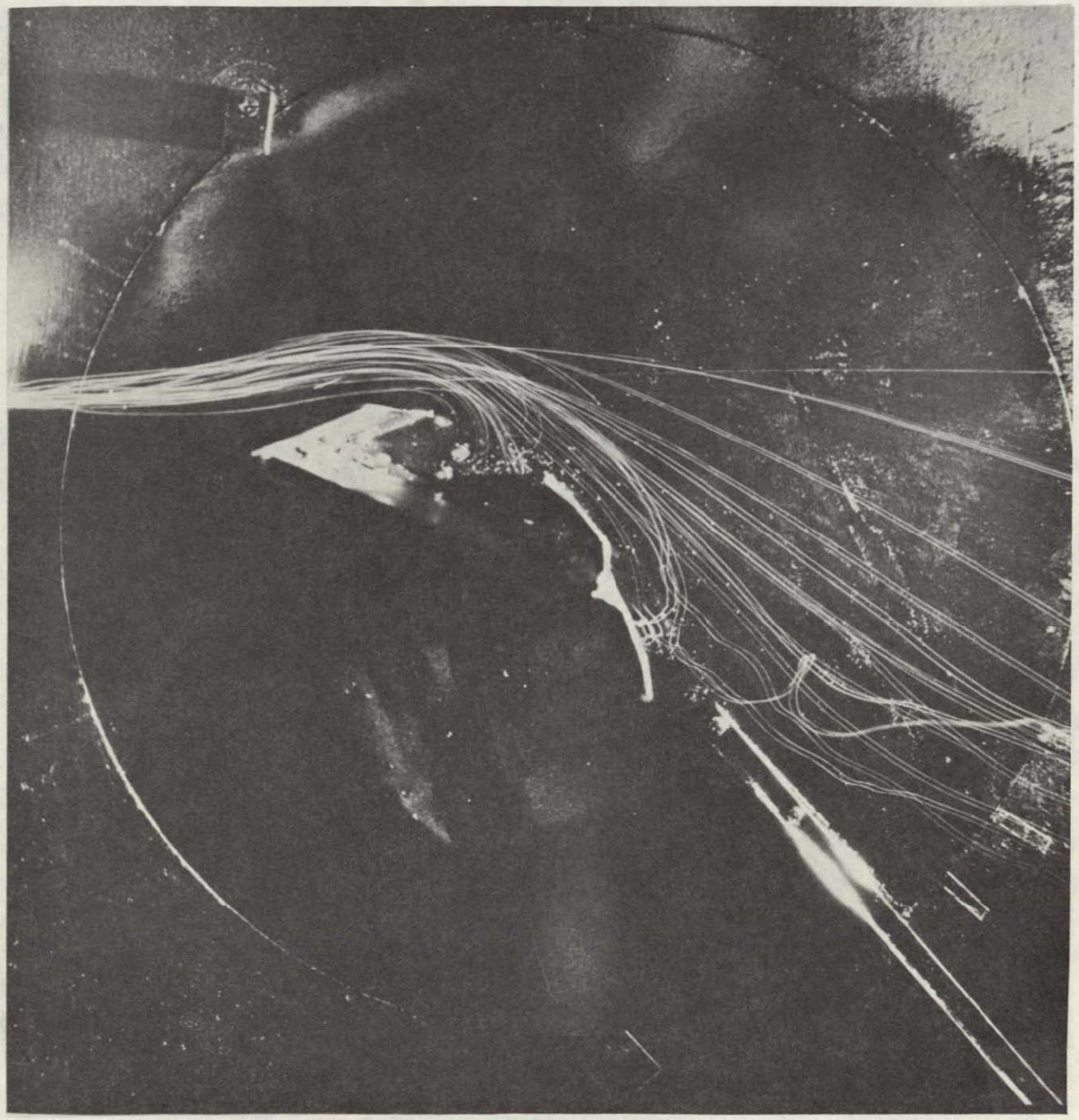

Figure 47.- Spanwise blowing on the rectangular wing for $\alpha = 20^{0}$ and $C_{\mu} = 0.30$; $\delta_{LE} = 45^{0}$; $\delta_{TE} = 30^{0}$; $x_n/c_r = 0.40$; $h/d = 1.0$.

Blowing On

Figure 48.- Spanwise blowing on the rectangular wing for $\alpha = 30^{0}$ and $C_{\mu} = 0.35$; $\delta_{LE} = 45^{0}$; $\delta_{TE} = 30^{0}$; $x_n/c_r = 0.40$; $h/d = 1.0$.

Blowing On

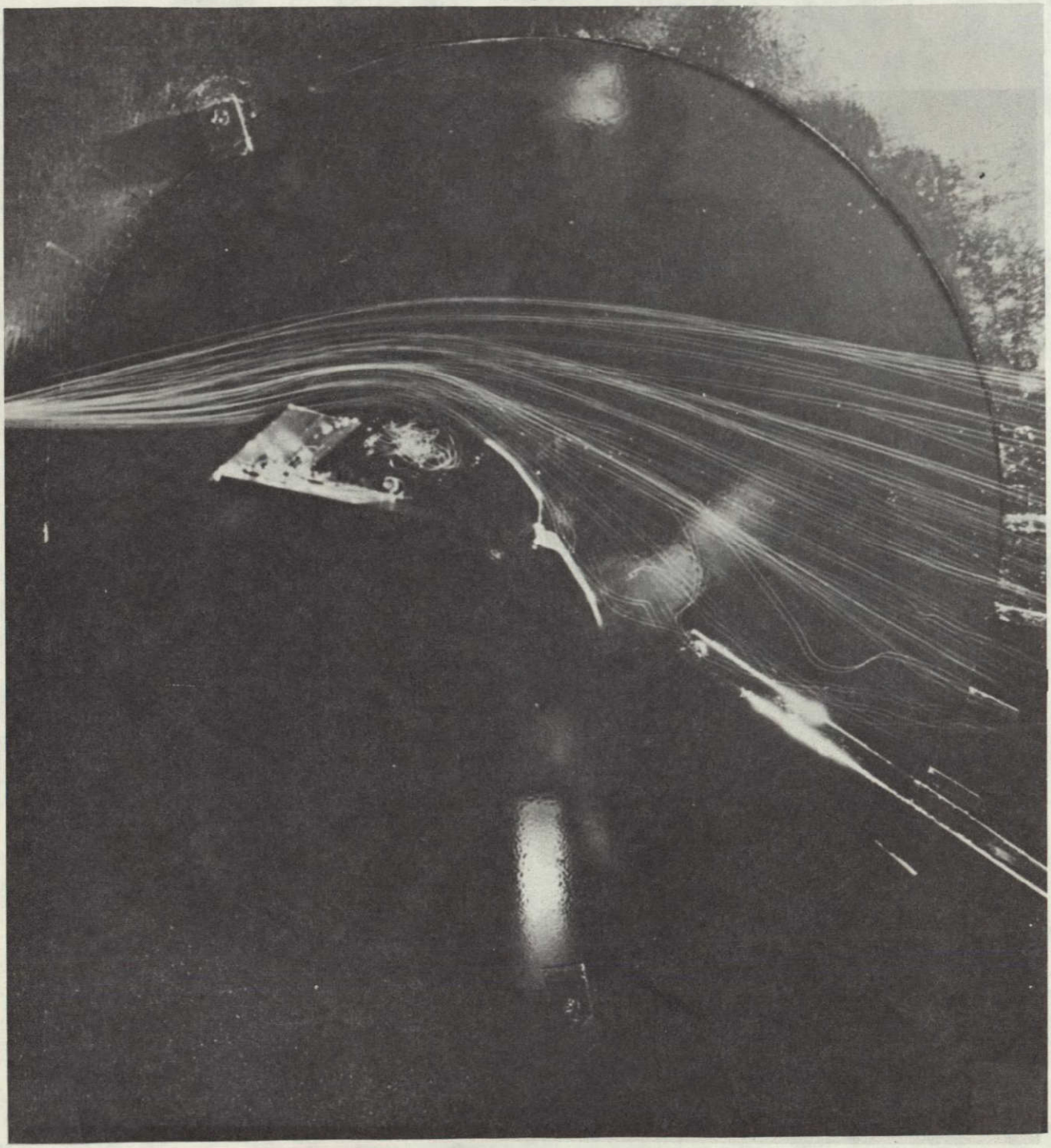

Figure 49. - Spanwise blowing on the rectangular wing for $\alpha = 20^{0}$ and $C_{\mu} = 0.45$; $\delta_{LE} = \delta_{TE} = 45^{0}$; $x_n/c_r = 0.40$; $h/d = 1.0$.

Blowing On

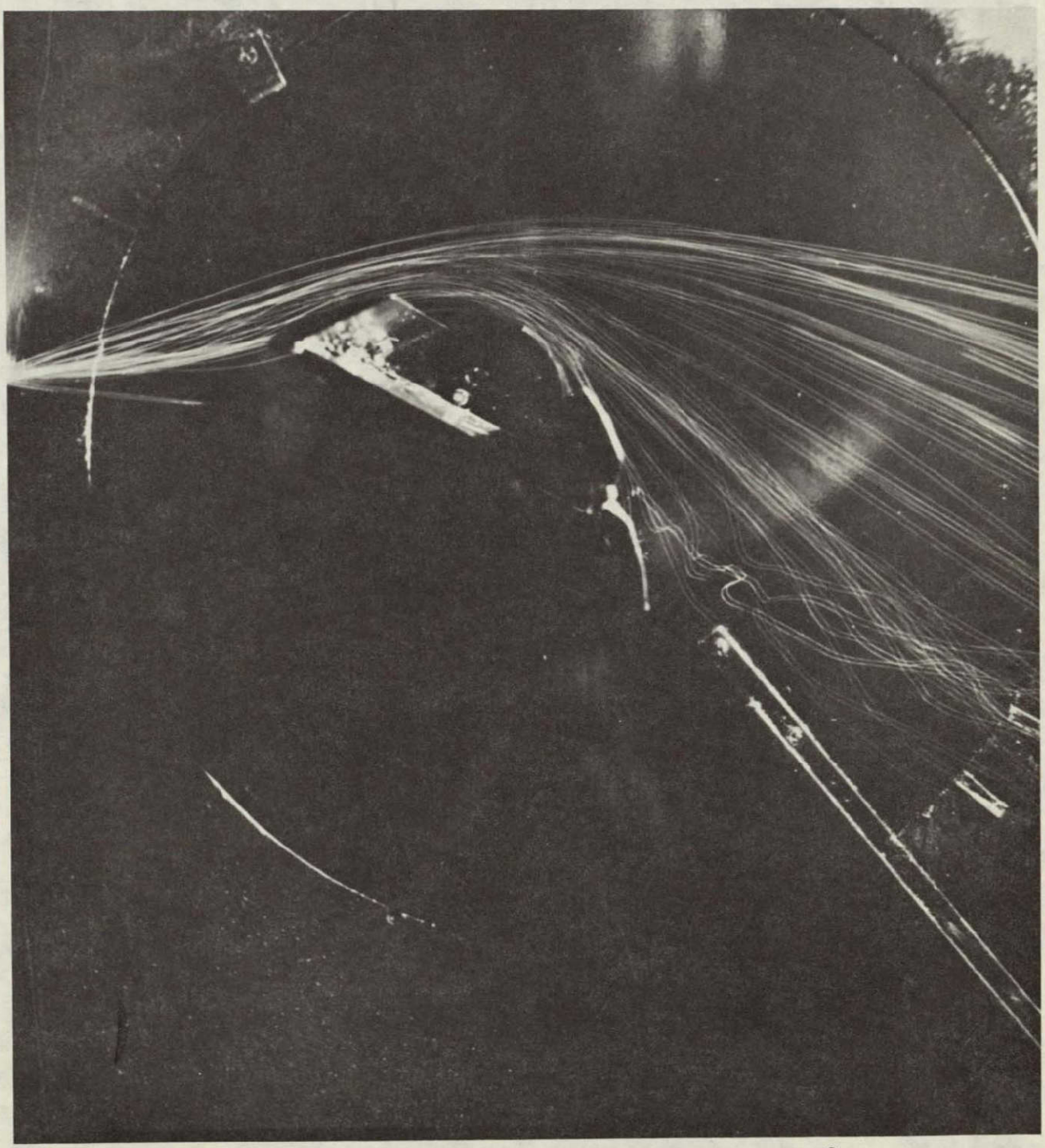

Figure 50. - Spanwise blowing on the rectangular wing for $\alpha = 30^{0}$ and $C_{\mu} = 0.45$; $\delta_{LE} = \delta_{TE} = 45^{0}$; $x_n/c_r = 0.40$; h/d = 1.0.

ORIGINAL PAGE IS
OF POOR QUALITY

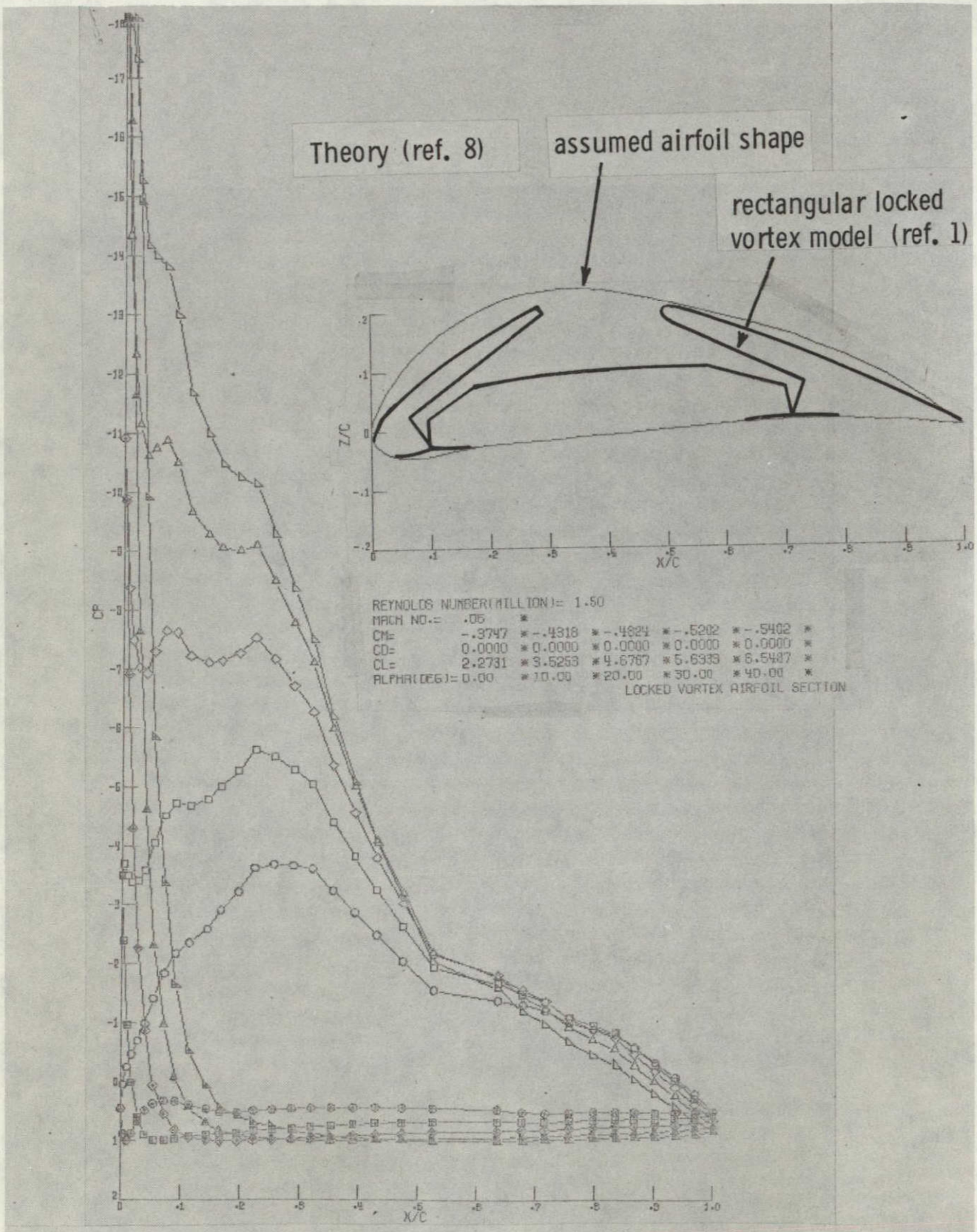

Figure 51.- Theoretical pressure coefficients and integrated longitudinal data for a thick, highly-cambered airfoil section for a range of angle of attack.

ORIGINAL PAGE IS
OF POOR QUALITY

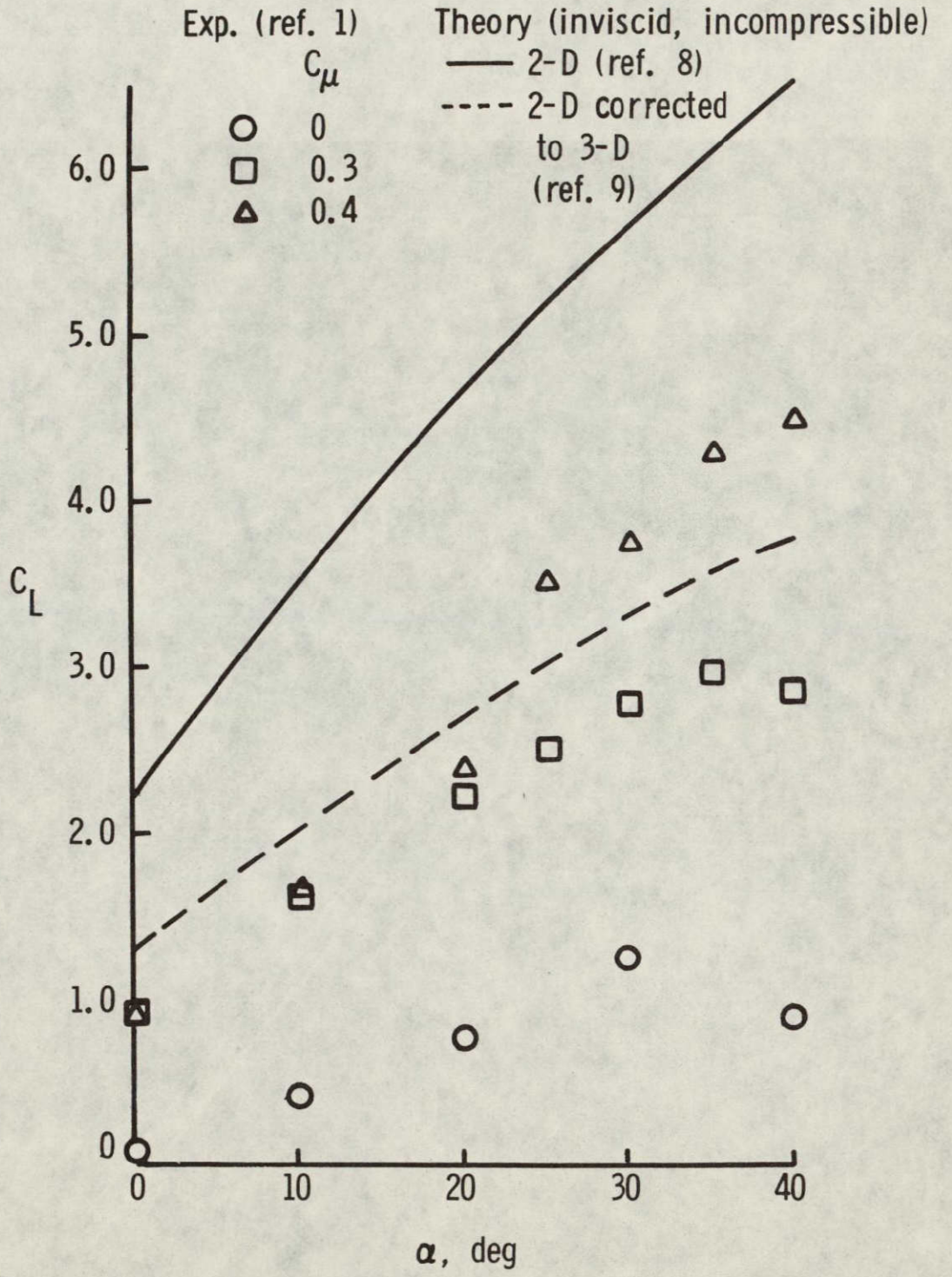

Figure 52.- Theoretical and experimental lift coefficients for the locked vortex rectangular wing; V_∞ = 68.9 fps; Re = 150,000; $\delta_{LE} = 30^0$; $\delta_{TE} = 20^0$.

Blowing Off

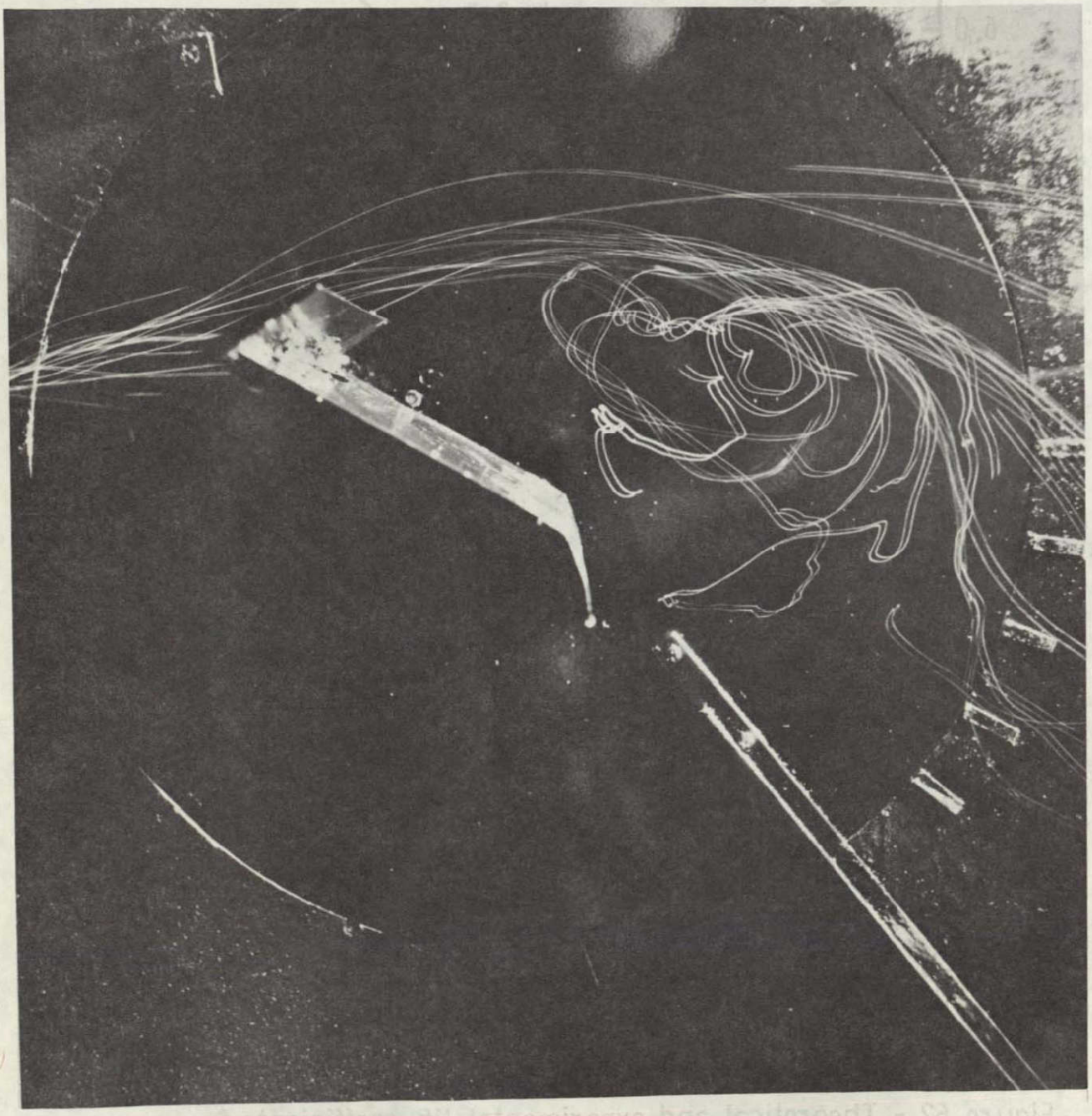

Figure 53. - Rectangular wing with upper surface TE flap off for $\alpha = 30^{o}$ and blowing off; $\delta_{LE} = 60^{o}$.

Blowing On

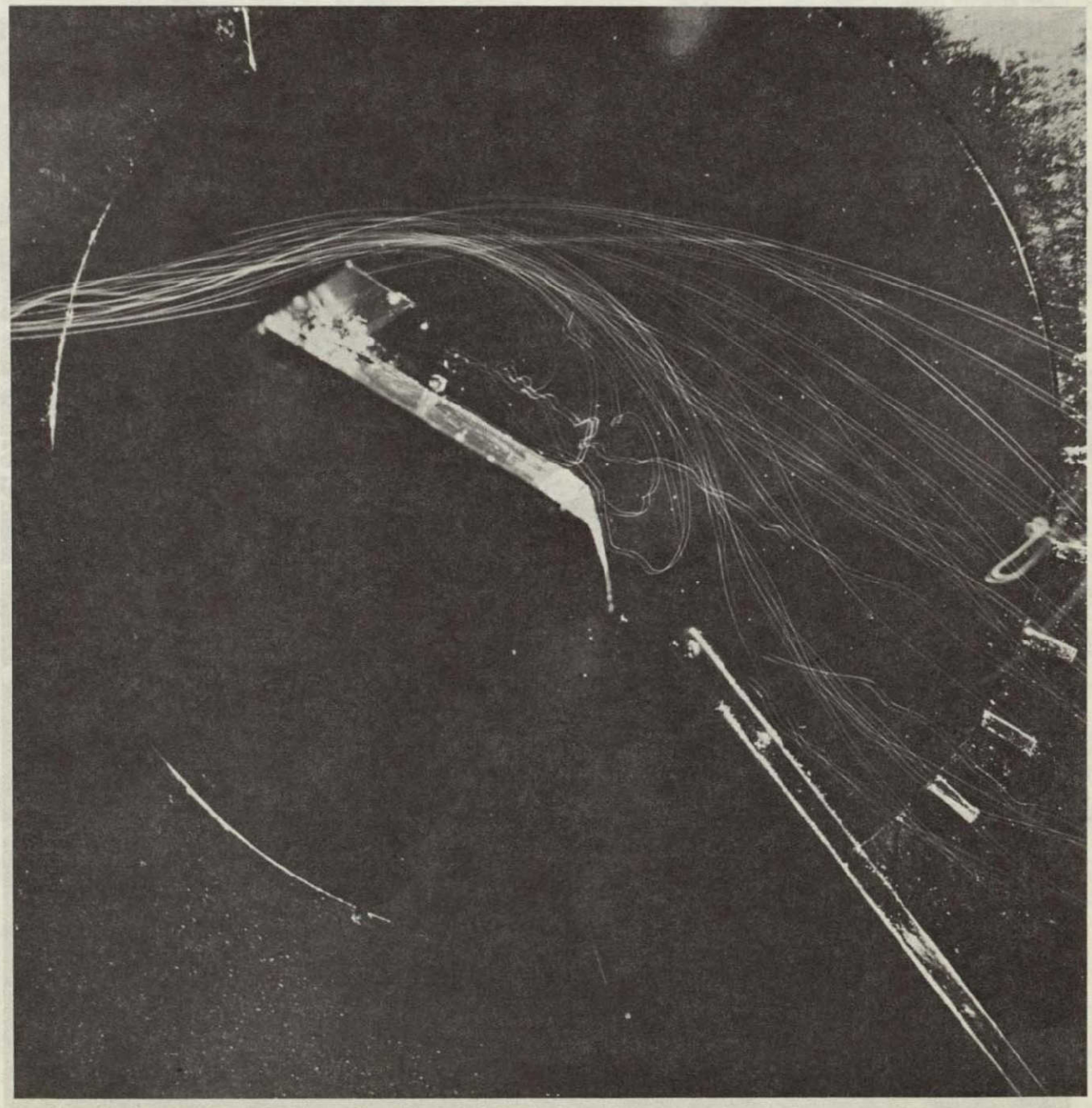

Figure 54. - Spanwise blowing on the rectangular wing without upper surface TE flap for $\alpha = 30^0$ and $C_\mu = 0.35$; $\delta_{LE} = 60^0$; $x_n/c_r = 0.40$; $h/d = 1.0$.

ORIGINAL PAGE IS
OF POOR QUALITY

Blowing On

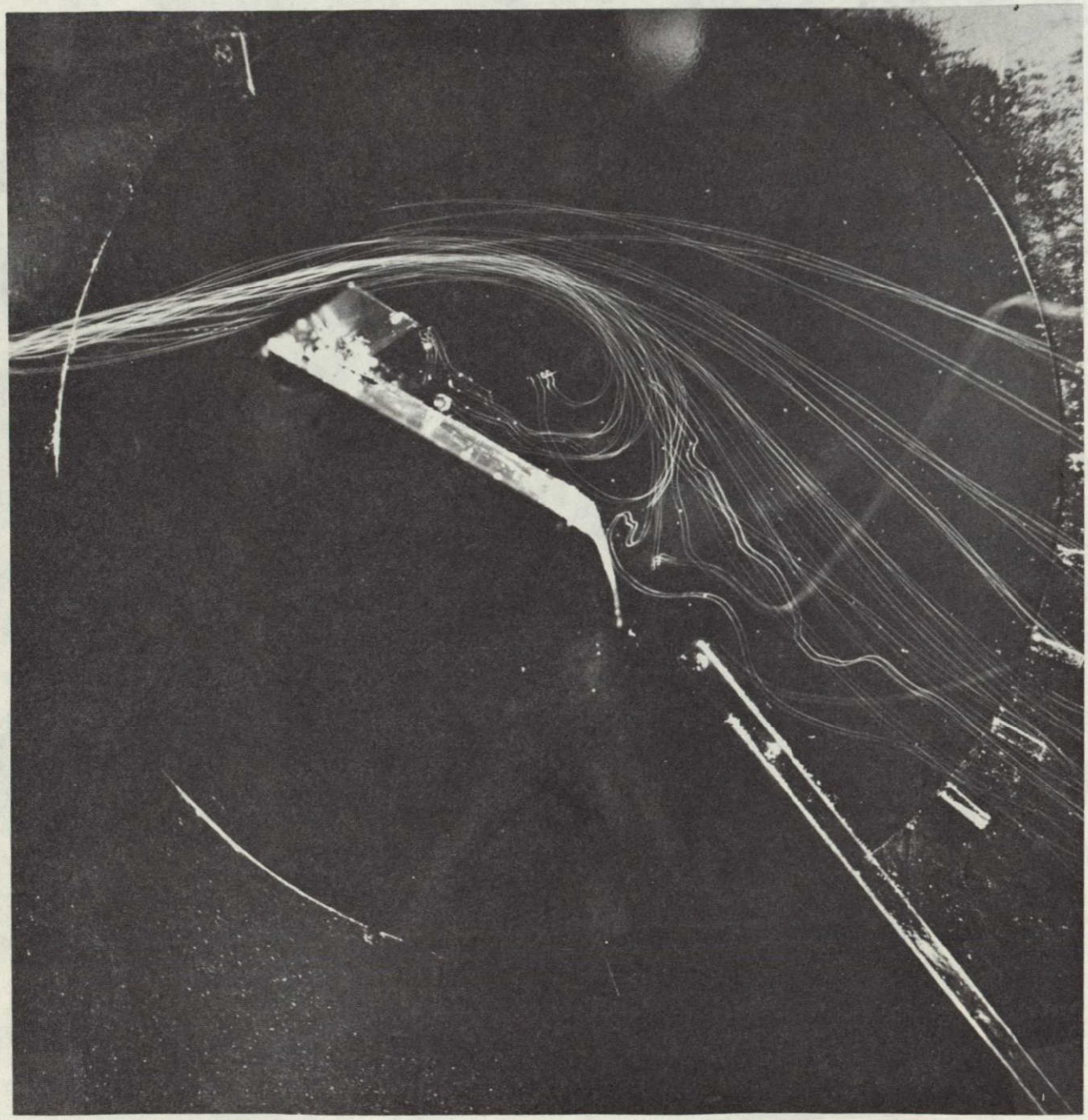

Figure 55. - Spanwise blowing on the rectangular wing without upper surface TE flap for $\alpha = 30^0$ and $C_\mu = 0.50$; $\delta_{LE} = 60^0$; $x_n/c_r = 0.40$; $h/d = 1.0$.

Blowing On

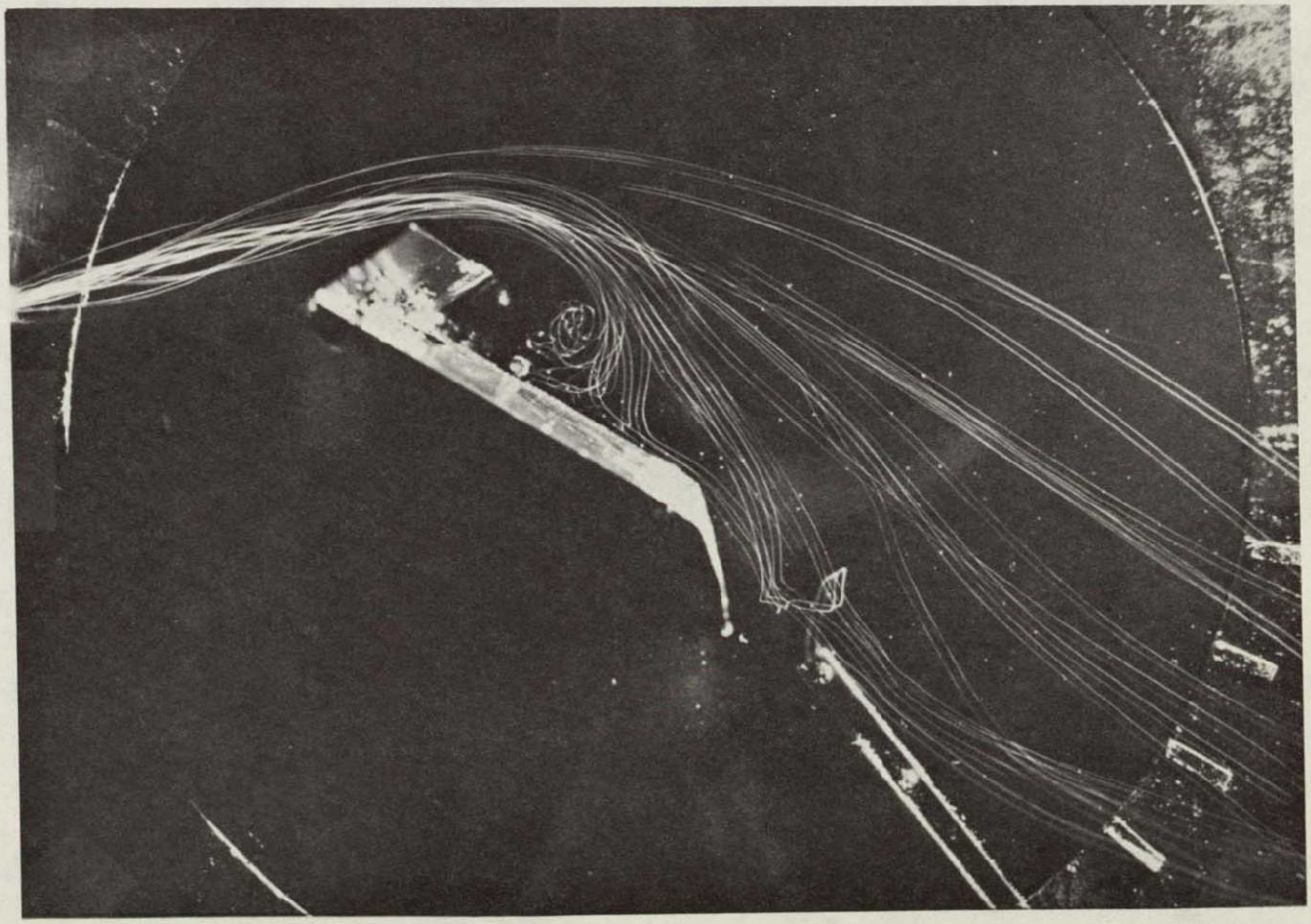

Figure 56. - Spanwise blowing on the rectangular wing without upper surface TE flap for $\alpha = 30^{0}$ and $C_{\mu} = 0.57$; $\delta_{LE} = 60^{0}$; $x_n/c_r = 0.40$; $h/d = 1.0$.

Blowing Off

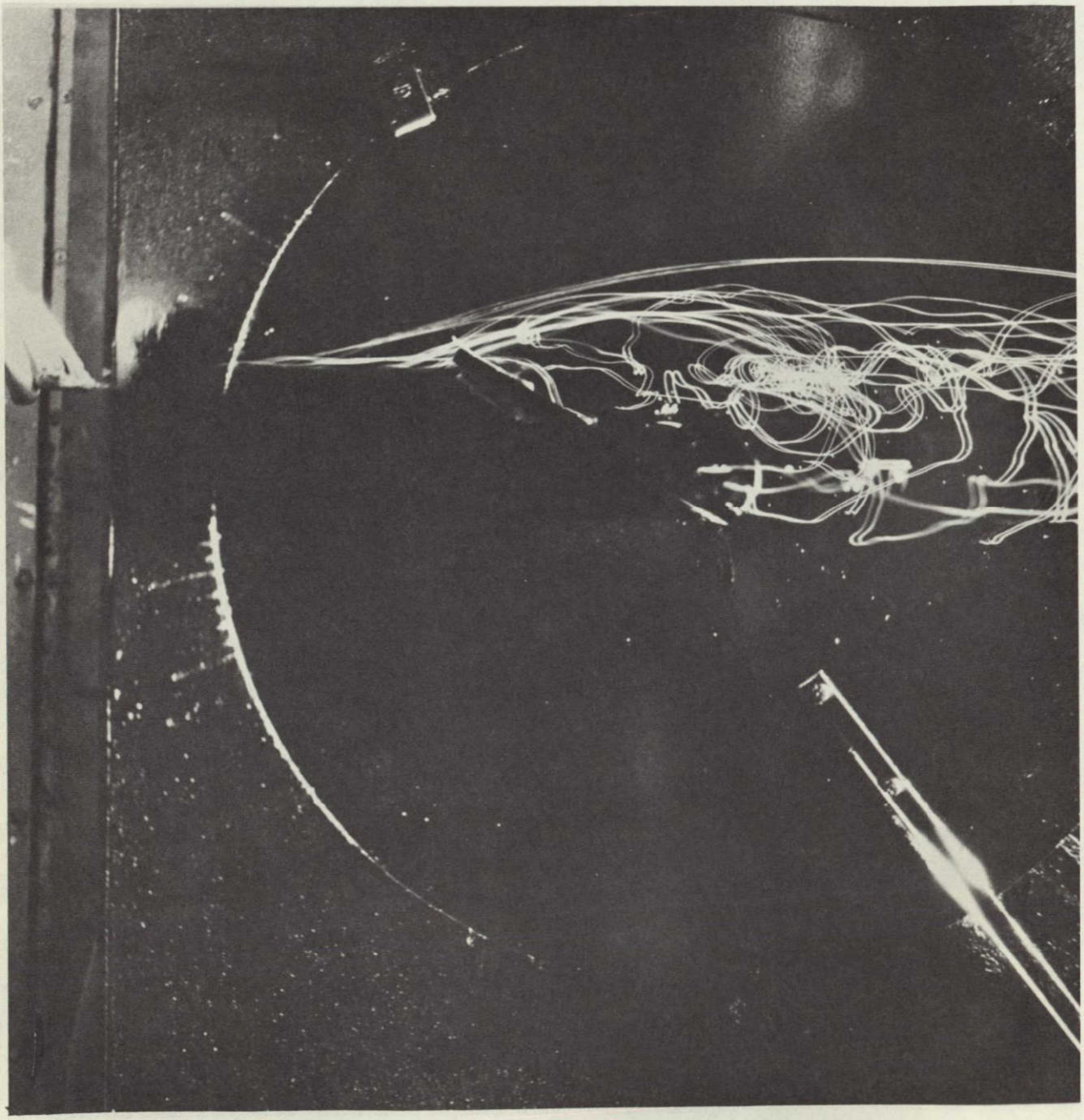

Figure 57.- Rectangular wing without LE flap for $\alpha = 30^{o}$ and blowing off; sharp LE; $\delta_{TE} = 30^{o}$.

Blowing On

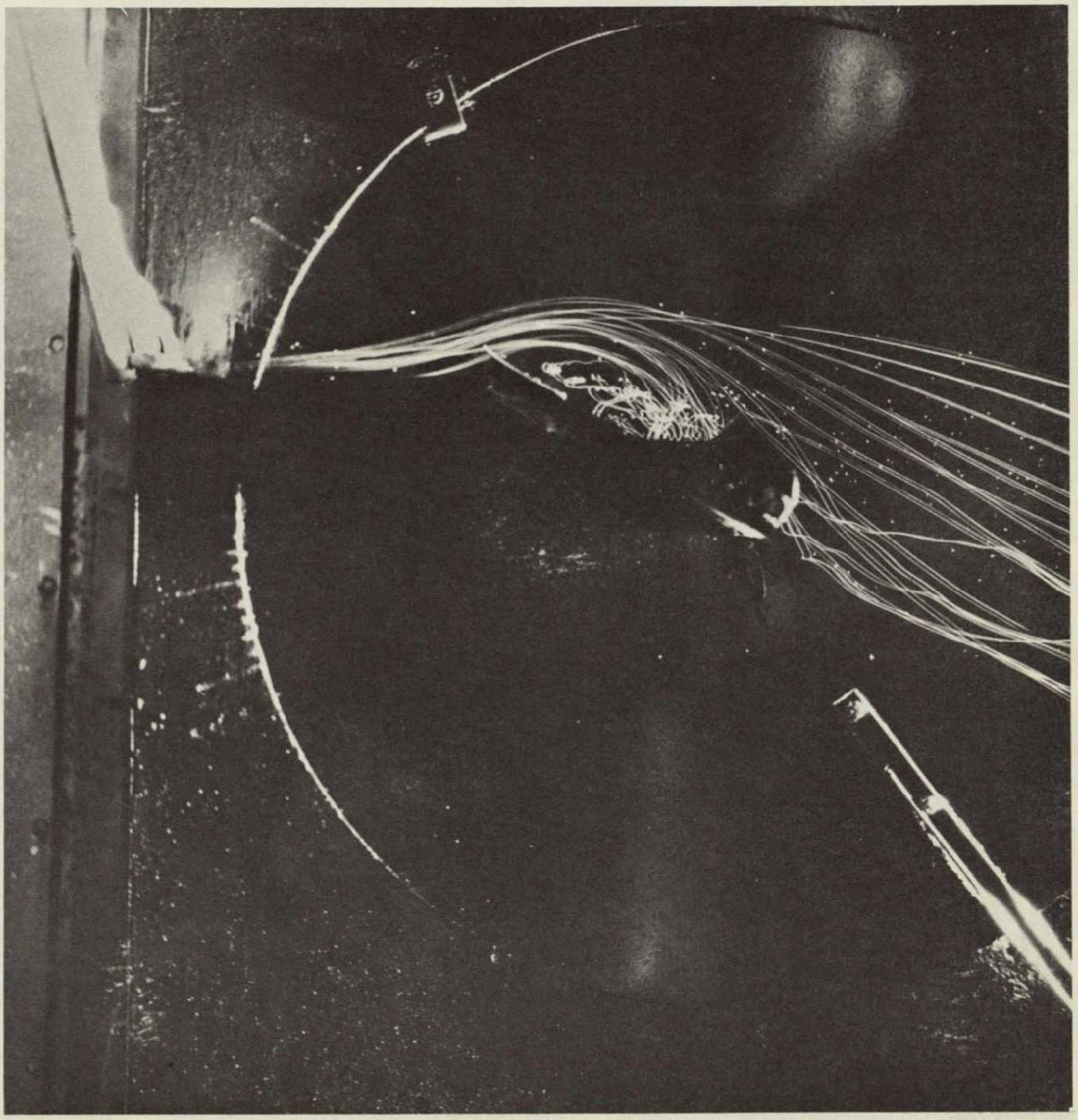

Figure 58. - Spanwise blowing on the rectangular wing without LE flap for $\alpha = 30^0$ and $C_\mu = 0.21$; sharp LE; $\delta_{TE} = 30^0$; $x_n/c_r = 0.40$; $h/d = 1.0$.

ORIGINAL PAGE IS
OF POOR QUALITY

Blowing On

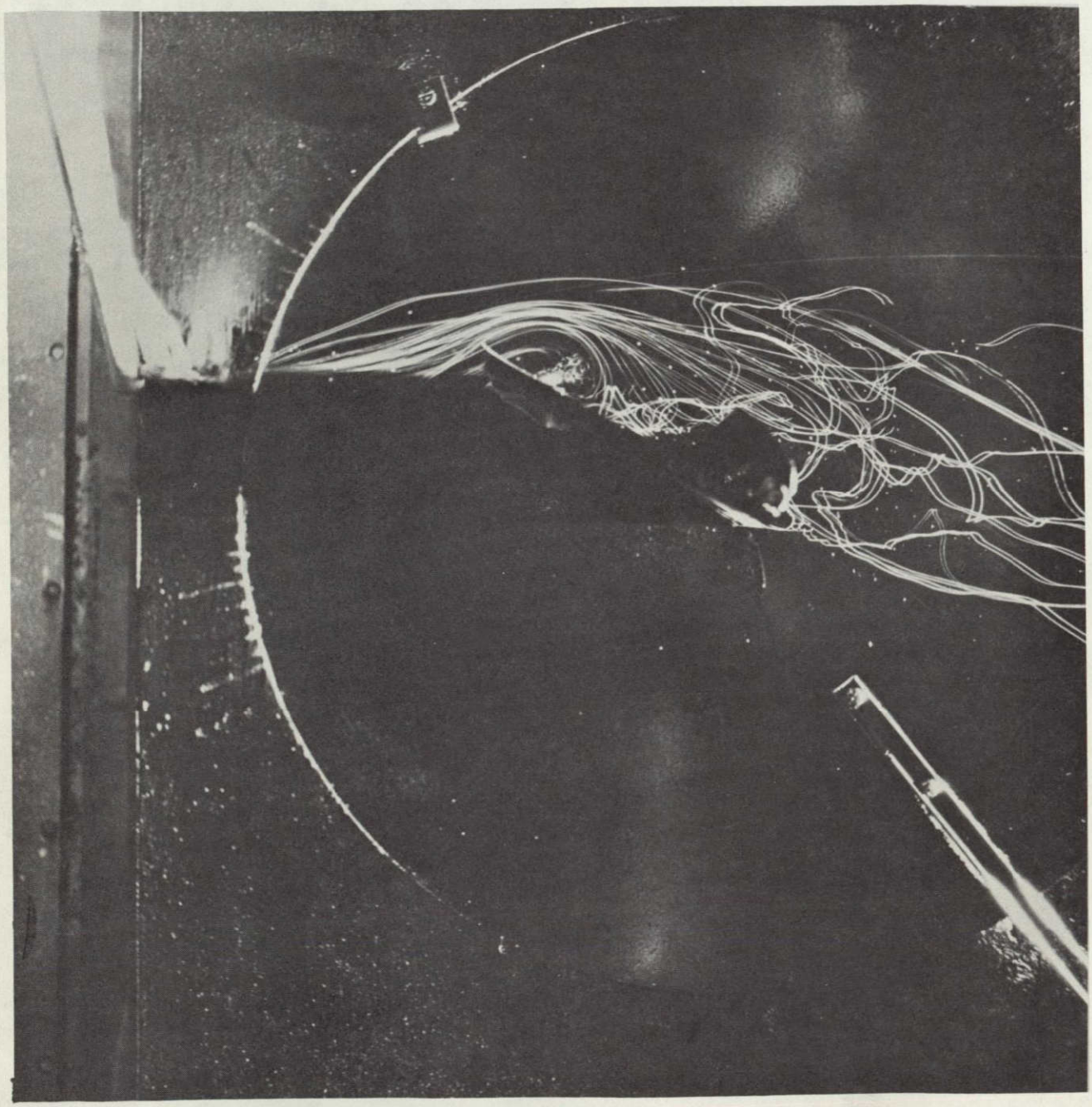

Figure 59. - Spanwise blowing on the rectangular wing without LE flap for $\alpha = 30^{0}$ and $C_{\mu} = 0.30$; sharp LE; $\delta_{TE} = 30^{0}$; $x_n/c_r = 0.40$; $h/d = 1.0$.

Blowing On

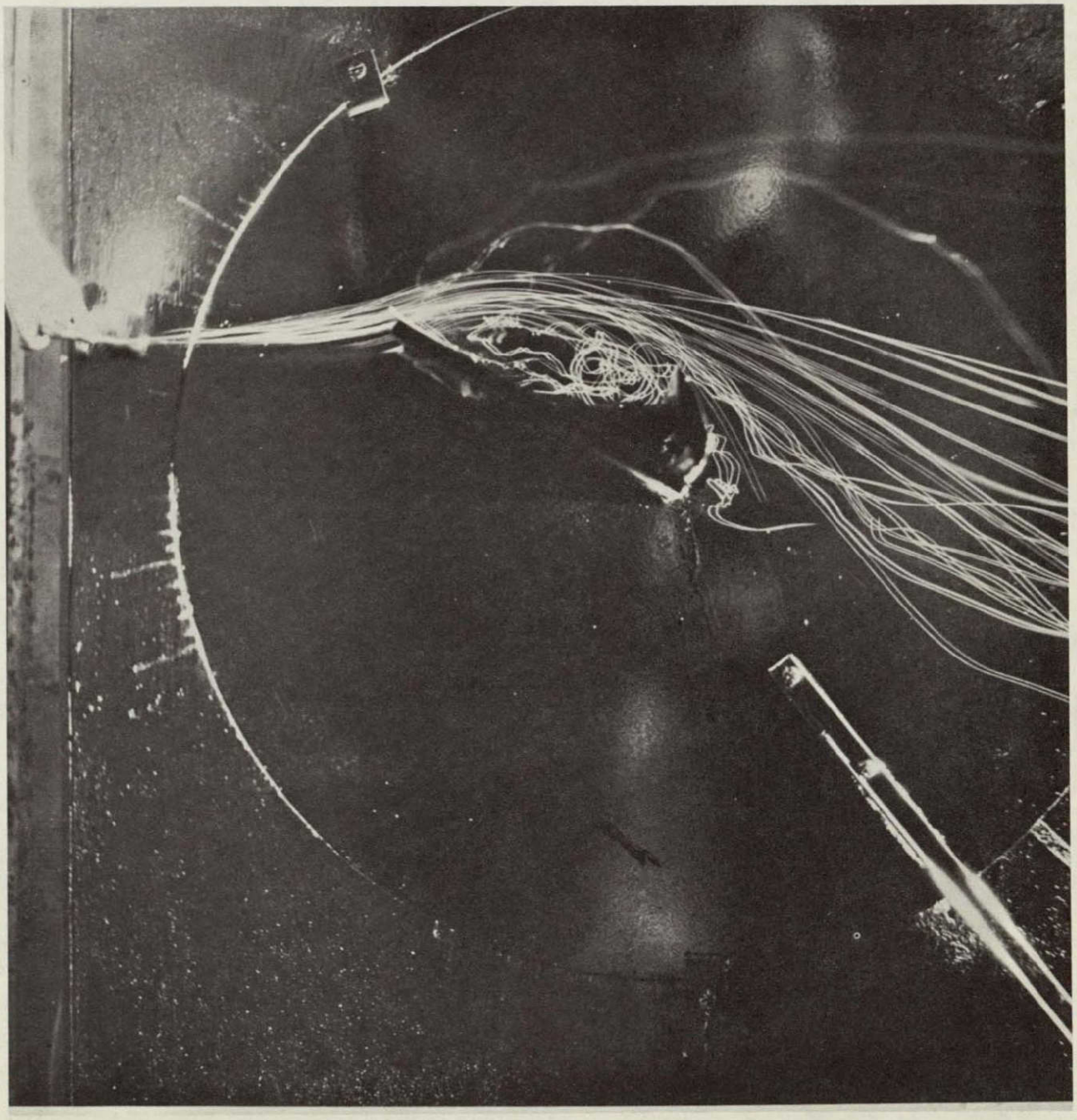

Figure 60. - Spanwise blowing on the rectangular wing without LE flap for $\alpha = 30^0$ and $C_\mu = 0.35$; sharp LE; $\delta_{TE} = 60^0$; $x_n/c_r = 0.40$; $h/d = 1.0$.

Blowing On

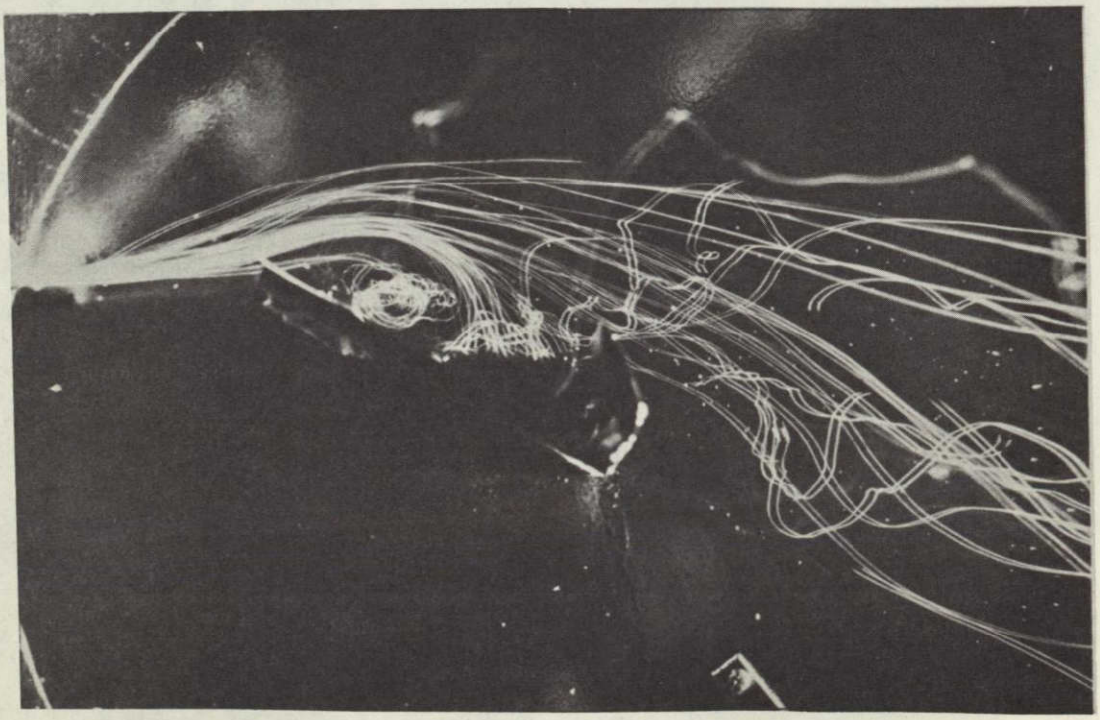

Figure 61. - Spanwise blowing on the rectangular wing without LE flap for $\alpha = 30^{0}$ and $C_{\mu} = 0.45$; sharp LE ; $\delta_{TE} = 60^{0}$; $x_n/c_r = 0.40$; $h/d = 1.0$.

Blowing On

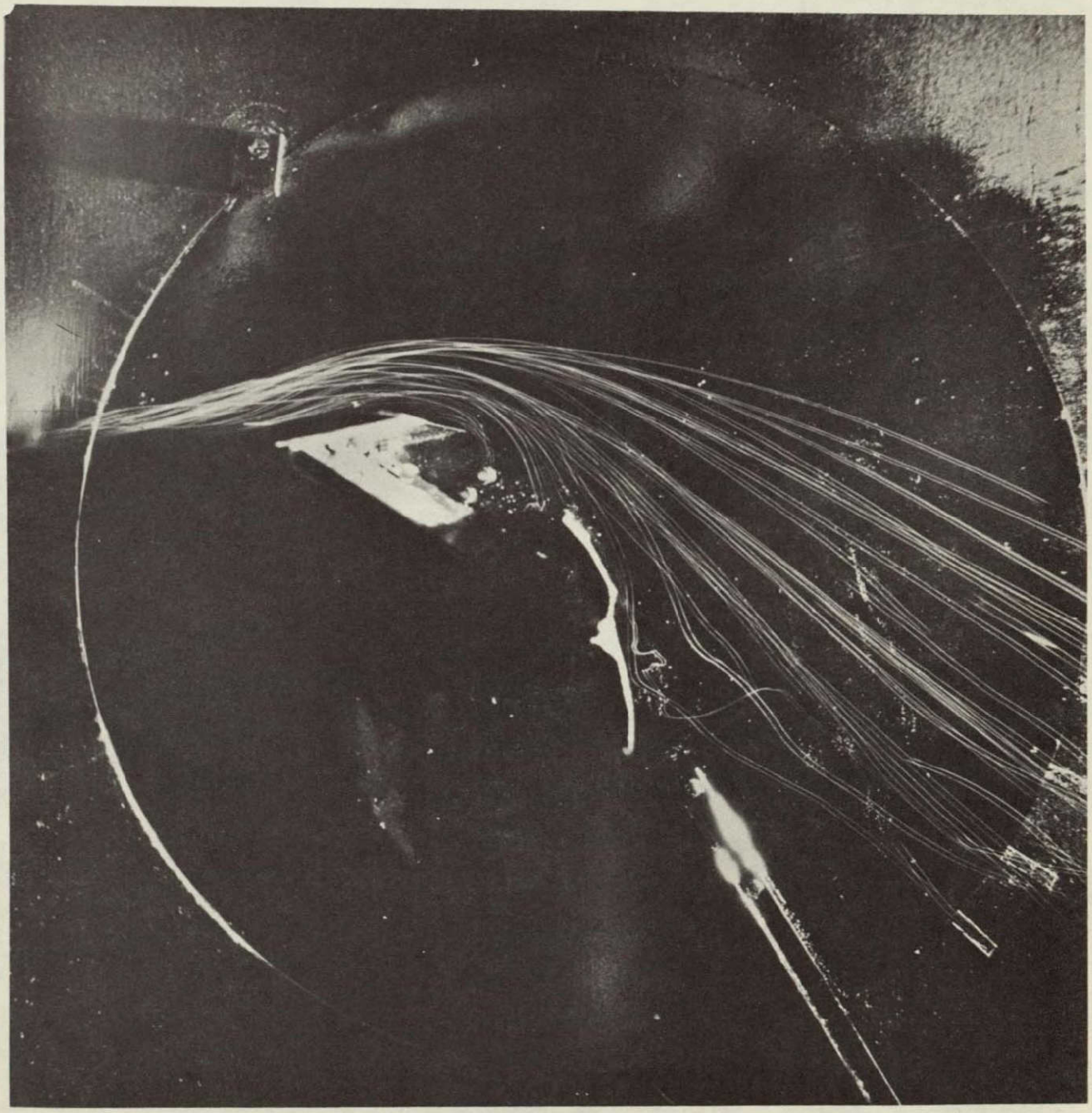

Figure 62. - Spanwise blowing from low nozzle location on the rectangular wing for $\alpha = 30^0$ and $C_\mu = 0.45$; $\delta_{LE} = \delta_{TE} = 45^0$; $x_n/c_r = 0.40$; $h/d = 1.0$.

Blowing On

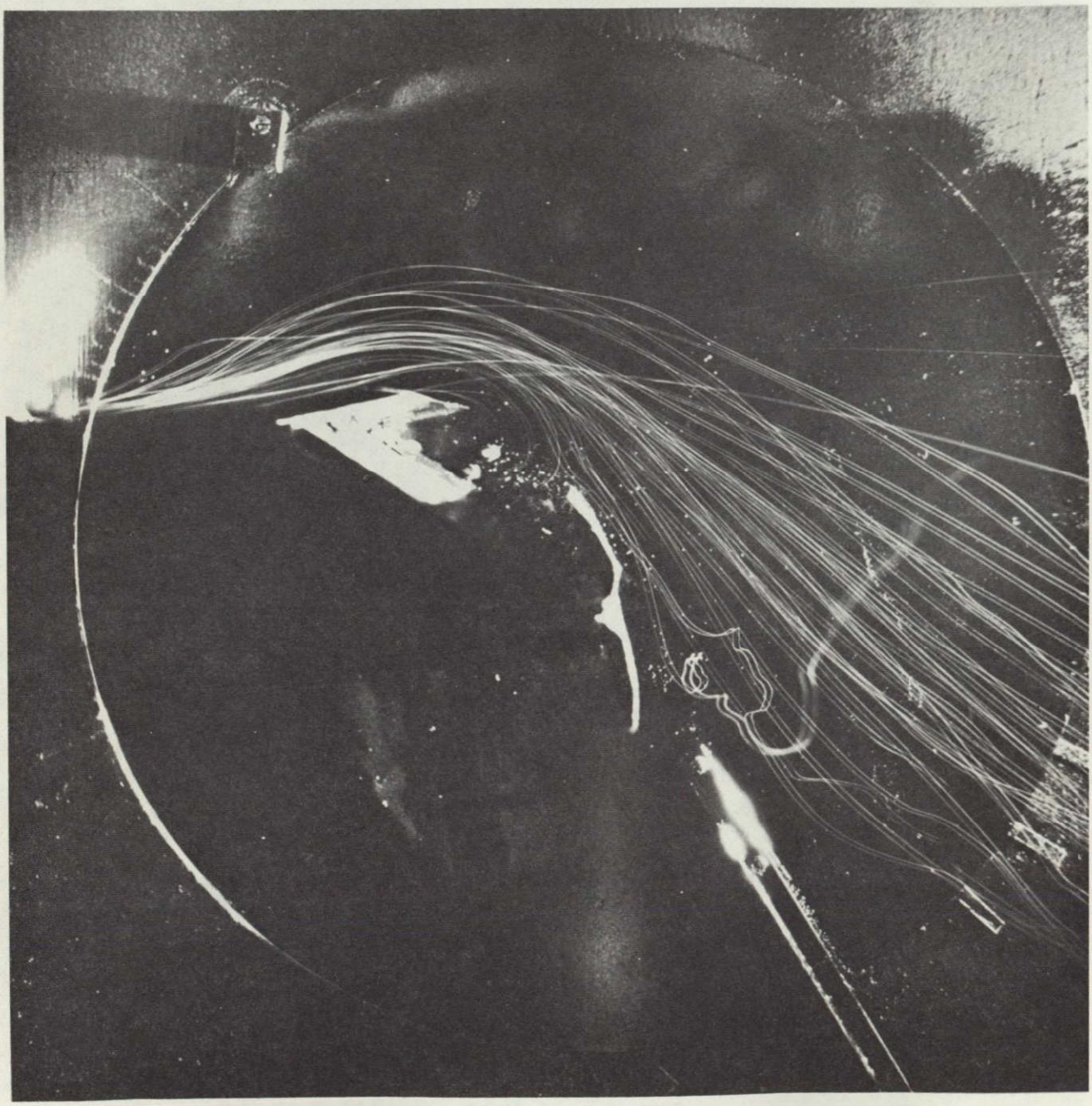

Figure 63. - Spanwise blowing from high nozzle location over the rectangular wing for $\alpha = 30^{o}$ and $C_{\mu} = 0.45$; $\delta_{LE} = \delta_{TE} = 45^{o}$; $x_n/c_r = 0.40$; $h/d = 4.0$.

Blowing On

Figure 64. - Spanwise blowing from low nozzle location on the rectangular wing for $\alpha = 30^{0}$ and $C_{\mu} = 0.50$; $\delta_{LE} = \delta_{TE} = 45^{0}$; $x_n/c_r = 0.40$; $h/d = 1.0$.

Blowing On

Figure 65. - Spanwise blowing from high nozzle location over the rectangular wing for $\alpha = 30^0$ and $C_\mu = 0.50$; $\delta_{LE} = \delta_{TE} = 45^0$; $x_n/c_r = 0.40$; $h/d = 4.0$.

Blowing On

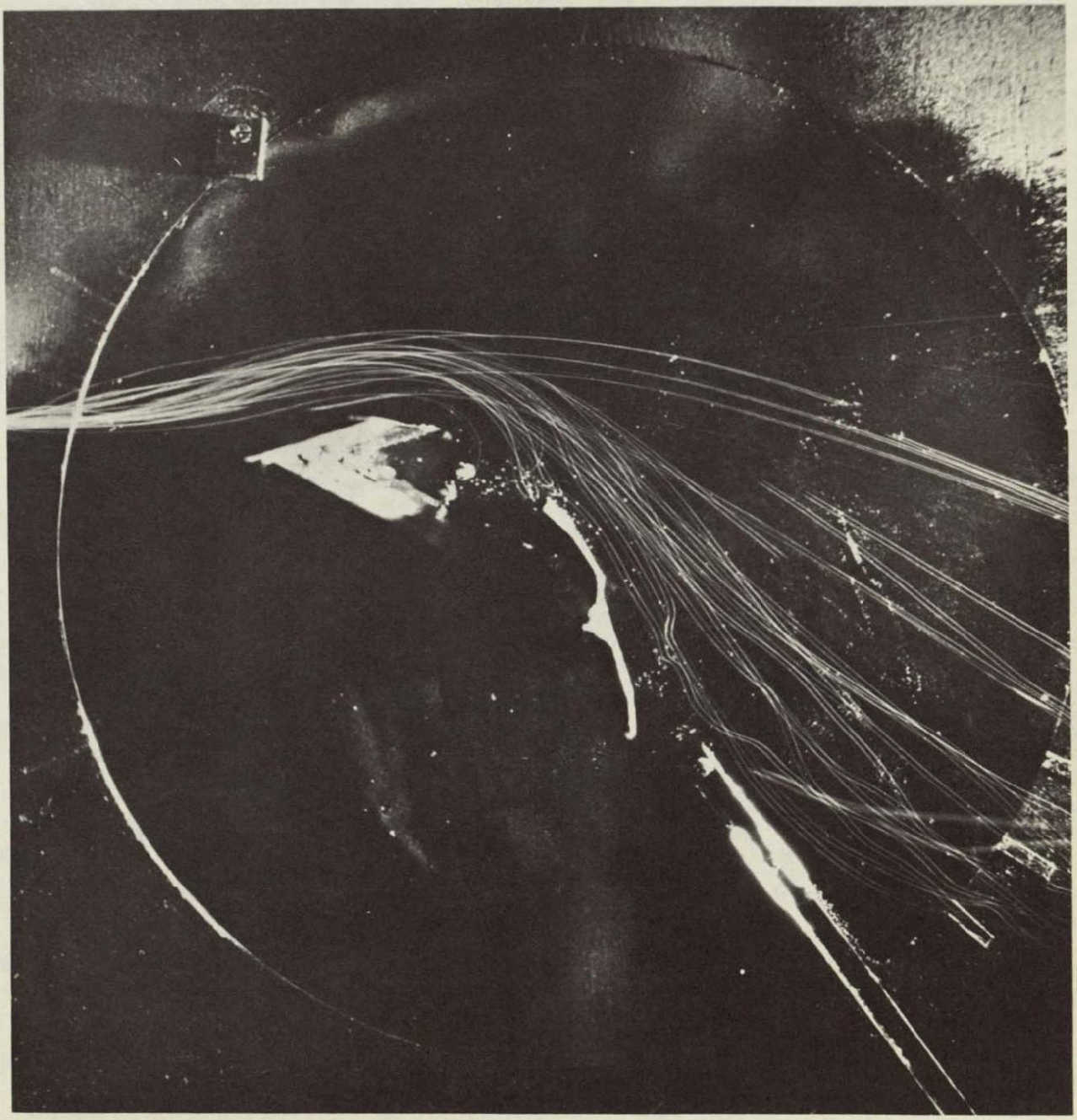

Figure 66. - Spanwise from low nozzle location on the rectangular wing for $\alpha = 30^0$ and $C_\mu = 0.57$; $\delta_{LE} = \delta_{TE} = 45^0$; $x_n/c_r = 0.40$; $h/d = 1.0$.

ORIGINAL PAGE IS
OF POOR QUALITY

Blowing On

Figure 67. - Spanwise blowing from high nozzle location over the rectangular wing for $\alpha = 30^0$ and $C_\mu = 0.57$; $\delta_{LE} = \delta_{TE} = 45^0$; $x_n/c_r = 0.40$; $h/d = 4.0$.

Blowing On

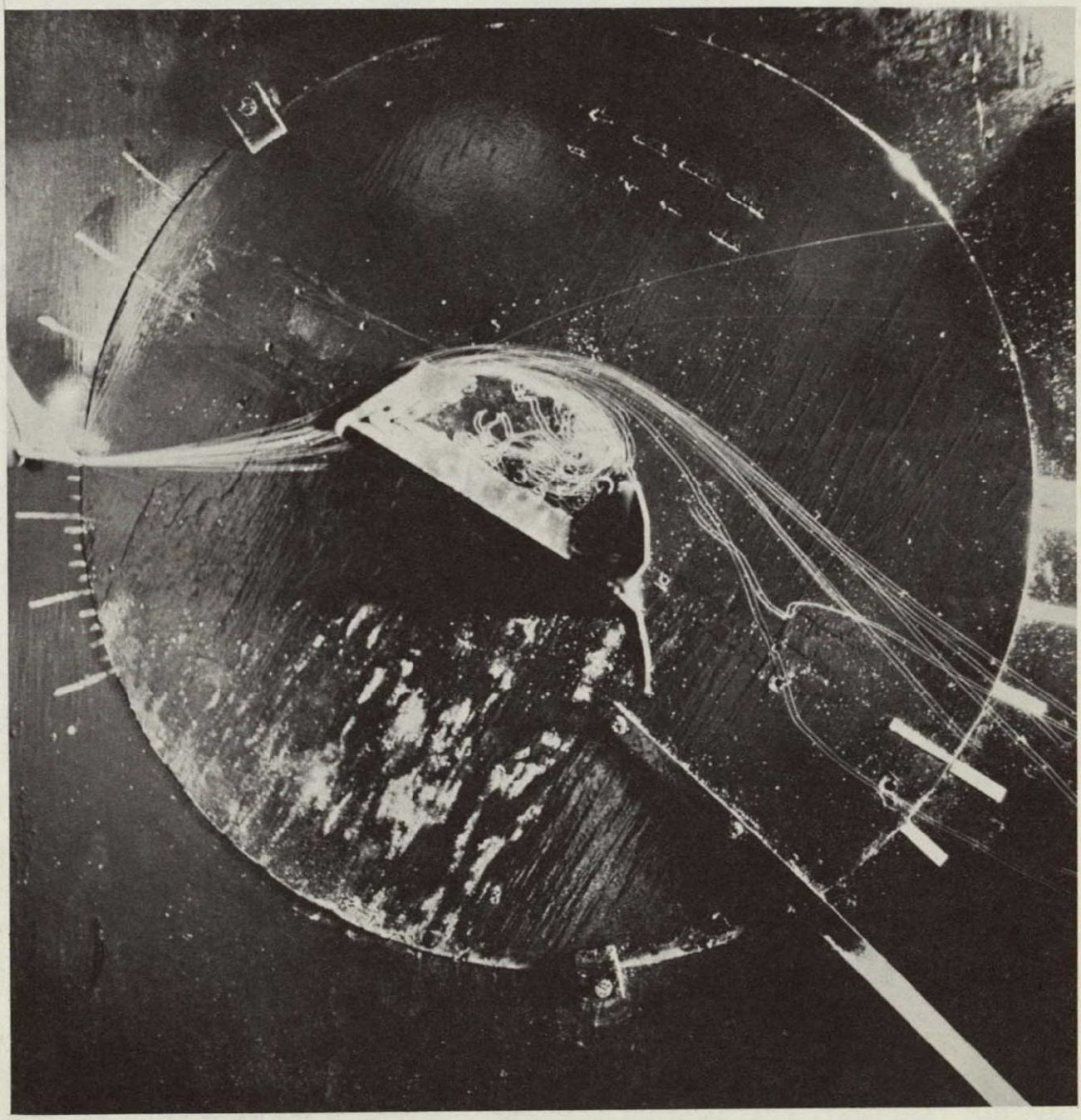

Figure 68.- Spanwise blowing from low nozzle location on the rectangular wing for $\alpha = 30^{0}$ and $C_{\mu} = 0.40$; $\delta_{LE} = \delta_{TE} = 60^{0}$; $x_n/c_r = 0.40$; $h/d = 1.0$.

Blowing On

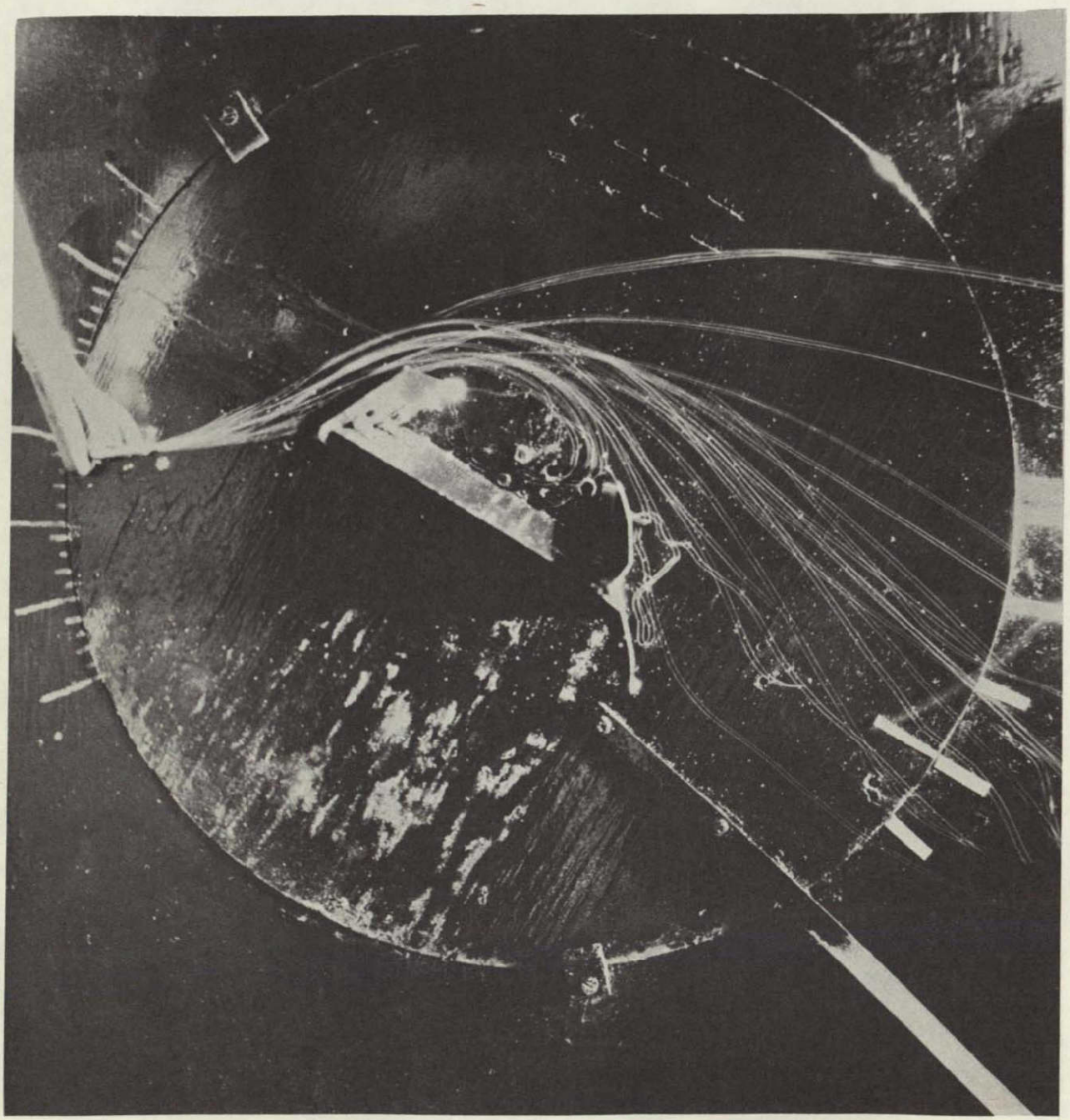

Figure 69. - Spanwise blowing from high nozzle location over the rectangular wing for $\alpha = 30^0$ and $C_\mu = 0.40$; $\delta_{LE} = \delta_{TE} = 60^0$; $x_n/c_r = 0.40$; $h/d = 4.0$.

Blowing On

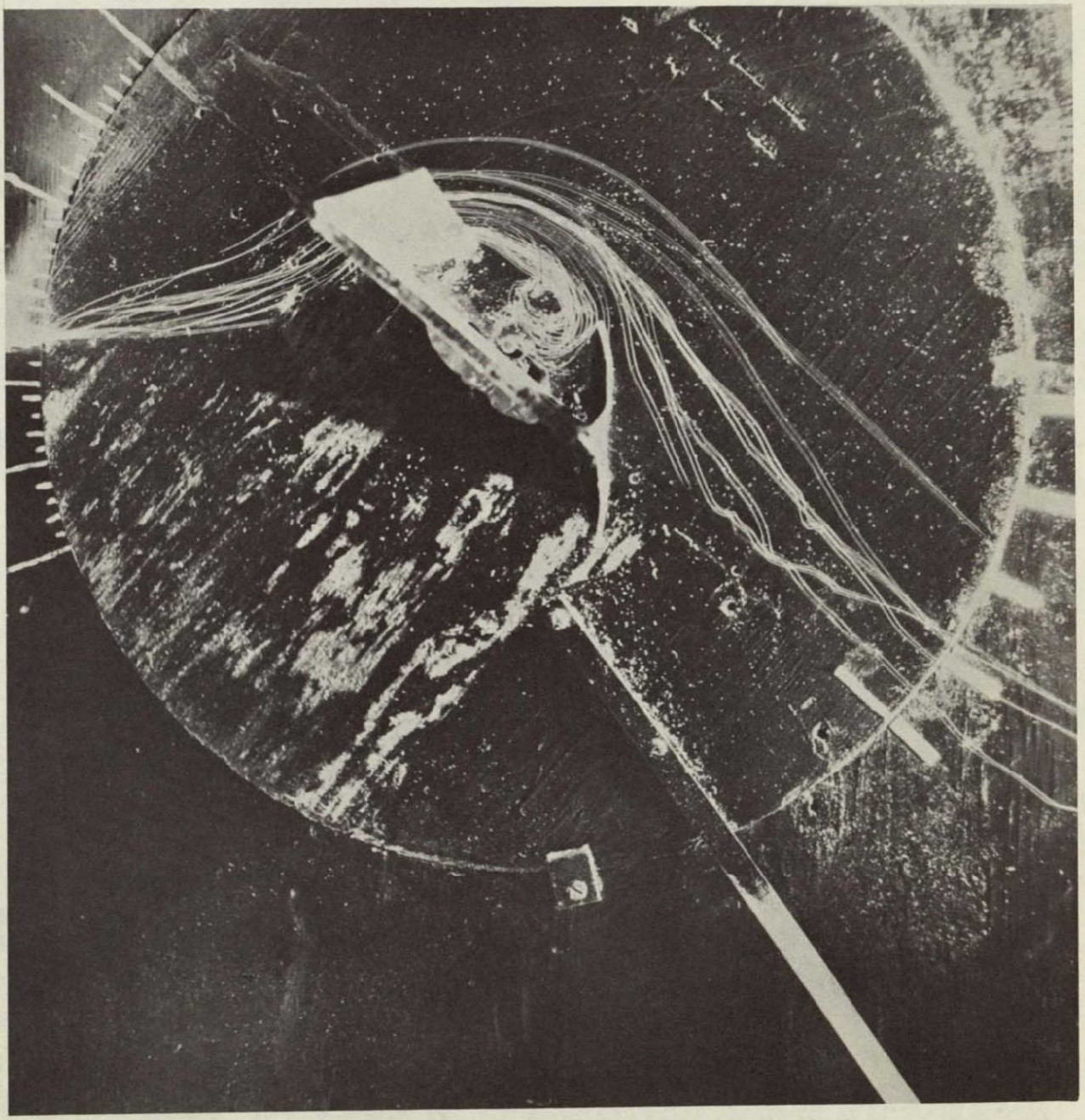

Figure 70. - Spanwise blowing from low nozzle location on the rectangular wing for $\alpha = 40^{0}$ and $C_{\mu} = 0.60$; $\delta_{LE} = \delta_{TE} = 60^{0}$; $x_n/c_r = 0.40$; $h/d = 1.0$.

Blowing On

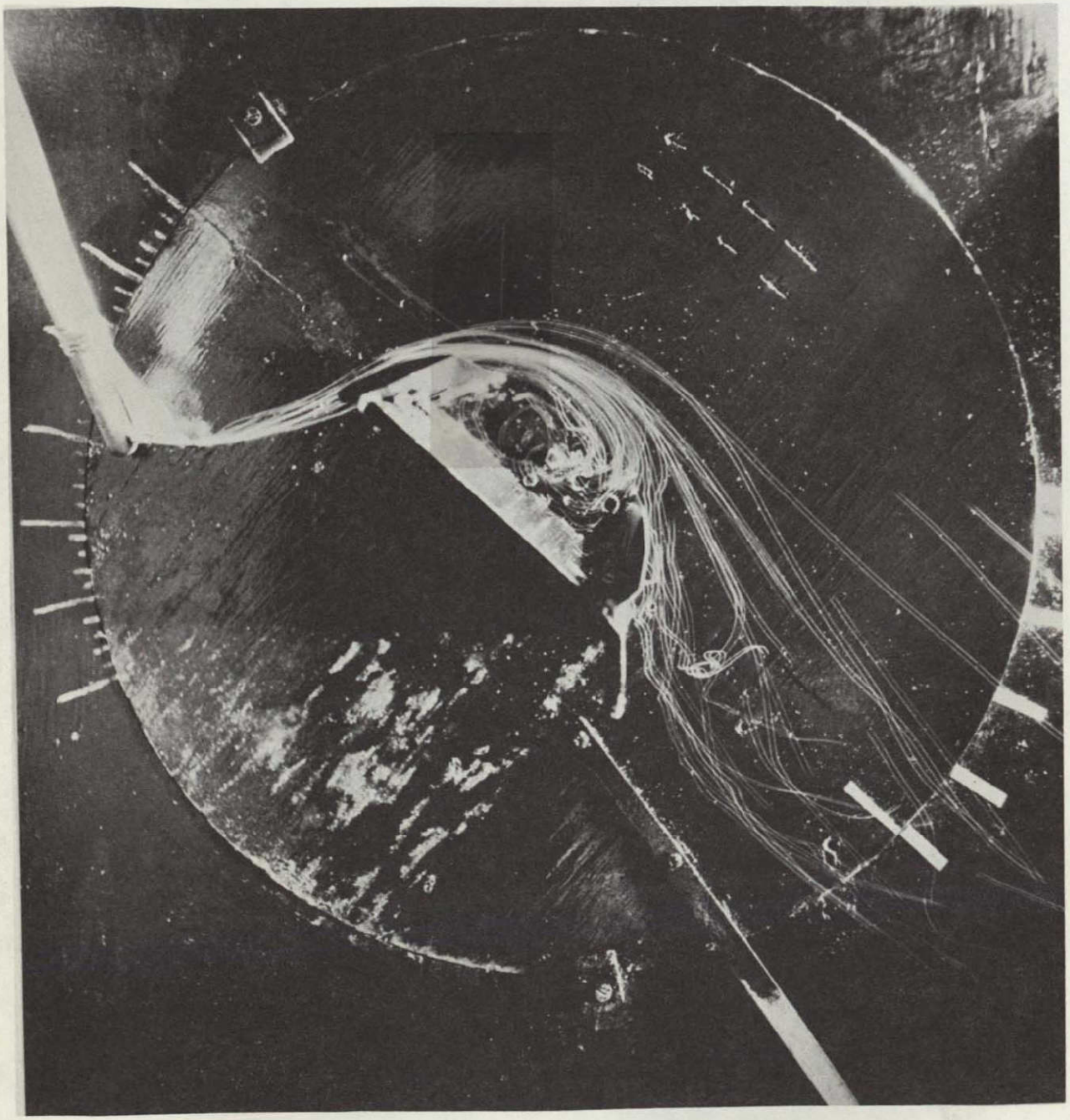

Figure 71. - Spanwise blowing from high nozzle location over the rectangular wing for $\alpha = 40^0$ and $C_\mu = 0.60$; $\delta_{LE} = \delta_{TE} = 60^0$; $x_n/c_r = 0.40$; $h/d = 4.0$.

Blowing Off

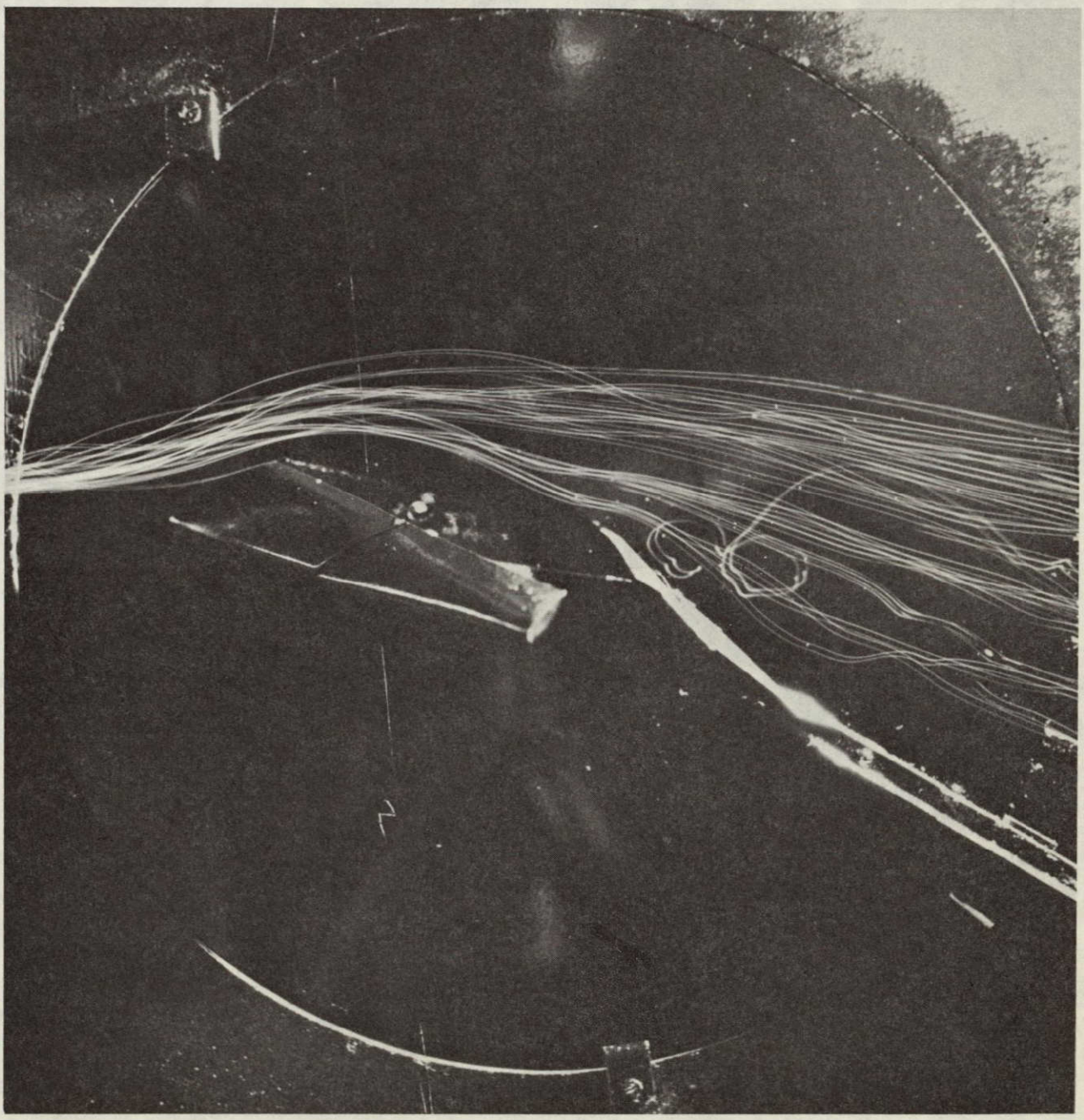

Figure 72. - Trapezoidal wing with 45^{0} leading edge sweep for $\alpha = 10^{0}$ and blowing off; $\delta_{LE} = \delta_{TE} = 60^{0}$.

ORIGINAL PAGE IS
OF POOR QUALITY

Blowing On

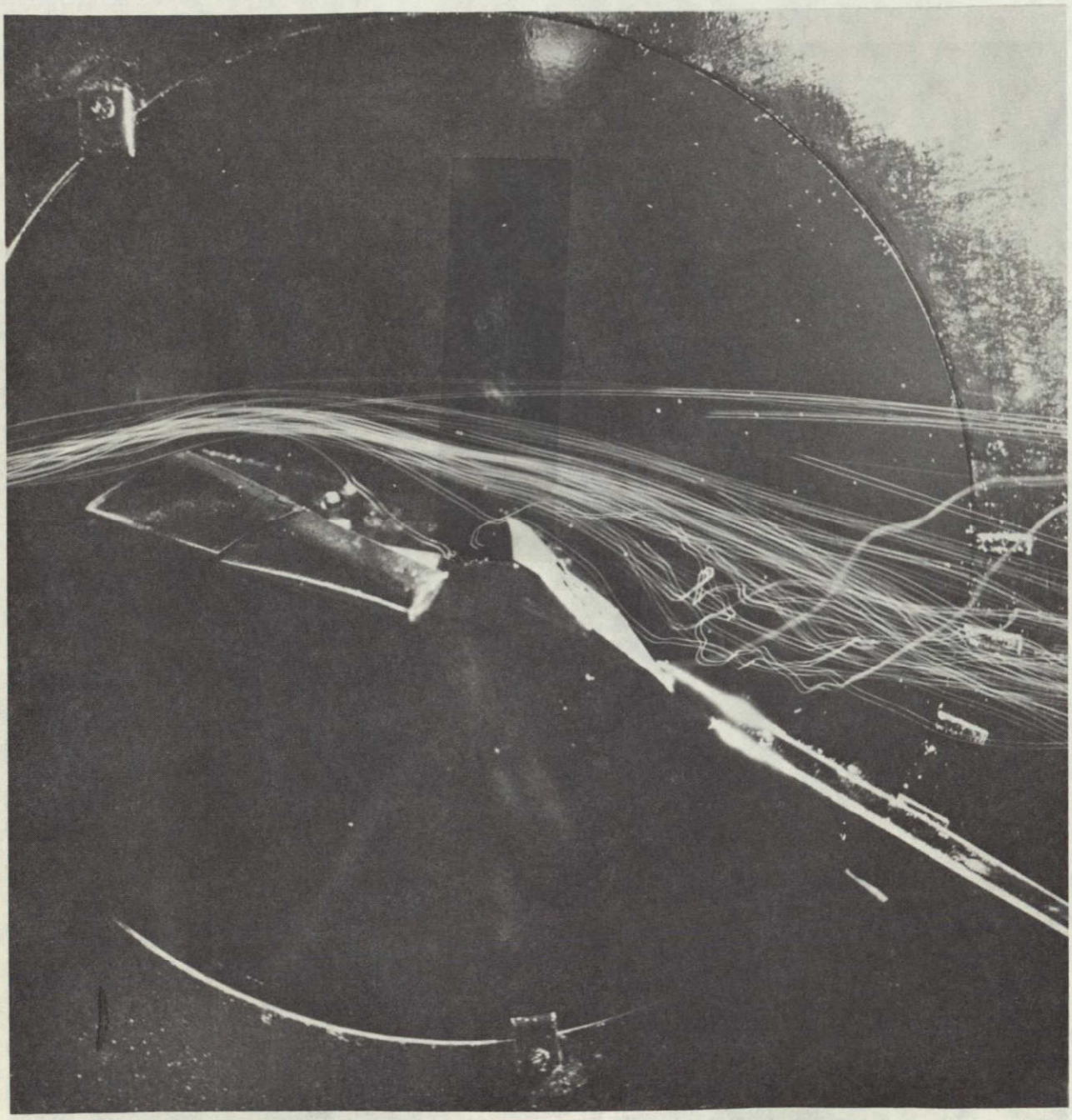

Figure 73. - Spanwise blowing on the 45^{0} swept trapezoidal wing for $\alpha = 10^{0}$ and $C_{\mu} = 0.04$; $\delta_{LE} = \delta_{TE} = 60^{0}$; $x_n/c_r = 0.40$; $h/d = 1.0$.

Blowing On

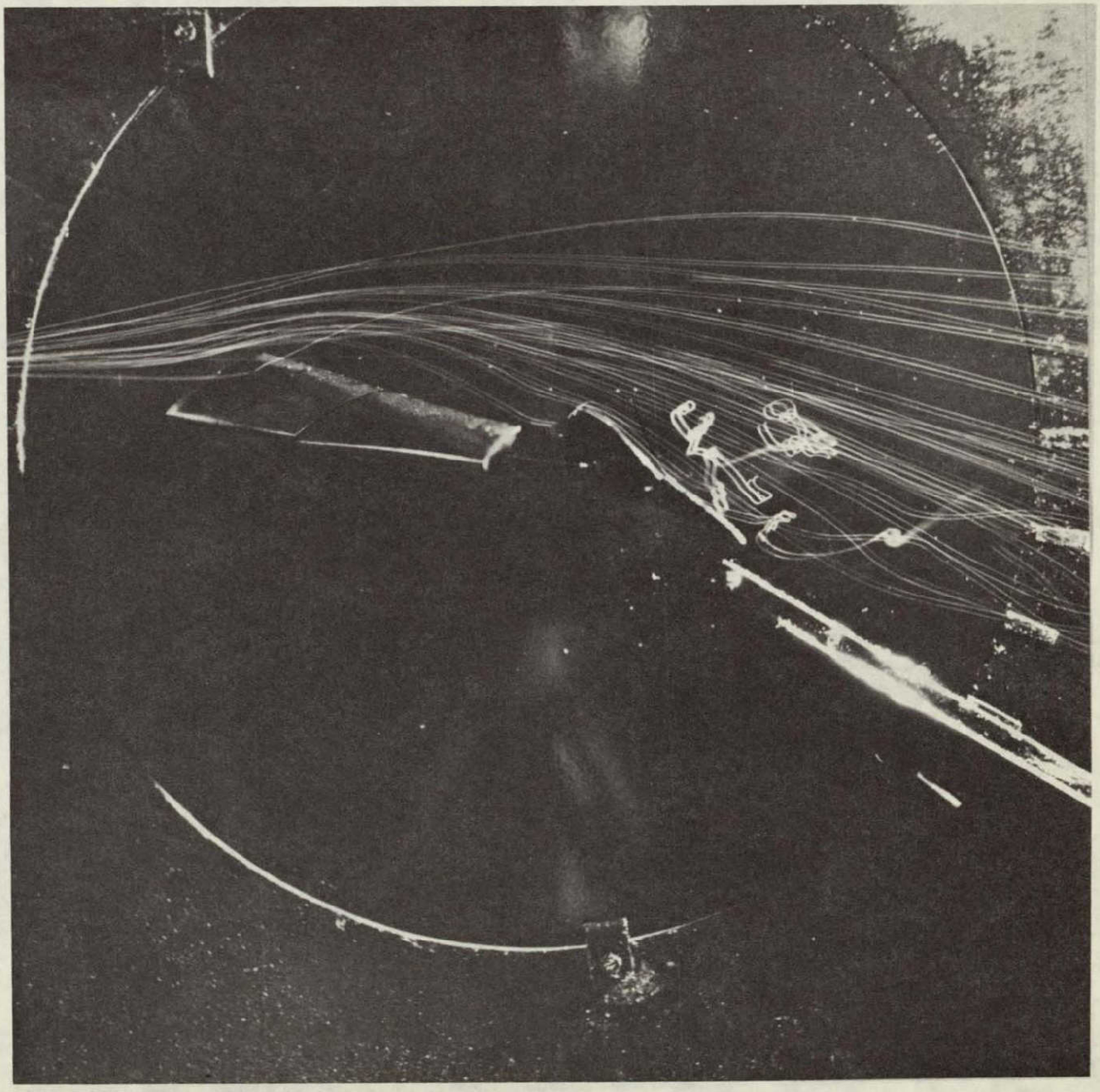

Figure 74. - Spanwise blowing on the 45^{o} swept trapezoidal wing for $\alpha = 10^{o}$ and $C_{\mu} = 0.057$; $\delta_{LE} = \delta_{TE} = 60^{o}$; $x_n/c_r = 0.40$; $h/d = 1.0$.

Blowing Off

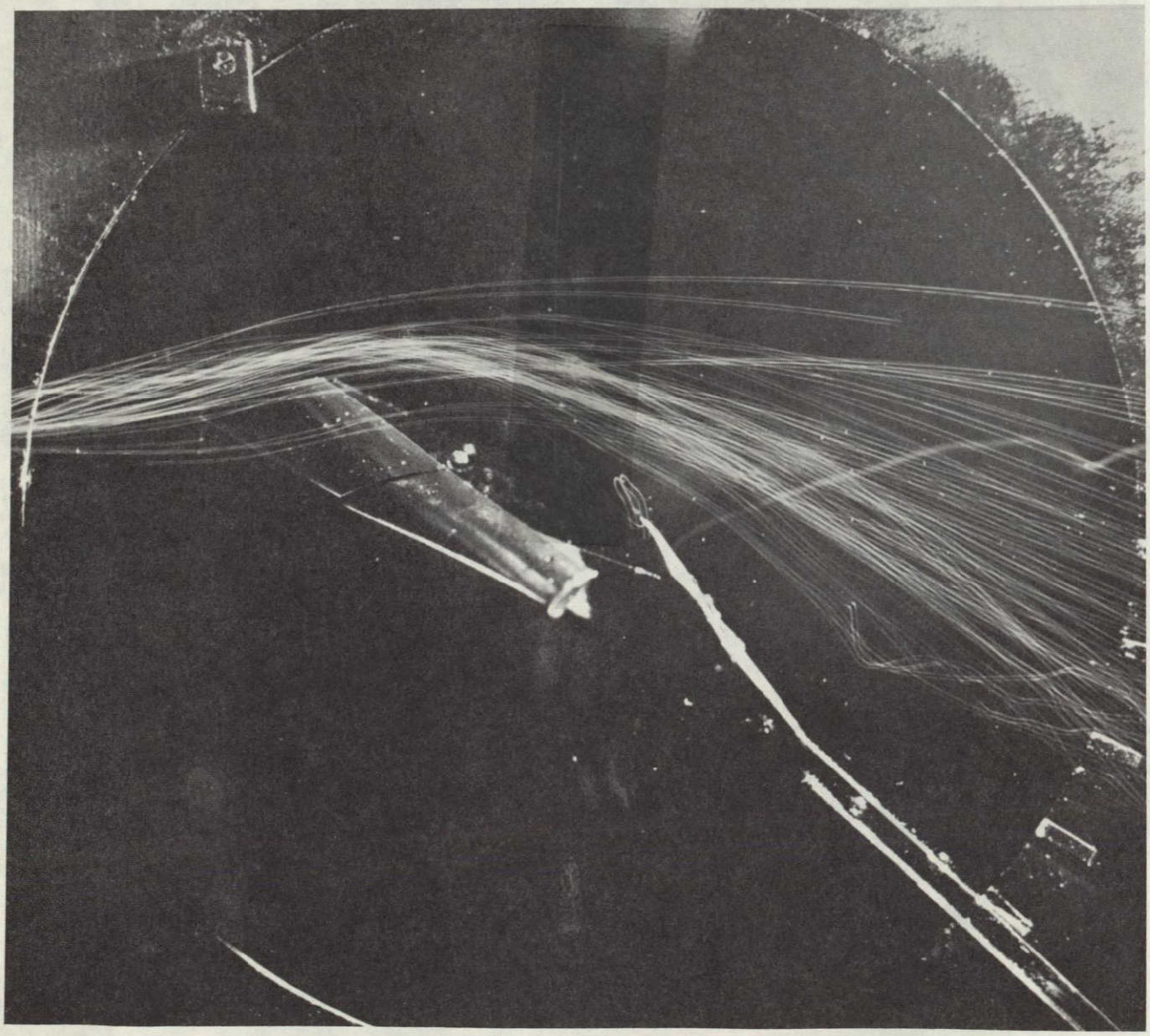

Figure 75. - Trapezoidal wing with 45^{0} leading edge sweep for $\alpha = 20^{0}$ and blowing off; $\delta_{LE} = \delta_{TE} = 60^{0}$.

Blowing On

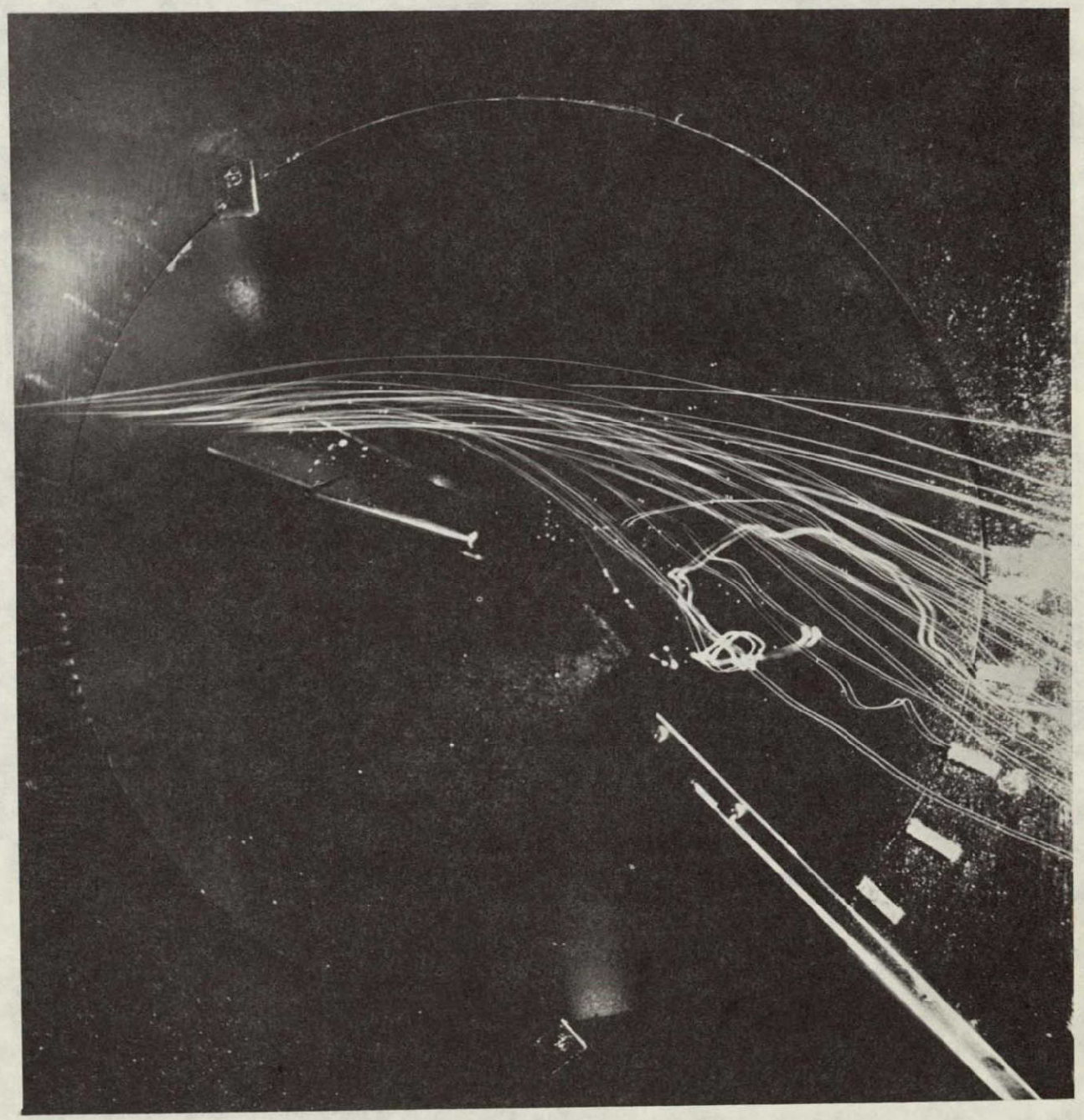

Figure 76. - Spanwise blowing on the 45^0 swept trapezoidal wing for $\alpha = 20^0$ and $C_\mu = 0.04$; $\delta_{LE} = \delta_{TE} = 60^0$; $x_n/c_r = 0.40$; $h/d = 1.0$.

ORIGINAL PAGE IS
OF POOR QUALITY

Blowing On

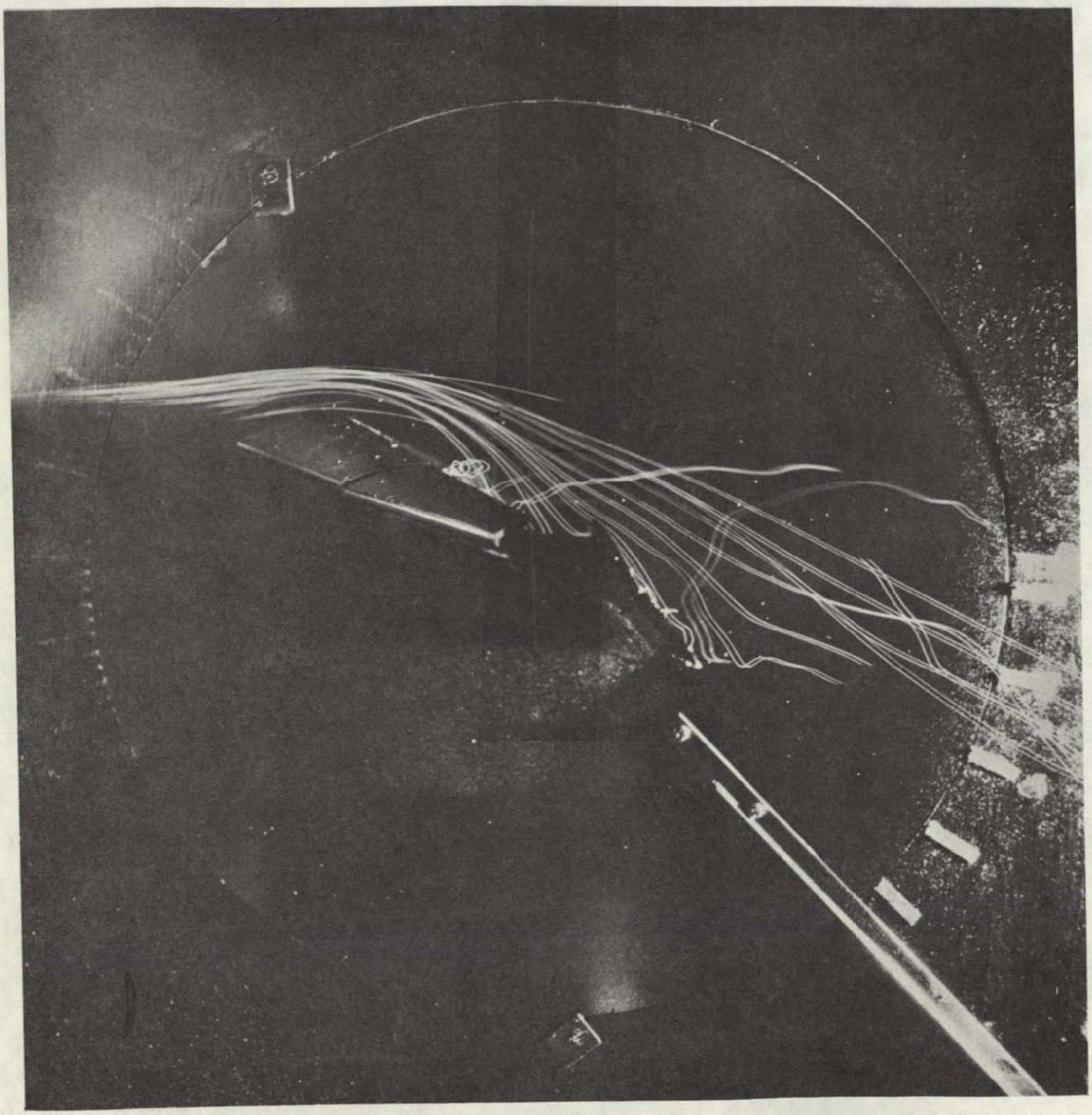

Figure 77.- Spanwise blowing on the 45^{o} swept trapezoidal wing for $\alpha = 20^{o}$ and $C_{\mu} = 0.057$; $\delta_{LE} = \delta_{TE} = 60^{o}$; c $x_n/c_r = 0.40$; $h/d = 1.0$.

Blowing On

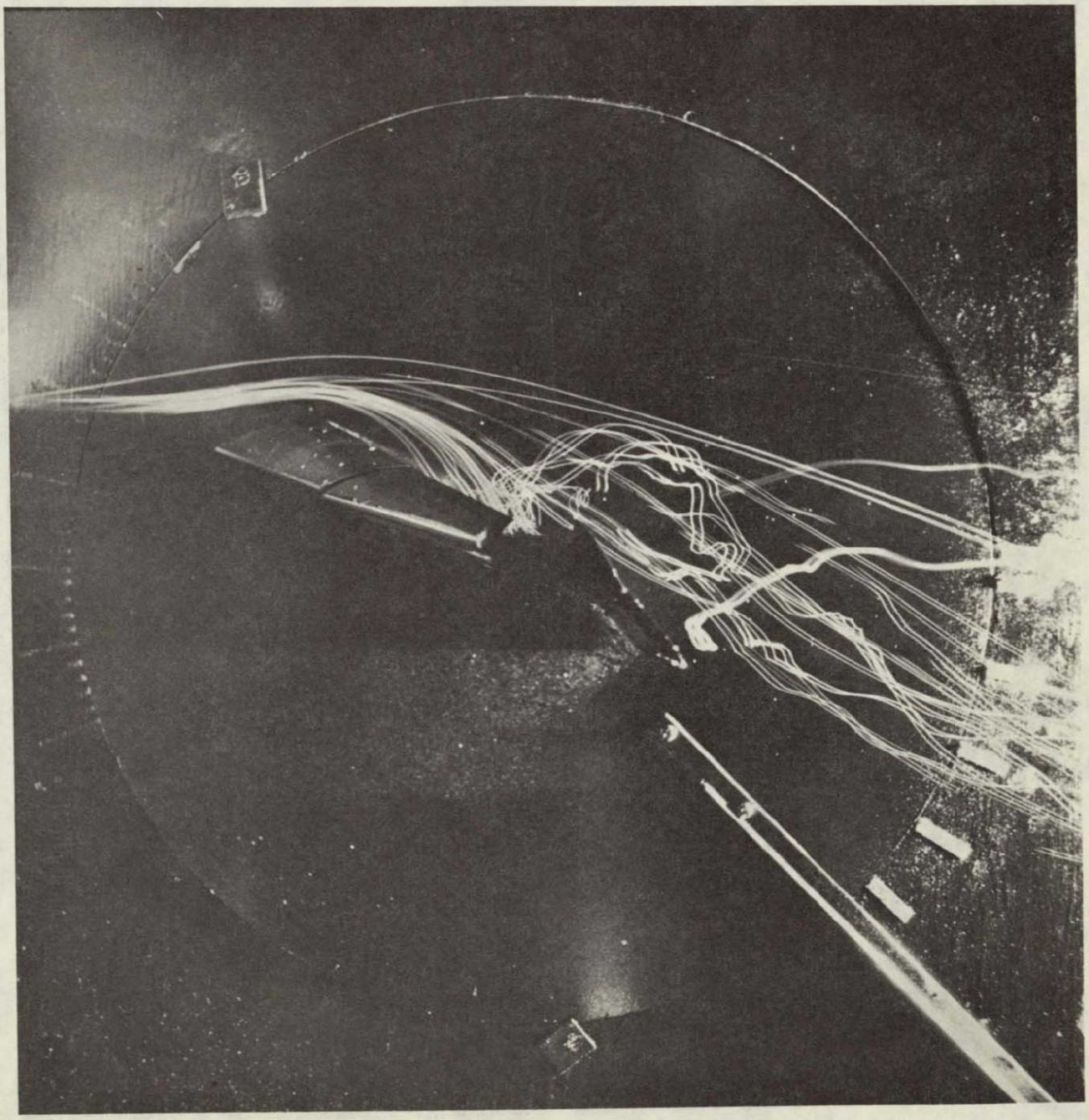

Figure 78. - Spanwise blowing on the 45° swept trapezoidal wing for $\alpha = 20^{\circ}$ and $C_{\mu} = 0.075$; $\delta_{LE} = \delta_{TE} = 60^{\circ}$; $x_n/c_r = 0.40$; $h/d = 1.0$.

Blowing Off

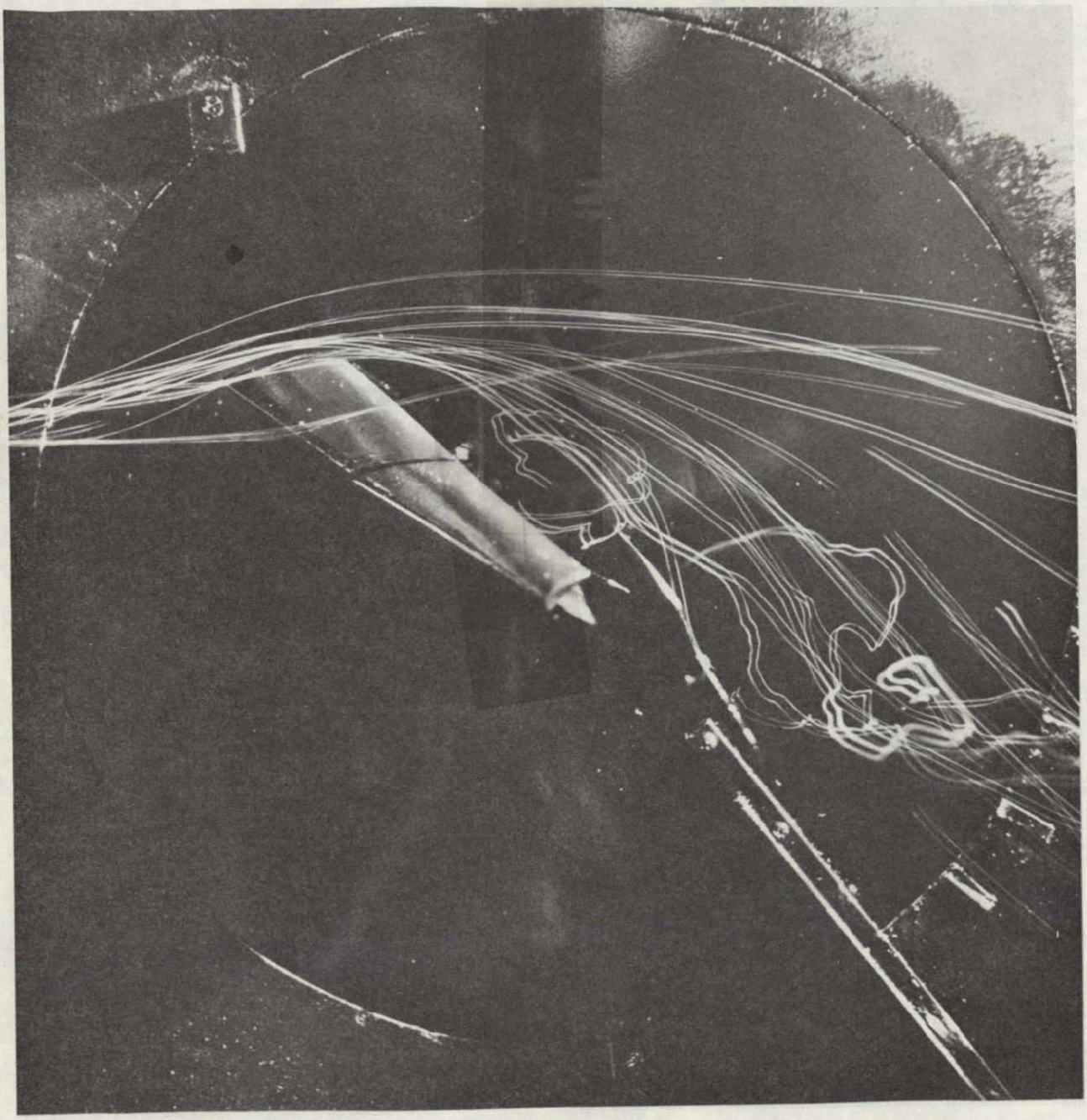

Figure 79.- Trapezoidal wing with 45^{o} leading edge sweep for $\alpha = 30^{o}$ and blowing off; $\delta_{LE} = \delta_{TE} = 60^{o}$.

Blowing On

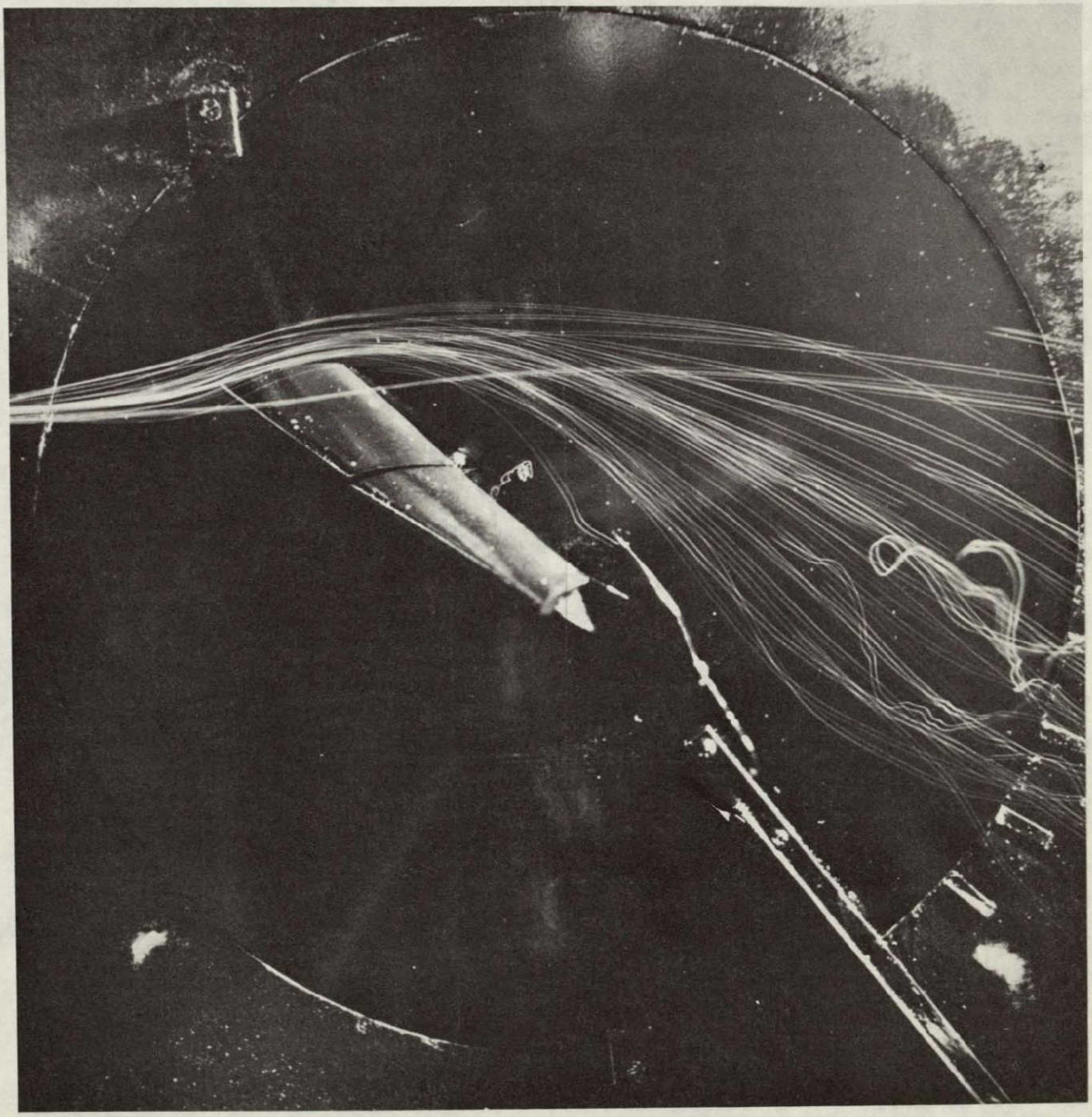

Figure 80. - Spanwise blowing on the 45° swept trapezoidal wing for $\alpha = 30^{\circ}$ and and $C_{\mu} = 0.057$; $\delta_{LE} = \delta_{TE} = 60^{\circ}$; $x_n/c_r = 0.40$; $h/d = 1.0$.

ORIGINAL PAGE IS
OF POOR QUALITY

Blowing On

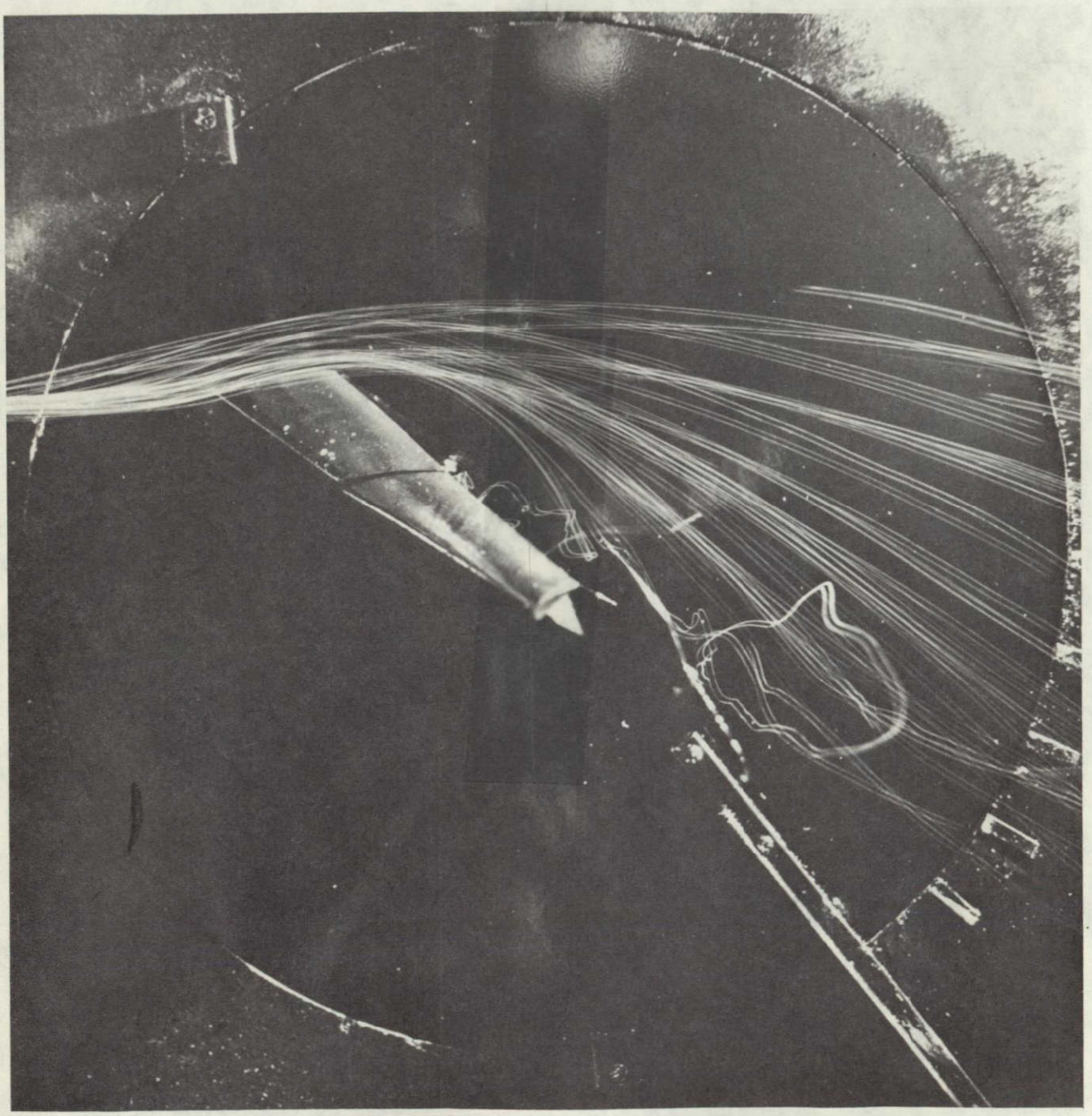

Figure 81. - Spanwise blowing on the 45^{0} swept trapezoidal wing for $\alpha = 30^{0}$ and $C_{\mu} = 0.065$; $\delta_{LE} = \delta_{TE} = 60^{0}$; $x_n/c_r = 0.40$; $h/d = 1.0$.

C.2

Blowing On

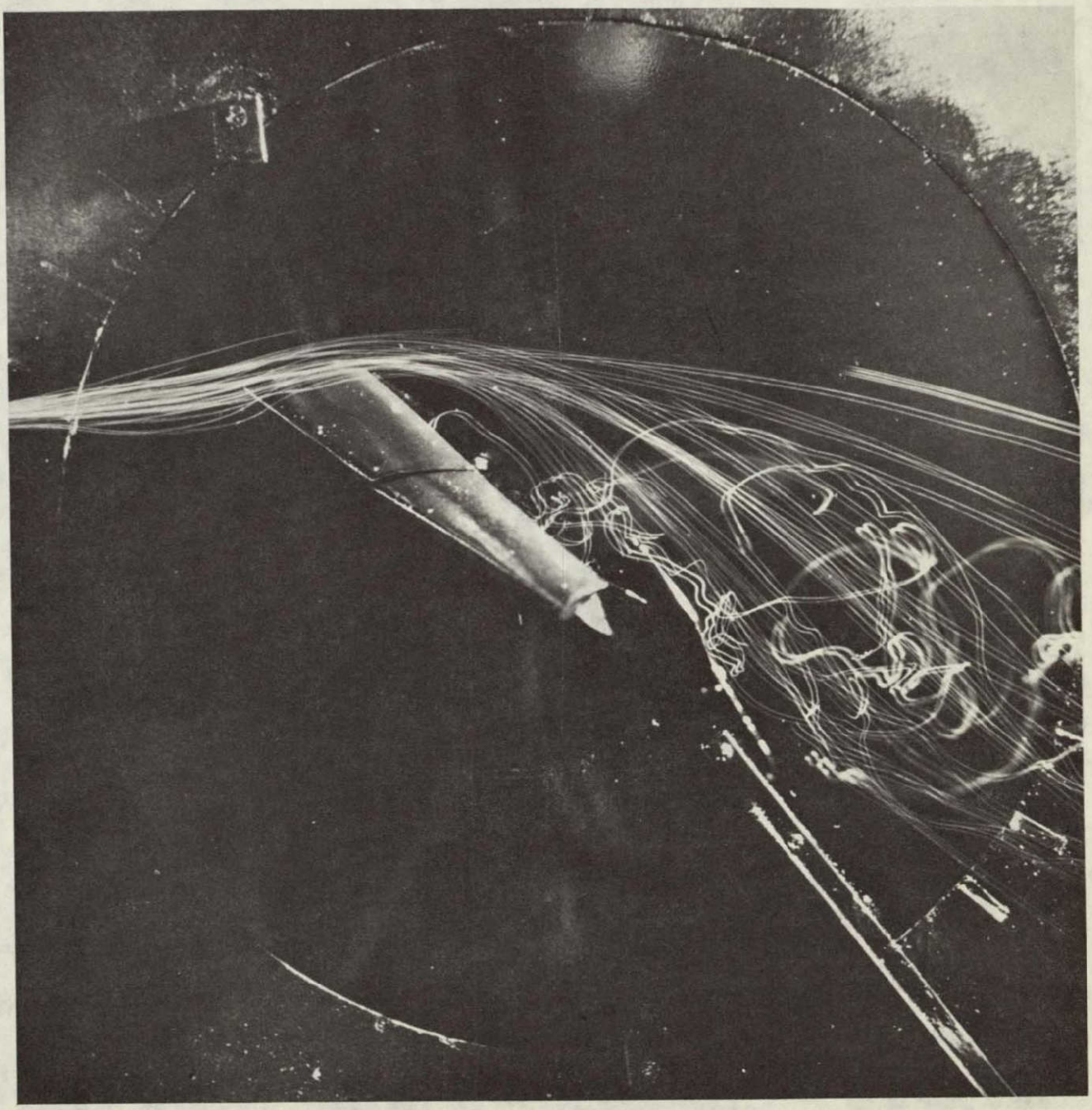

Figure 82. - Spanwise blowing on the 45^{0} swept trapezoidal wing for $\alpha = 30^{0}$ and $C_{\mu} = 0.095$; $\delta_{LE} = \delta_{TE} = 60^{0}$; $x_n/c_r = 0.40$; $h/d = 1.0$.

ORIGINAL PAGE IS
OF POOR QUALITY

Blowing Off

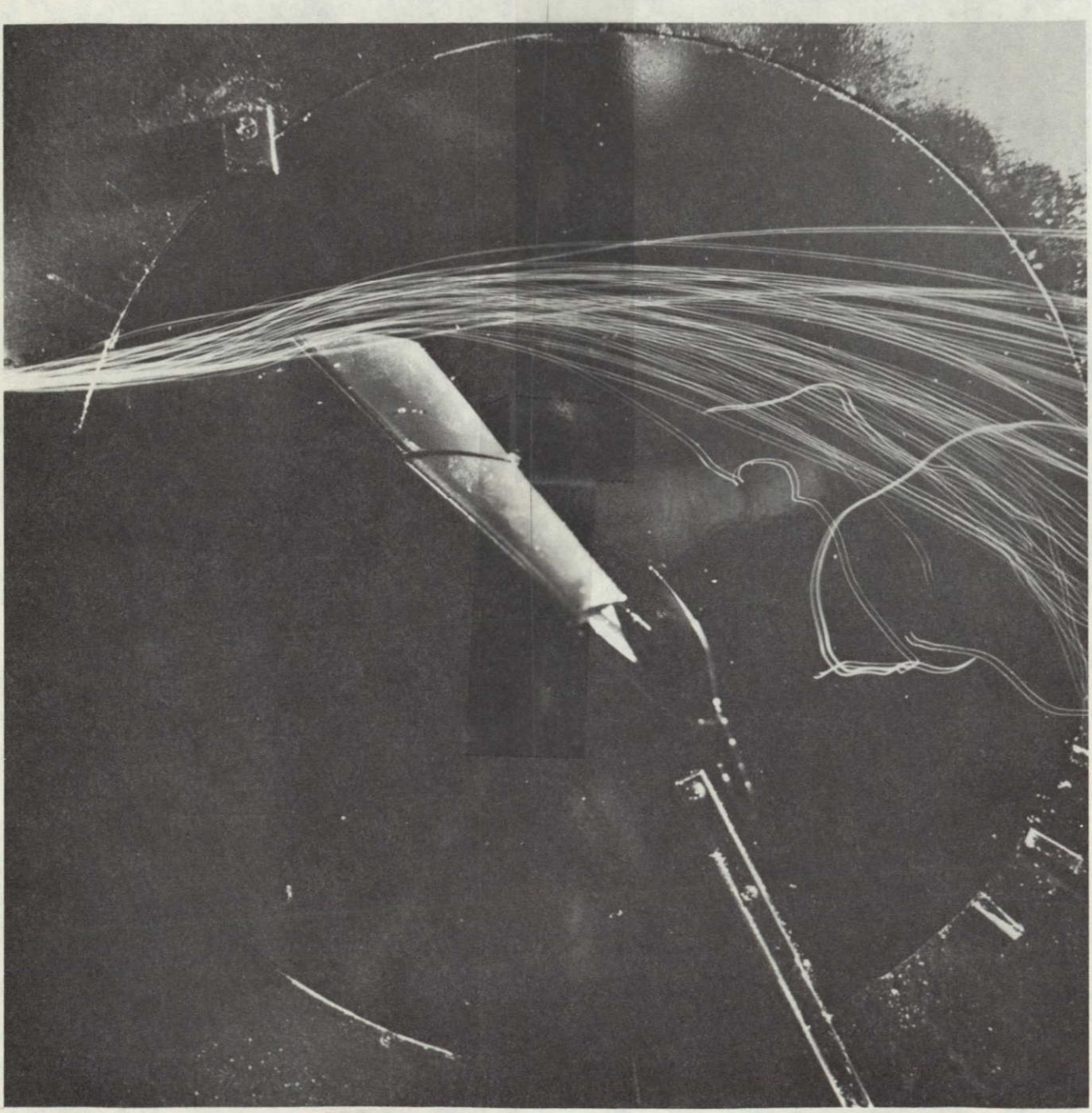

Figure 83. - Trapezoidal wing with 45^{0} leading edge sweep for $\alpha = 40^{0}$ and blowing off; $\delta_{LE} = \delta_{TE} = 60^{0}$.

Blowing On

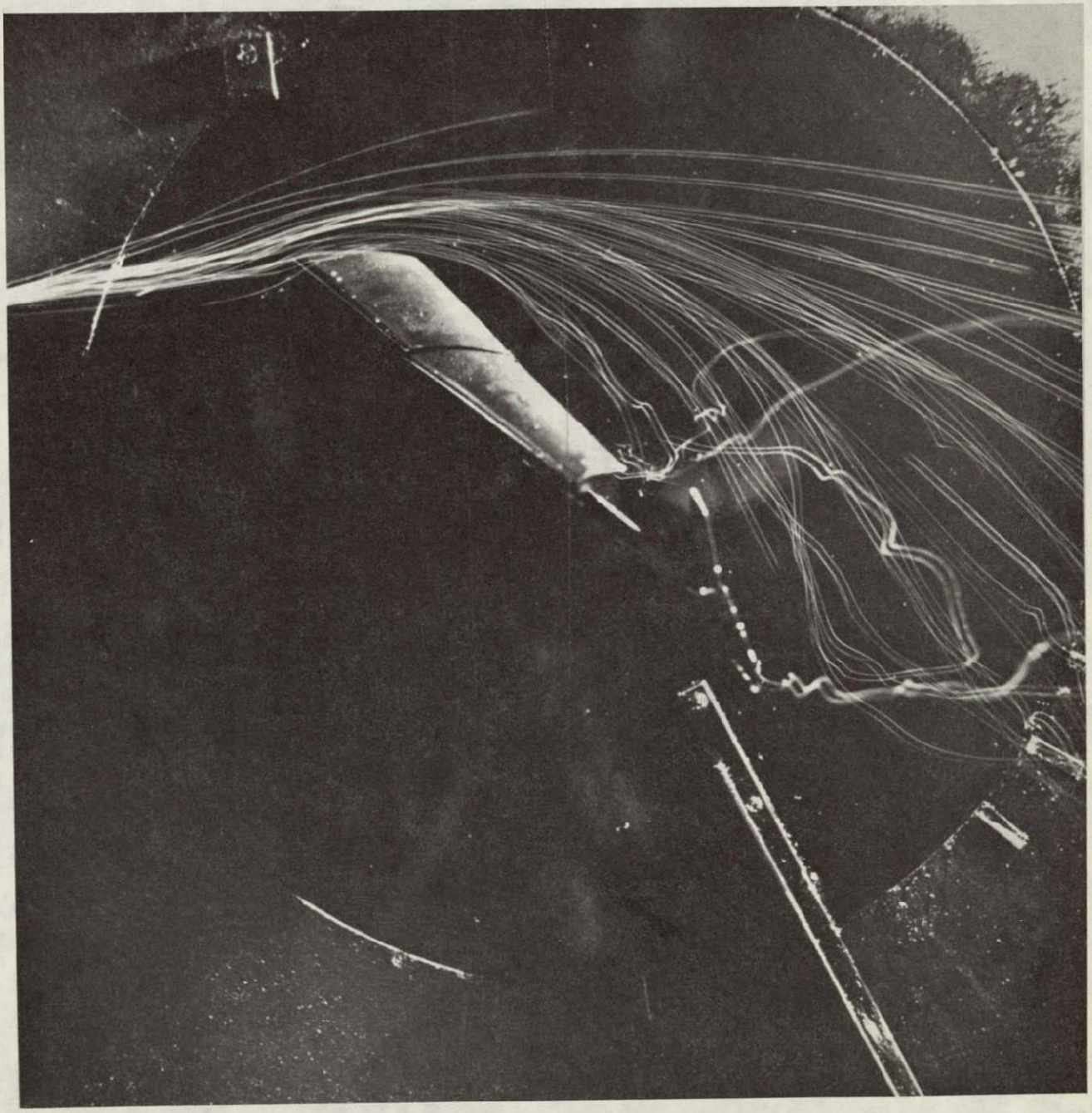

Figure 84. - Spanwise blowing on the 45^{0} swept trapezoidal wing for $\alpha = 40^{0}$ and $C_{\mu} = 0.057$; $\delta_{LE} = \delta_{TE} = 60^{0}$; $x_n/c_r = 0.40$; $h/d = 1.0$.

ORIGINAL PAGE IS
OF POOR QUALITY

Blowing On

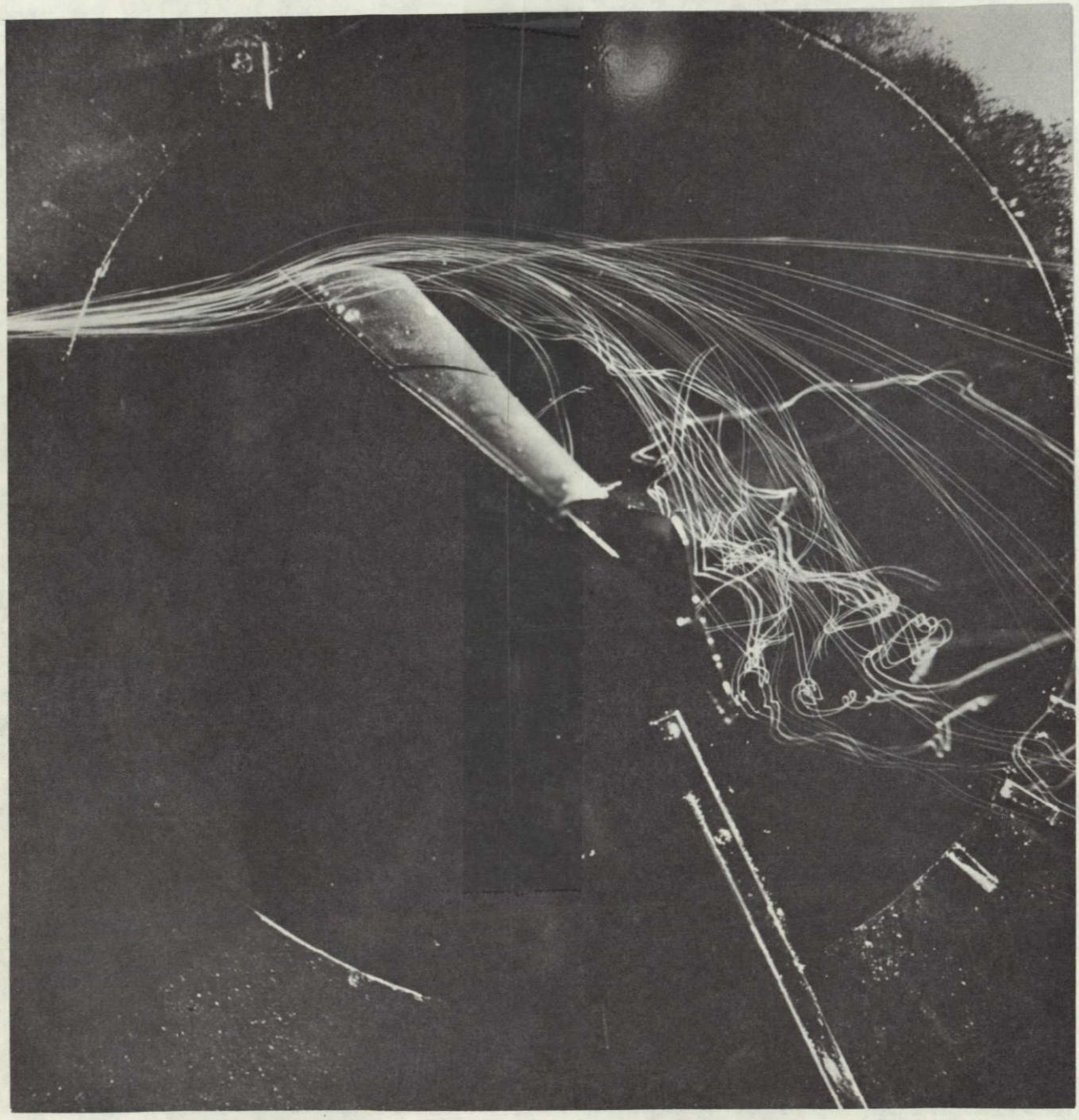

Figure 85.- Spanwise blowing on the 45^{0} swept trapezoidal wing for $\alpha = 40^{0}$ and $C_{\mu} = 0.075$; $\delta_{LE} = \delta_{TE} = 60^{0}$; $x_n/c_r = 0.40$; $h/d = 1.0$.

Blowing On

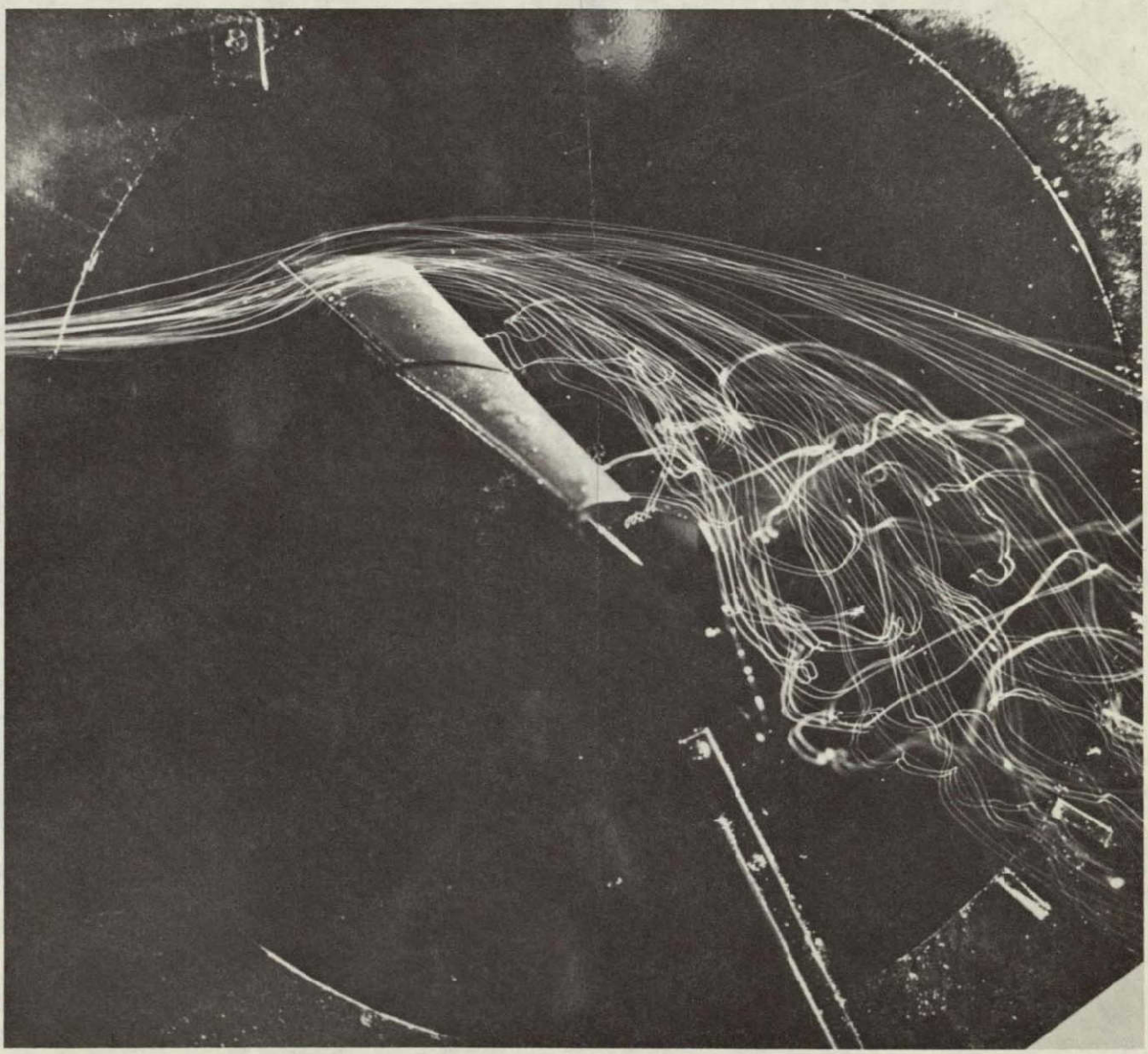

Figure 86. - Spanwise blowing on the 45^{o} swept trapezoidal wing for $\alpha = 40^{o}$ and $C_{\mu} = 0.095$; $\delta_{LE} = \delta_{TE} = 60^{o}$; $x_n/c_r = 0.40$; $h/d = 1.0$.

ORIGINAL PAGE IS
OF POOR QUALITY